A causal role of theta oscillations in memory and hippocampal physiology

Hyun Choong Yong

Integrated Program in Neuroscience

McGill University, Montreal

September 2022

A thesis submitted to McGill University in partial fulfillment of the requirements of the degree of Doctor of Philosophy in Neuroscience

Table of Contents

Abstract

Episodic memory is the ability to remember one's first person experiences embedded in a spatial and temporal context (Tulving, 1972). In the case of patient Henry Molaison (H.M.), he was not able to form any new long-term episodic memories following bilateral lesions of the medial temporal lobe (Corkin et al., 1997; Scoville & Milner, 1957). This spawned a massive research program investigating the medial temporal lobe to pinpoint neural mechanisms that subserve spatial and temporal aspects of episodic memory. Although potential neural correlates of spatial components of episodic memory have been identified (Hafting et al., 2005; J. O'Keefe & Dostrovsky, 1971), how the brain supports the 'when' component of episodic memory remains largely elusive. Recently, time cells, which have temporally-tuned receptive fields, have been identified in the hippocampal formation (Kraus et al., 2015; Pastalkova et al., 2008), and are implicated to have a crucial role in supporting the 'when' component of episodic memory (Eichenbaum, 2014). However, the causal relationship between these time cells and working memory remains unclear. Similarly, hippocampal theta oscillations are thought to support working memory, primarily through the generation of time cell sequences (Y. Wang et al., 2015).

My PhD thesis is aimed at causally examining these relationships by optogenetically silencing the medial septal GABAergic theta-generating circuit during the delay portion of a working memory task. Optogenetic manipulations of GABAergic neurons disrupted theta oscillations with temporal and spatial specificity. Moreover, without hippocampal theta oscillations, many time cells exhibited remapping and new time cells were recruited; collectively resulting in a new time cell sequence during the delay period. Despite this remapping of time cells on a random selection of theta-reduced trials, behavioral performance was unimpaired,

demonstrating that working memory is not dependent on a single or unique time cell sequence during the delay period. Moreover, a subset of time cells that encode animal's past or future trajectories maintained their firing fields during theta-reduced trials, suggesting another potential mechanism that might have supported animal's behavior.

Résumé

La mémoire épisodique est la capacité à se souvenir de ses expériences à la première personne intégrées dans un contexte spatial et temporel (Tulving, 1972). Dans le cas du patient Henry Molaison (H.M.), il n'a pas été en mesure de former de nouveaux souvenirs épisodiques à long terme suite à des lésions bilatérales du lobe temporal médial (Corkin et al., 1997 ; Scoville & Milner, 1957). Cela a engendré un programme de recherche massif étudiant le lobe temporal médian pour identifier les mécanismes neuronaux qui sous-tendent les aspects spatiaux et temporels de la mémoire épisodique. Bien que des corrélats neuronaux potentiels des composantes spatiales de la mémoire épisodique aient été identifiés (Hafting et al., 2005; J. O'Keefe & Dostrovsky, 1971), la façon dont le cerveau prend en charge la composante « quand » de la mémoire épisodique reste largement insaisissable. Récemment, des cellules temporelles, qui ont des champs récepteurs accordés dans le temps, ont été identifiées dans la formation de l'hippocampe (Kraus et al., 2015 ; Pastalkova et al., 2008), et sont impliquées pour avoir un rôle crucial dans le soutien du « quand » composante de la mémoire épisodique (Eichenbaum, 2014). Cependant, la relation causale entre ces cellules temporelles et la mémoire de travail reste incertaine. De même, on pense que les oscillations thêta de l'hippocampe soutiennent la mémoire de travail, principalement par la génération de séquences de cellules temporelles (Y. Wang et al., 2015).

Ma thèse de doctorat vise à examiner de manière causale ces relations en faisant taire optogénétiquement le circuit générateur de thêta GABAergique septal médial pendant la partie retard d'une tâche de mémoire de travail. Les manipulations optogénétiques de ces neurones ont perturbé les oscillations thêta avec une spécificité temporelle et spatiale. De plus, sans oscillations thêta de l'hippocampe, de nombreuses cellules temporelles présentaient un

remappage et de nouvelles cellules temporelles étaient recrutées ; aboutissant collectivement à une nouvelle séquence de cellules temporelles pendant la période de retard. Malgré ce remappage des cellules temporelles sur une sélection aléatoire d'essais thêta-réduits, les performances comportementales n'ont pas été altérées, démontrant que la mémoire de travail ne dépend pas d'une seule ou unique séquence de cellules temporelles pendant la période de retard. De plus, un sous-ensemble de cellules temporelles dans lesquelles les trajectoires passées ou futures de l'animal ont maintenu leurs champs de tir pendant les essais à thêta réduit, suggérant un autre mécanisme potentiel qui aurait pu soutenir le comportement de l'animal.

Not only so, but we also glory in our sufferings, because we know that suffering produces perseverance; perseverance, character; and character, hope. - Romans 5:3-5

Acknowledgements

First and foremost, I would like to thank my supervisor, Dr. Mark Brandon. Without his unyielding support and mentorship, I would not have been able to complete my PhD. He fostered an environment that allowed scientific freedom to pursue ideas and provided necessary support and guidance to see through to the end. He put together such a great team of scientists, and it was a great privilege to work with them. I would like to thank my advisory committee members, Dr. Tak Pan Wong, Dr. Sylvain Williams, and Dr. Lalit Srivastava for their guidance throughout my PhD. I would like to thank my former and current colleagues for wonderful discussions and interactions I had with them over the years: Andres Nieto-Posadas (MD-PhD), Robert Rozeske (PhD), Justin Quinn Lee (PhD), Alexandra Keinath (PhD), Jennifer Robinson (PhD), Cecilia Kramer (PhD), Marie Oule (PhD), Coralie-Anne Mosser (PhD), Zaki Ajabi (PhD), Saishree Badrinarayanan (MSc), Leonie Runtz (MSc), Mohammad Hassan Yaghoubi (MSc), Zeeshan Haqqee (MSc), Eric Morgan (BSc), Raphael Lavoie (MSc), and Sooyeon Kim (BSc). I would like to also thank my collaborator, HaoRan Chang (BSc). A special thanks to Johnson Ying (BSc) who has been invaluable to my scientific success.

Last but not the least, I would like to thank my wife, Sooyeon Kim. I would not have made it to PhD without your dedication, patience, and support. Thank you very much.

Contribution to Original Knowledge

My PhD thesis presents causal evidence that theta oscillations are not required to maintain working memory in the hippocampus. Moreover, it demonstrates that a single reliable neuronal code is not a prerequisite for stable memory performance while it leaves a possibility that a small subset of stable hippocampal neurons might be sufficient to support successful memory performance.

Contribution of Authors

In all cases, Hyun Choong Yong led the study design, data acquisition, and data analysis. HaoRan Chang contributed to data analysis in Chapter 2. Writing of the thesis including figure construction, was completed by Hyun Choong Yong unless stated otherwise.

List of Figures

Chapter 1.

Chapter 2.

Chapter 3.

List of abbreviations

DG	Dentate gyrus
MS	Medial septum
CA	Cornu ammonis
MEC	Medial entorhinal cortex
LEC	Lateral entorhinal cortex
SWR	Sharp-wave ripples
REM	Rapid eye movement
SBD	Same birthday neurons
DBD	Different birthday neurons

Chapter 1: Introduction

Episodic memory is the ability to remember one's first-person experiences embedded in a spatial and temporal context (Tulving, 1972). When asked to describe what one did over the weekend, one is relying on their episodic memory to describe a sequence of events that are unfolding within specific spatial contexts. In the case of patient Henry Molaison (H.M.), bilateral lesions of the medial temporal lobe including the hippocampus left him unable to form any new long-term episodic memory (Corkin et al., 1997; Scoville & Milner, 1957). His memory deficits were severe to the extent that he seemed to be unable to remember that he had surgery. This unexpected discovery provided the earliest and strongest evidence that a key role of the medial temporal lobe is to encode new memories. Consequently, this spawned a massive research program to identify neural mechanisms that enable the medial temporal lobe to encode spatial and temporal aspects of episodic memory.

From a theoretical perspective, the three key components of episodic memory are *where*, *when*, and *what* (Tulving, 1972). Spatially modulated cells, such as place cells (J. O'Keefe & Dostrovsky, 1971), grid cells (Hafting et al., 2005), head direction cells (Taube et al., 1990) and boundary vector cells (Solstad et al., 2008), found in the hippocampus and the medial entorhinal cortex (MEC) are thought to subserve the *where* component of episodic memory (Buzsáki & Moser, 2013; John O'Keefe & Nadel, 1978). It is hypothesized that the *what* component is supported by the lateral entorhinal cortex (LEC) because its neurons fire in the vicinity of objects while being less spatially modulated compared to neurons in the MEC (Deshmukh & Knierim, 2011; Hargreaves et al., 2005; Knierim et al., 2014). For the *when* component, time cells found in the hippocampus (Pastalkova et al., 2008) and MEC (Kraus et al., 2015) may be crucial

(Eichenbaum, 2014). These time cells fire at specific moments in time during the delay period of working memory tasks, and are thought to play a crucial role in bridging a temporal gap between discontinuous events (Eichenbaum, 2014). However, a circuit mechanism for time cell generation remains largely unknown although it has been suggested that theta oscillations are involved (Y. Wang et al., 2015).

In Chapter 1, detailed descriptions of hippocampal and septal anatomy will be provided. These anatomical descriptions will be coupled with a hypothesized function of each area based on the current literature. The anatomy and function section will be followed by discussion of hippocampal rhythms. Finally, this chapter will conclude with a discussion of time cells.

1.1. The anatomy and function of the hippocampal formation and septal nuclei

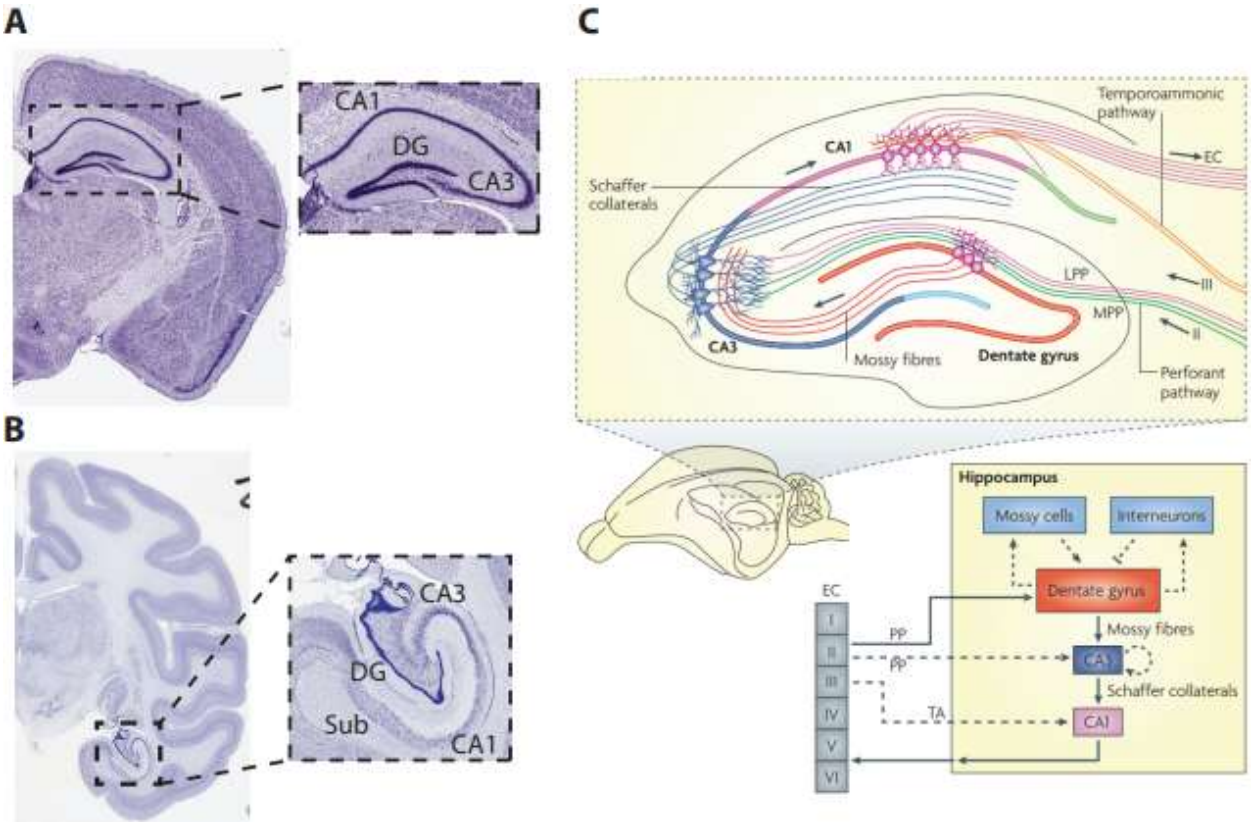

Figure 1-1. The hippocampus.

(A-B) Nissl-stained coronal views of the hippocampus in rodents (A) and primates (B). Insets are zoomed images of the hippocampus. Note that the primate hippocampus is located along the ventral surface of the brain while the rodent hippocampus is found below the cortex. Sub: subiculum.

(C) A gross overview of the classical trisynaptic circuit. MPP: medial perforant pathway, LPP: lateral perforant pathway, EC: entorhinal cortex

Parts **A-B** were adapted from BrainMaps (Mikula et al., 2007), and Part **C** was adapted from Deng et al. (2010).

1.1.1. Dentate gyrus (DG)

Granule cells are the principal cells of the dentate gyrus (DG), which is made up of three main sublayers: (1) the molecular layer, (2) the granule cell layer, and (3) the polymorphic layer, or the hilus. Being the most superficial layer, the molecular layer contains dendrites of granule cells, and these dendrites extend to the superficial portion of the molecular layer in the shape of a cone. The granule cell layer consists of cell bodies of granule cells, which send projections to CA3. These axonal projections from the DG to CA3 are called mossy fibers. The polymorphic layer, the deepest layer, contains mossy fibers as well as mossy cells and other types of interneurons. Mossy fibers project to mossy cells, which send their axons back to the molecular layer, potentially modulating output of granule cells (Hsu et al., 2016; Scharfman, 2016).

Furthermore, the DG receives its inputs from layer II of the entorhinal cortex through connections called the perforant pathway (Witter, 2007b). The perforant pathway terminates in

the molecular layer, and its terminals are highly organized based on the origin of its axons (Hjorth-Simonsen & Jeune, 1972; Hjorth-Simonsen, 1972; Stanfield et al., 1979). Axon terminals arising from the LEC occupy the most superficial third of the molecular layer, while axons from the MEC terminate in the middle third. Projections from mossy cells are found in the inner third of the molecular layer.

The DG is hypothesized to be involved in pattern separation, a process by which similar events are encoded with dissimilar patterns of neuronal activities (Gilbert et al., 2001; J. K. Leutgeb et al., 2007; Neunuebel & Knierim, 2014; Treves & Rolls, 1994). Previous studies showed that dentate granule cells remapped more than CA3 neurons when an environment was slightly altered (J. K. Leutgeb et al., 2007), and had very sparse activities (N. B. B. Danielson et al., 2016; GoodSmith et al., 2017; M. W. Jung & McNaughton, 1993; Neunuebel & Knierim, 2012). These works support a classical view that the DG plays an important role in parsing overlapping inputs from the entorhinal cortex with sparse coding (Marr, 1969; B. L. McNaughton & Nadel, 1990; Yassa & Stark, 2011). However, recent works challenge this notion since dentate granule cells remapped less than dentate mossy cells and hippocampal pyramidal neurons when environments were changed (Hainmueller & Bartos, 2018; Senzai & Buzsáki, 2017). In light of these recent works, the role of the DG in pattern separation is currently under revision (H. Lee et al., 2020).

1.1.2. CA3

Located adjacent to the DG, CA3 is made up of five sublayers: (1) the stratum lacunosum-moleculare, (2) the stratum radiatum, (3) the stratum lucidum, (4) the stratum pyramidale, and (5) the stratum oriens, ordered from superficial to deep. Pyramidal cells, whose

cell bodies are found in the stratum pyramidale, are the principal cell of CA3, as well as CA1 and CA2. While their apical dendrites are found in the stratum lacunosum-moleculare and the stratum radiatum, their basal dendrites are confined in the stratum oriens. Axons of CA3 pyramidal cells project to CA1, and these projections are called Schaffer collaterals. Although it has been shown that CA3 send projections to CA2 (Sekino et al., 1997), this projection remains largely elusive.

Moreover, CA3 receives direct inputs from the DG through mossy fibers, which terminate in the stratum lucidum and target proximal dendrites. DG-CA3 contact sites via mossy fibers can be distinguished by the presence of thorny excrescences (Amaral, 1978). A recent study, however, discovered that a group of distal CA3 pyramidal neurons does not receive mossy fiber inputs and have thorny excrescences (Hunt et al., 2018). They had different physiological properties and contributed differently to sharp-wave ripple (SWR) events, suggesting heterogeneity in populations of hippocampal principal cells, which were largely considered to be homogeneous (Graves et al., 2012; Hunt et al., 2018; Lee et al., 2014). In addition to DG inputs, CA3 receives direct inputs from the perforant pathway with fibers from the LEC and MEC terminating in the superficial and deep portion of the stratum lacunosum-moleculare, respectively (Witter, 1993). One notable aspect of this projection is that proximal CA3 pyramidal neurons receive little to no inputs via the perforant pathway, but are largely driven by DG inputs (Ishizuka et al., 1990; Witter, 2007a), suggesting heterogeneity or a gradient of inputs along the transverse axis of CA3 (Q. Sun et al., 2017).

Given its extensive recurrent collaterals, CA3 is hypothesized to be involved in pattern completion, a process by which degraded or partial inputs lead to retrieval of a full memory trace

(Marr, 1971; Rolls, 2016; Treves & Rolls, 1994). A previous study demonstrated that CA3 place cells had more stable fields compared to CA1 place cells when cues were rotated (I. Lee et al., 2004). Moreover, it was suggested that different degrees of pattern completion are carried out along the transverse axis of CA3 (H. Lee et al., 2015; Lu et al., 2015). Lee et al. (2015) showed that when cues were rotated, place cells in CA3 remapped to the extent that no evidence of pattern completion, but rather pattern separation was observed. However, as they recorded from more distal portion of CA3, place cells were resilient to changes in the environment, suggesting that proximal CA3 is involved in pattern separation, and intermediate and distal CA3 are involved in pattern completion (H. Lee et al., 2020).

1.1.3. CA2

CA2 is a narrow area located between CA3 and CA1, and its anatomy and function have been relatively studied less than other hippocampal subfields because it is difficult to experimentally target CA2 given its size and location. Initially, CA2 was considered to be distinct from CA3 because pyramidal neurons in CA2 did not express thorny excrescences in their dendrites, indicating that they do not receive direct inputs from mossy fibers arising from the DG (Lorente De Nó, 1934). A recent study, however, showed that CA2 receives monosynaptic inputs from the DG, calling for an update to the classical definition of CA2 (Kohara et al., 2014). It has been suggested that termination sites of axons arising from the supramammillary nucleus and the paraventricular nucleus of the hypothalamus may demarcate the border between CA3 and CA2 better given their extensive and specific projections to CA2 (Cui et al., 2013; Dudek et al., 2016; L. Zhang & Hernández, 2013). Similar to CA1, CA2 receives inputs from CA3 via Schaffer collaterals (Lorente De Nó, 1934), but the function of this pathway remains unknown.

One line of research suggests that CA2 has a significant role in social memory (Dudek et al., 2016; Tzakis & Holahan, 2019). It has been shown that mice were not able to recognize familiar mice when CA2 was inactivated or lesioned (Hitti & Siegelbaum, 2014; Stevenson & Caldwell, 2014). Moreover, during SWRs, a process theorized to be important for memory consolidation (Dupret et al., 2010; Fernández-Ruiz et al., 2019; Girardeau et al., 2009; Jadhav et al., 2012; Karlsson & Frank, 2009; Wilson & McNaughton, 1994), CA2 pyramidal neurons that had been active during social interaction were reactivated (Oliva et al., 2020). Manipulating these SWRs to either shorten or prolong reactivation events impaired or improved social memory, respectively (Oliva et al., 2020). These findings are consistent with what was observed with spatial memory (Fernández-Ruiz et al., 2019). In addition, within the hippocampus proper, receptors for vasopressin, which is known to have an important role in social behavior and aggression (Wersinger et al., 2002; Wersinger et al., 2008), are more or less exclusively expressed in CA2 (Young et al., 2006). Taken together, these studies suggest that CA2 has a crucial role in social memory.

1.1.4. CA1

CA1 is the main output structure of the hippocampus proper, sitting at the top of the trisynaptic circuit. Although CA1 shares many anatomical similarities with CA3, there are some key differences. First, CA1 does not have the stratum lucidum since CA1 does not receive mossy fiber inputs from the DG. Second, CA1 pyramidal neurons do not have recurrent connections like CA3 although it was recently suggested that they might be more interconnected than previously thought (Geiller et al., 2022). A recent study demonstrated that when a CA1 pyramidal neuron was optogenetically stimulated, a subset of nearby CA1 pyramidal neurons started to fire and gained a place field close to the stimulated pyramidal neuron (Geiller et al.,

2022). Third, CA1 does not receive direct inputs from the entorhinal cortex through the perforant pathway, but through the temporoammonic pathway that originates from layer III of the entorhinal cortex. However, pyramidal neurons in the layer II of the MEC directly project to CA1 (Kitamura et al., 2014).

Similar to CA3, axons arising from the entorhinal cortex project to the stratum lacunosum-moleculare and are topographically organized with the LEC and MEC fibers preferentially terminating in the distal and proximal portions of CA1, respectively. CA3 Schaffer collaterals terminate in the stratum radiatum with proximal and distal CA3 projecting to distal and proximal portions of CA1, respectively (Van Strien et al., 2009). Recent studies showed that axons from CA2 preferentially terminate in the stratum oriens rather than the stratum radiatum (Hitti & Siegelbaum, 2014; Shinohara et al., 2012).

In addition to heterogeneous but highly organized input patterns along the proximodistal axis of CA1, pyramidal cells in CA1 have different anatomical and functional properties depending on their location of cell bodies along the stratum pyramidale (Lorente De Nó, 1934). Superficial pyramidal cells located closer the stratum radiatum show immunoreactivity to calbindin, whereas deep pyramidal cells located closer to the stratum oriens do not (Baimbridge et al., 1991; Lee et al., 2014). Deep CA1 pyramidal cells are more heavily innervated by CA2 inputs (Kohara et al., 2014). The LEC projects more densely to superficial CA1 pyramidal cells while the MEC projects uniformly throughout the superficial-deep axis (Y. Li et al., 2017). Moreover, during embryonic development, deep CA1 pyramidal cells are born around 2-3 days earlier than superficial CA1 pyramidal cells (Cembrowski et al., 2016).

Differences in anatomical connectivity, as well as timing of neurogenesis during embryonic development, may give rise to electrophysiological differences observed along the superficial-deep axis of CA1 (Soltesz & Losonczy, 2018). Deep CA1 pyramidal cells had higher firing rates and burst more than superficial CA1 pyramidal cells (Mizuseki et al., 2011). When environmental cues were changed, superficial CA1 pyramidal cells remapped less compared to deep CA1 pyramidal cells that were more modulated by goal locations (Danielson et al., 2016) or landmarks (Geiller et al., 2017). Depending on their location along the superficial-deep axis, CA1 pyramidal cells receive differential inputs from GABAergic interneurons (Lee et al., 2014; Valero et al., 2015) and have distinctive recruitment patterns during SWRs (Stark et al., 2014). These results show that CA1 pyramidal cells have substantial differences in their anatomy and function along not only the transverse axis, but also the superficial-deep axis.

As the main output structure of the hippocampus proper, CA1 sends projections to the subiculum as well as deep layers of the entorhinal cortex. Distal and proximal CA1 project to proximal and distal subiculum, respectively. Moreover, projections from CA1 to the entorhinal cortex closely follow input patterns. Distal and proximal CA1 send their axons to deep layers of the LEC and MEC, respectively (Naber et al., 2001; Tamamaki & Nojyo, 1995). The dorsolateral portion of the entorhinal cortex receives inputs from the septal portion of CA1 while the ventromedial portion of the entorhinal cortex is targeted by the temporal portion of CA1 (Naber et al., 2001; Van Strien et al., 2009).

One of the most widely studied function of CA1 is its representation of space, fueled by the discovery of place cells (O'Keefe & Dostrovsky, 1971). These place cells fire at a specific location in the environment, and are sensitive to changes to external cues or landmarks (Leutgeb

et al., 2005; Muller & Kubie, 1987). These key properties of place cells led to the development of the cognitive map theory, which posits that the hippocampus utilizes place cells to construct and store a mental representation of the external world (O'Keefe & Nadel, 1978). A recent study has shown that positive reinforcement of a place cell during sleep increased time exploring the area encoded by the reinforced place cell, demonstrating a causal role of place cells in spatial navigation (De Lavilléon et al., 2015; Jadhav et al., 2012). However, the function of CA1 goes far beyond the spatial domain as it has been demonstrated that CA1 encodes variables in nonspatial domain such as time (Pastalkova et al., 2008), sound (Sakurai, 2002), odor (Eichenbaum et al., 1987), and task-relevant motor action (Aronov et al., 2017). These results suggest that the hippocampus may provide neuronal representations of variables relevant to solve a task at hand instead of exclusively encoding spatial variables (Aronov et al., 2017).

1.1.5. The entorhinal cortex

As the main gateway between the hippocampus and the neocortex, the entorhinal cortex provides the hippocampus with cortical inputs and distributes highly processed hippocampal outputs to the neocortex (Canto et al., 2008; Witter et al., 2017). Thus, CA1 projections to deep layers of the entorhinal cortex close the entorhinal-hippocampal loop that is instantiated by the entorhinal cortex via either the perforant pathway or the temporoammonic pathway. The entorhinal cortex receives its inputs from numerous structures, including the postrhinal, perirhinal, and piriform cortex. For output, the entorhinal cortex sends projections back to its input structures by reciprocating cortical afferents (Canto et al., 2008).

The entorhinal cortex can further be divided into the LEC and the MEC, and they subserve different functions. As previously described, the LEC is thought to be involved in

'what' aspect of episodic memory (Deshmukh & Knierim, 2011; Hargreaves et al., 2005; Neunuebel & Knierim, 2014; C. Wang et al., 2018). A recent study demonstrated that the LEC represented objects using the egocentric frame of reference while the MEC used the allocentric framework (C. Wang et al., 2018). This finding suggests that the LEC integrates 'what' information with 'where' information from the perspective of an observer instead of simply representing 'what' aspect of episodic memory (C. Wang et al., 2018).

The MEC represents an animal's location with grid cells, which fire at regular intervals to form hexagonally organized firing fields (Hafting et al., 2005). Given that locations of their firing fields were invariant between different environments, it was initially hypothesized that they provide a universal spatial metric (B. L. McNaughton et al., 2006; Moser et al., 2008). This hypothesis, however, has been challenged because recent studies demonstrated that grid cells are modulated by the shape of environments similar to place cells (Krupic et al., 2015; Stensola et al., 2015). Furthermore, the role of grid cells in generation of hippocampal place cells remains unclear after numerous studies showed that grid cells are not required to generate place fields in both familiar and novel environments (Brandon et al., 2014; Hales et al., 2014; Y. Wang et al., 2015). Other than spatial navigation, it has been shown that the MEC has a role in processing temporal information (Heys & Dombeck, 2018; Kraus et al., 2015)

1.1.6. Septal nuclei

Located in the midline, septal nuclei are largely conserved across vertebrates (Lanuza & Martínez-García, 2009). Septal nuclei can be subdivided into the lateral septum (LS) and medial septum (MS). These two regions have different anatomical connections and functional properties, which will be described below.

1.1.6.1.Lateral septum (LS)

The lateral septum (LS) in rodents is located along the midline and surrounded by lateral ventricles. The LS contains primarily GABAergic neurons (Risold & Swanson, 1997a; Wong et al., 2016; Zhao et al., 2013). The LS receives inputs not only from the hippocampus, but also from the entorhinal cortex, medial prefrontal cortex, and MS (Sheehan et al., 2004). Based on connectivity with the hippocampus, the LS can be subdivided into the dorsomedial, dorsolateral, ventrolateral, and ventromedial regions, receiving its inputs from dorsal CA1, dorsal CA3, ventral CA3, and ventral CA1, respectively (Oh et al., 2014; Rizzi-Wise & Wang, 2021). Moreover, CA2 projects to the dorsal portion of the LS (Leroy et al., 2018). While the LS sends most of their projections to subcortical regions such as hypothalamus and ventral tegmental area, the LS also sends sparse projections to the cortex (Risold & Swanson, 1997b; Sheehan et al., 2004).

The function of the LS within the hippocampo-septal network remains largely unknown. As the major subcortical structure targeted by the hippocampus, the LS contains place cells (Leutgeb & Mizumori, 2002; Zhou et al., 1999; Takamura et al., 2006; van der Veldt et al., 2021; Wirtshafter & Wilson, 2020) and is able to decipher hippocampal place cell outputs using theta phase codes (Tingley & Buzsáki, 2018). Additionally, it has been suggested that excitatory inputs from CA2 to the LS promotes aggressive behavior in mice (Leroy et al., 2018). These studies suggest that the LS may have similar roles as the hippocampus in social memory and spatial navigation.

1.1.6.2.Medial septum (MS)

The medial septum-diagonal band of Broca (MS-DBB) is located along the midline with the MS encapsulated by the LS, and the DBB situated close to the ventral surface of the brain. The MS-DBB receives its inputs from numerous structures including the hippocampus, the amygdala, and the thalamus, while sending projections to several structures including the hippocampus and the entorhinal cortex (Gonzalez-Sulser et al., 2014; Swanson & Cowan, 1979). GABAergic (Freund & Antal, 1988), cholinergic (Frotscher & Léránth, 1985), and glutamatergic neurons (Colom et al., 2005; Manseau et al., 2005; J. Robinson et al., 2016; Sotty et al., 2003) are three cell types found in the MS-DBB. All of them send long projections to the hippocampus, but they have different targets. GABAergic neurons primarily terminate on hippocampal interneurons (Freund & Antal, 1988; Unal et al., 2015), but cholinergic and glutamatergic neurons send their collaterals to both pyramidal cells and interneurons in the hippocampus (Frotscher & Léránth, 1985; Y. Sun et al., 2014; Unal et al., 2015; Widmer et al., 2006). Notably, CA1 interneurons receive around 67%, 12%, and 21% of their MS-DBB inputs from GABAergic, cholinergic, and glutamatergic neurons, respectively (Sun et al., 2014). In contrast, for CA1 pyramidal cells, 27%, 66%, and 7% of their inputs arise from GABAergic, cholinergic, and glutamatergic neurons, respectively (Sun et al., 2014).

In line with different input patterns from the MS-DBB to the hippocampus, each cell type subserves a different function in the septo-hipocampal network. Cholinergic neurons have an important role in regulating hippocampal SWRs as the activation of cholinergic neurons leads to suppression of SWRs (Vandecasteele et al., 2014; Zhang et al., 2021). Also, it has been demonstrated that cholinergic neurons are required for fear learning because of their involvement in activating interneurons that inhibit inputs arriving via the temporoammonic pathway (Lovett-

Barron et al., 2014). Glutamatergic neurons are considered to be involved in locomotion (Fuhrmann et al., 2015), although their functions remain largely elusive. Finally, GABAergic neurons are considered to work as a pacemaker of hippocampal theta oscillations by rhythmically disinhibiting pyramidal neurons in the hippocampus (Tóth et al., 1997).

1.2. Hippocampal rhythms

1.2.1. Theta oscillations

Theta oscillations (4-12 Hz) were initially described in rabbits (R. Jung & Kornmüller, 1938), and were subsequently discovered in cats, rats, monkeys, and humans (Bohbot et al., 2017; Goyal et al., 2020; Green & Arduini, 1954; Jutras et al., 2013; Vanderwolf, 1969). Being one of the most studied brain rhythms in rodents, theta oscillations are observed throughout the hippocampus during active exploration, quiet wakefulness, and rapid eye movement (REM) sleep (Buzsáki, 2002; Vanderwolf, 1969).

1.2.1.1.The role of the MS in the generation of hippocampal theta oscillations

GABAergic neurons in the MS are thought be a pacemaker of hippocampal theta oscillations (Colgin, 2013; Tóth et al., 1997). Firing rhythmically at theta frequencies, these neurons are phase-locked to hippocampal theta oscillations that are recorded around 80ms after a spike (Hangya et al., 2009; Simon et al., 2006). These GABAergic neurons in the MS are equipped with hyperpolarization-activated cyclic nucleotide-gated (HCN) channels, which allow them to generate rhythmic firing patterns (Varga et al., 2008). Moreover, these neurons send long projections to interneurons in the hippocampus, which result in rhythmic disinhibition of pyramidal neurons at theta frequencies (Tóth et al., 1997).

However, this view was recently challenged because the hippocampus preparation *in vitro* spontaneously generated theta oscillations in the absence of inputs from the MS (Goutagny et al., 2009). Theta oscillations were observed in CA1 even when CA3 was removed. Furthermore, theta oscillations recorded from dorsal CA1 was not coherent with theta oscillations recorded from ventral CA1 when intermediate CA1 was inhibited. These suggested that the hippocampus has not only internal machinery capable of generating theta oscillations in the absence of MS inputs, but also independent theta oscillators throughout the hippocampus. Although the hippocampus can generate theta oscillations on its own *in vitro*, many studies indicate that the MS is required for theta oscillations *in vivo*. Inactivation of the MS with muscimol, a $GABA_A$ receptor agonist, led to a near-complete reduction of theta oscillations in the hippocampus and the MEC (Brandon et al., 2011, 2014; Koenig et al., 2011; Y. Wang et al., 2015). A recent study showed that optogenetic inhibition of GABAergic neurons *in vivo* significantly reduced theta oscillations during REM sleep (Boyce et al., 2016). Together, these results demonstrate that inputs from the MS, especially from GABAergic neurons, are needed for theta oscillations *in vivo*.

Cholinergic neurons in the MS are needed to generate a specific type of theta oscillations, called atropine-sensitive or type 2 theta (Kramis et al., 1975). Type 2 theta is observed when animals are immobile, but attentive, and can be abolished with an acetylcholine receptor antagonist called atropine (Kramis et al., 1975). Type 1 theta, observed during periods of REM sleep and active exploration, is resistant to atropine. Although cholinergic neurons in the MS are involved in the generation of type 2 theta, it is unlikely that these neurons generally work as a pacemaker for theta oscillations. First, cholinergic neurons do not fire rhythmically at theta frequencies, and have low firing rates (Simon et al., 2006). Second, optogenetic stimulation of

cholinergic neurons in the MS have little to no effects on theta power in behaving animals (Dannenberg et al., 2019; Vandecasteele et al., 2014) despite of cholinergic tone increasing with locomotion and decreasing with immobility (Kopsick et al., 2022; Y. Zhang et al., 2021). Instead of being a pacemaker of theta oscillations, cholinergic neurons may have an important role in modulating other network activities as described in the previous section.

1.2.1.2.The function of theta oscillations

Hippocampal theta oscillations are hypothesized to be involved in learning and memory. The earliest evidence supporting this hypothesis came from a study that administered foot shocks to rodents (Landfield et al., 1972). This study showed that the magnitude of theta oscillations recorded in the electroencephalogram was positively correlated with the degree to which rats remembered an aversive foot shock. Subsequent studies further demonstrated that the magnitude of theta oscillations is correlated with behavior or memory performance in both animals and humans (Berry & Thompson, 1978; Klimesch et al., 1996; Liebe et al., 2012; Macrides et al., 1982; Osipova et al., 2006; Rutishauser et al., 2010). For example, a study showed that successful memory recall in humans could be predicted by phase-locking of single unit activities to hippocampal theta oscillations (Rutishauser et al., 2010). Animals with reversible or irreversible MS lesions were impaired in memory tasks such as a delayed spatial alternation task and radial arm maze task (M'Harzi & Jarrard, 1992; Mitchell et al., 1982; Mizumori et al., 1990; Robbe & Buzsáki, 2009; Winson, 1978). Furthermore, electrical stimulation of the fornix following pharmacological inhibition of the MS in theta frequency to restore theta rhythmicity in the hippocampus rescued spatial memory (N. McNaughton et al., 2006).

These studies implicate theta oscillations in learning and memory, but do not establish a causal relationship between the two. Studies described above were correlational in nature, or did not have cell-type specificity in their circuit manipulation to conclude that theta oscillations are crucial for memory. A recent study addressed this issue by specifically targeting GABAergic neurons in the MS using optogenetics (Boyce et al., 2016). This study showed that mice were impaired in novel place object recognition and fear-conditioning tasks following disruption of theta oscillations during REM sleep. Moreover, several studies drove theta oscillations to oscillate outside of their endogenous frequency range by either cooling down (Petersen & Buzsáki, 2020) or optogenetically pacing the MS (Quirk et al., 2021). These manipulations caused significant impairment in memory performance although hippocampal place cell codes were not impaired despite changes in theta frequencies (Petersen & Buzsáki, 2020; Zutshi et al., 2018). This raises a possibility that downstream structures cannot decipher neural codes transferred outside of endogenous theta frequencies.

1.2.2. Gamma oscillations

Gamma oscillations (30-120Hz) are thought to support information transfer between neural assemblies by transiently binding them to fire together (Engel et al., 2001; Fries et al., 2007; Gray et al., 1989). In the hippocampal formation, information transfer from CA3 or the MEC is considered to be driven by low gamma (30-60Hz) and high gamma (60-120Hz), respectively (Colgin et al., 2009). It has been reported that low gamma and high gamma are stronger in the stratum radiatum and the stratum lacunosum-moleculare, respectively. This is in line with how CA3 and the MEC differentially target CA1 sublayers (Belluscio et al., 2012; Schomburg et al., 2014). Furthermore, CA1 spikes that fired during low gamma states conveyed significantly less spatial information when CA3 input was disrupted, while CA1 spikes during

high gamma states were not impaired (Middleton & McHugh, 2016). Disruption of high gamma oscillations disrupted MEC-dependent spatial learning, but had no effects on LEC-dependent object learning (Fernández-Ruiz et al., 2021). These studies further demonstrate that two non-overlapping gamma frequency bands pass on information from different structures. Fast-spiking parvalbumin (PV) basket cells are considered to be essential to generate gamma oscillations (Bartos et al., 2007). Being highly active during gamma oscillations, they are phase-locked to gamma oscillations (Bragin et al., 1995; Csicsvari et al., 2003; Mann et al., 2005). Stimulation or inhibition of these PV interneurons using optogenetics led to amplification or reduction of gamma oscillations, respectively (Cardin et al., 2009; Sohal et al., 2009). In addition to basket cells, other types of interneurons such as cholecystokinin-expressing basket cells and axo-axonic cells may play a role in the generation of gamma oscillations. However, their roles remain to be studied (Bartos et al., 2007).

1.3. Time cells in the hippocampal formation

Early lesion studies in rodents demonstrated that the hippocampus is needed to remember a sequence of events (Chiba et al., 1994; Fortin et al., 2002; Kesner et al., 2002). In one study, rats were required to (1) choose an odor that appeared earlier in the sequence or (2) choose an odor that was not presented in the sequence (Fortin et al., 2002). Rats with bilateral hippocampal lesions were impaired in the first task, providing strong evidence that the hippocampus is required to bind temporally distant events in order. Furthermore, this impairment was not driven by the animal's inability to recognize odors because they were not impaired in the second task.

A subsequent study suggested that CA1 may have neural mechanisms to connect discontinuous events in order (Manns et al., 2007). Single-unit recordings from dorsal CA1

showed that hippocampal activity gradually changed when animals were learning a sequence of odors as if the hippocampus was timestamping experience with evolving activity. A pair of odors that appeared closer to each other in the sequence had more similar activity patterns compared to a pair of odors that was presented further apart. This study suggested that CA1 might be able to support the 'when' component of episodic memory by encoding temporal context with evolving neural activity.

However, this conclusion was confounded because animals were able to freely move around throughout behavior. Given that the hippocampus is able to represent space with its place cells (J. O'Keefe & Dostrovsky, 1971), evolving activity observed in CA1 might have been driven by changes in animals' location instead of time. To investigate whether hippocampal neurons could generate a code for temporal dimension independent of changes in spatial location, one study controlled the animal's location by adding a running wheel to the stem portion of a T-maze (Pastalkova et al., 2008). Here, animals were trained to perform a delayed spatial alternation task, in which animals need to alternate between the left and right arm of the maze while running on the wheel during the delay period. The running wheel fixed the animal's location during the delay period when the hippocampus is hypothesized to be needed to bridge discontinuous events. Surprisingly, CA1 neurons fired at specific moments in time during the delay period and formed a sequence to tile up the entire delay period. Moreover, this sequence differed between left-going and right-going trials, suggesting that they bridge gaps between discontinuous alternation (Pastalkova et al., 2008). In a subsequent study, these cells were named 'time cells' (MacDonald et al., 2011), and became another area of active research in the hippocampus.

These time cells exhibit temporally-tuned receptive fields that tile the delay period of a working memory task forming a 'time cell sequence', which might play a role in maintaining the contents of working memory during the delay (Heys & Dombeck, 2018; Kraus et al., 2013, 2015; MacDonald et al., 2011, 2013; MacDonald & Tonegawa, 2021; Pastalkova et al., 2008; N. T. M. Robinson et al., 2017; Sabariego et al., 2019; Salz et al., 2016; Shimbo et al., 2021; Taxidis et al., 2020; Y. Wang et al., 2015). However, whether time cell sequences are necessary and/or sufficient to support working memory remains unclear. In prior work, time cells were observed while animals engaged in a memory task, and the fidelity of those time cell sequences correlated with memory performance (Gill et al., 2011; MacDonald et al., 2013; Pastalkova et al., 2008; N. T. M. Robinson et al., 2017; Y. Wang et al., 2015). Importantly, time cell sequences also failed to emerge in a similar task that did not include a memory component (Gill et al., 2011; Pastalkova et al., 2008). Since these reports, however, time cell sequences have been observed in a 'looping task' with no memory demand (Mau et al., 2018), and do not emerge during the trace period of trace fear conditioning (Ahmed et al., 2020). Time cell sequences failed to differentiate between odors although a number of time cells increased with training (Taxidis et al., 2020). Moreover, in one study, ablation of inputs from the medial entorhinal cortex spared hippocampal time cell sequences while memory performance was impaired (Sabariego et al., 2019). These reports thus suggest that time cell sequences could arise independently of working memory processes. Finally, studies that use direct and immediate optogenetic perturbations to the entorhinal-hippocampal circuit have reported concurrent disruptions of both time cell activity and memory (MacDonald & Tonegawa, 2021; N. T. M. Robinson et al., 2017). We suspect that these conflicting findings could be due to the methodologies used - lesion studies allow time for homeostatic regulation or other compensatory

mechanisms (Maldonado et al., 2008; Otchy et al., 2015), while direct and immediate perturbation of hippocampal activity has the potential to influence a wide array of hippocampal and cortical processes, other than the activity of hippocampal time cell sequences (N. Li et al., 2019).

Beyond the search for the function of time cell sequences, computational models have generated clear hypotheses for how the hippocampus generates time cell sequences. Several popular models rely on hippocampal theta oscillations (6-10Hz), including models that use rhythmic persistent spiking and oscillatory interference (Hasselmo, 2008; Hasselmo & Stern, 2014), and/or theta-rhythmic inhibition to advance activity across the network (Haimerl et al., 2019; Y. Wang et al., 2015). These models have received important experimental support from one study that used long-acting muscimol to silence the MS, resulting in reduced theta power, disrupted time cell responses, and impaired memory performance (Y. Wang et al., 2015). One important caveat to this study is that muscimol inhibits all MS cell types (GABAergic, cholinergic, and glutamatergic) which are hypothesized to support independent proposed mnemonic functions (Hasselmo M. E., 1999; Roland et al., 2014). Further, these inactivations are maintained throughout an entire testing session - not specifically during the delay period. For these reasons, it has not been possible to attribute the perturbation in time cell sequences and the deficits in memory performance directly to the absence of theta oscillations and time cells during the delay portion of this task. Future studies are needed to study a causal role of theta oscillations in working memory and time cells.

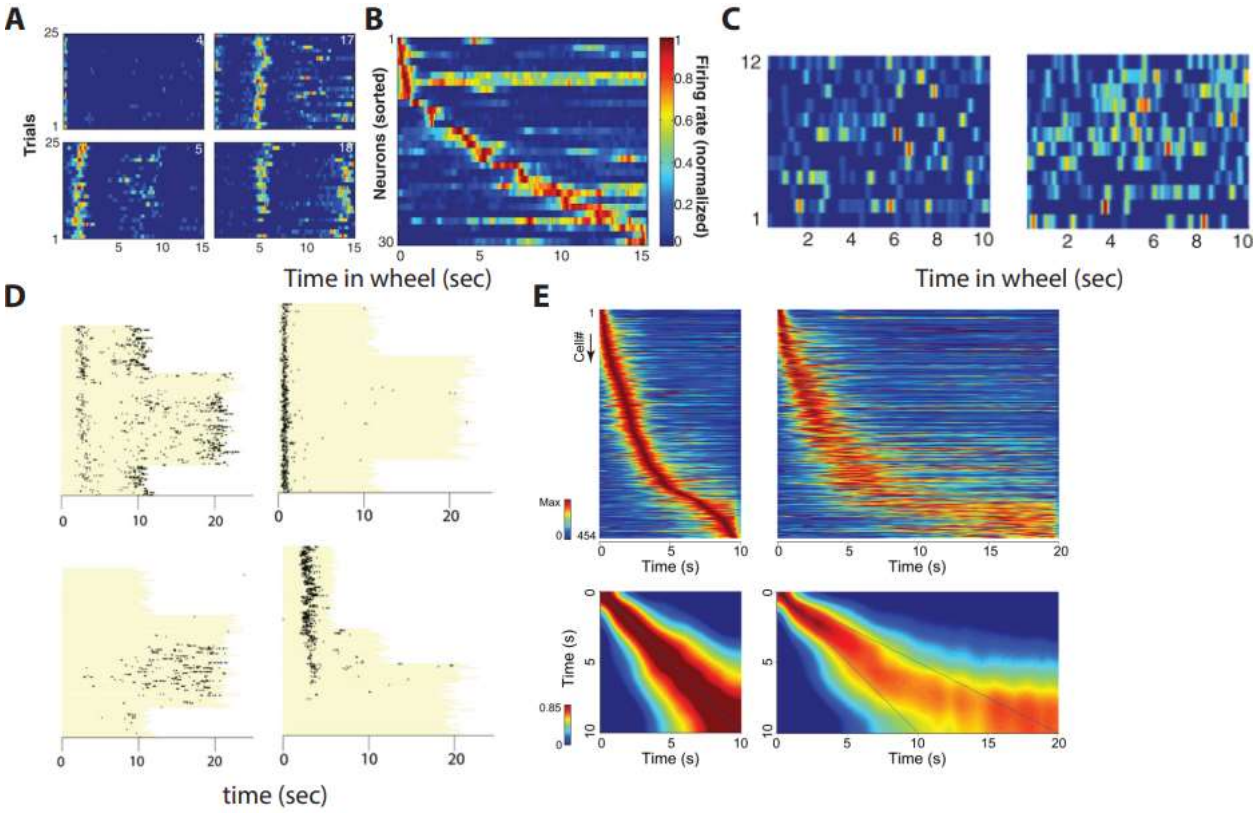

Figure 1-2. Properties of time cells

(A) Time cells fire at specific moments during the delay period similar to place cells firing at specific locations.

(B) Time cells tile up the entire delay period of a working memory task.

(C) Time cells are not observed without memory demands. When animals spontaneously ran on a running wheel inside their home cage, no time fields were observed (Pastalkova et al., 2008).

(D) Time cells remap, or 're-time', when temporal variables are changed similar to place cells changing their firing field locations when external cues are changed (MacDonald et al., 2011).

(E) Time cells may simply extend their fields instead of completely remapping when temporal variables are changed (Heys & Dombeck, 2018; Shimbo et al., 2021).

Parts **A-C** were adapted from Pastalkova et al. (2008), **D** from MacDonald et al. (2011), and **E** from Shimbo et al. (2021).

1.4. Hypothesis and specific aims

Time cells are considered to be essential to support 'when' component of episodic memory by bridging discontinuous events. However, a circuit mechanism involved in time cell generation remains elusive. To untangle the complex relationship between theta oscillations, time cell sequences, and working memory, we are going to utilize an optogenetic strategy to selectively silence the GABAergic population in the MS - a cell population necessary for the generation of theta oscillations in the hippocampus (Boyce et al., 2016). This approach will allow us to control the power of theta oscillations with similar efficiency to muscimol infusions selectively during the delay period in a delayed T-maze alternation task.

We hypothesize that theta oscillations play a crucial role in working memory task, and time cells would produce a reliable sequence to bridge temporal gaps between discontinuous events. Specifically, **we hypothesize that with optogenetic inhibition of theta oscillations, memory performance as well as time cell activities in the hippocampus will be disrupted**.

To test this hypothesis, my thesis will address the following aims:

- Our first aim is to address the efficacy and specificity of optogenetic inhibition of septal GABAergic neurons in freely moving mice. In chapter 2, we selectively inhibited GABAergic neurons in the MS only when animals were running on the treadmill during the delay period.

- Our second aim is to address the role of theta oscillations in working memory and time cells. In chapter 2, we observed how inactivation of theta impacted working memory and time cell firing.
- Our third aim is to address the electrophysiological property of time cells in mice. All electrophysiological recordings of time cells have been done only in rats. In chapter 2, we used a transgenic mouse line called VGAT::Cre, and reported time cells recorded in mice.

Chapter 2: Theta oscillations, time cells, and working memory

2.1. Materials and methods

2.1.1. Subjects

VGAT-ires-Cre male mice (the Jackson Laboratory, stock #01692) were housed individually on a 12-h light/dark cycle. Only male mice were used in this experiment, as female VGAT-ires-Cre mice were considerably smaller (**Table 2-4**) and have increased difficulty to support the weight of electrophysiology preamplifier, tether, and optic patch cord. All experiments were carried out during the light cycle, and all experiment procedures were approved by McGill University and Douglas Hospital Research Centre Animal Use and Care Committee (protocol #2015-7725) and performed following Canadian Institutes of Health Research Guidelines. The previous work has demonstrated the selectivity of this transgenic mouse line for GABAergic neurons in the MS (Boyce et al., 2016).

2.1.2. Surgeries

Prior to surgery, mice were initially anesthetized with isoflurane (5% at 1.5% oxygen) and injected subcutaneously with carprofen (0.01mg/g) and 1mL of sterile saline. Mice were maintained at 0.5%-2.5% isoflurane with 1.5% oxygen throughout the surgery. Eye lubricant and a heating pad were used to keep eyes hydrated and maintain the body temperature, respectively. All surgeries were carried out on a stereotaxic frame (David Kopf Instruments, Inc). Prior to surgeries, all surgical tools were sterilized with a glass bead sterilizer. Two surgeries were needed to prepare them for recording (viral injection surgery and optic fiber/microdrive implantation surgery).

Male mice at 8-12 weeks of age were injected with 600nL of AAV2/DJ-Ef1α-Flex-ArchT-GFP ($1.1x10^{13}$) or AAV2/DJ-Ef1α-Flex-GFP ($8.2x10^{12}$), obtained from the Neurophotonics Centre at the University of Laval. Mice received a single injection at AP: +0.82 / ML: 0.00 / DV: -4.80 with a glass pipette connected to Nanoject II injector (Drummond Scientific, Inc) at a flow rate of 23nL/s, or at AP: +0.82 / ML: -0.5 / DV: -4.8 (angled at 4.5° towards the midline) with a 28G cannula connected to a pump (Harvard Apparatus). Glass pipette or cannula was retracted after waiting for 10 minutes following the injection.

Two to four weeks following the injection surgery, an optic fiber (CF230, Thorlabs; implant site: AP: +0.82 / ML: -0.5/ DV: -3.64 at 4.5°) and a microdrive (Versa drive, Axona Ltd; implant site: AP: -1.8 / ML: +1.6) were implanted above the MS and dorsal CA1, respectively. Prior to implant surgery, tetrodes were gold-plated using the NanoZ (Neuralynx) to lower the impedance below 250kΩ at 1004Hz. Two stainless anchor screws (B000FN0J58, Antrin Online) were placed in front of the inferior cerebral vein, and the optic fiber was secured to the skull with dental cement (Patterson Dental, Inc). After dental cement was dry, two more anchor screws were placed on the contralateral hemisphere. A third craniotomy was made on top of the cerebellum to place a ground screw. After putting the microdrive and the ground screw in place, both holes were initially secured with a silicone adhesive (Kwik-Sil, World Precision Instruments) and then covered with dental cement. Once the cement was dry, tetrodes were lowered 250um below the surface of the brain.

Mice were maintained on the heating pad and monitored until they fully recovered after each surgery. For the first seven days after each surgery, mice were given a soft diet along with

carprofen gel (MediGel CPF, ~5 mg kg−1 each day) as an analgesia and a diet boost (DietGel Boost).

2.1.3. Behavioral training on the delayed alternation with treadmill T-maze task

At least seven days following the implant surgery, mice were placed on water restriction and their weight was maintained above the 85% of their *ad libitum* weight throughout the experiment. On the first day, mice were habituated to the T-maze (MazeEngineers, Inc) by allowing them to freely explore the T-maze for 30 minutes. Water droplets were placed throughout the maze except for the treadmill area to encourage explorative behavior. Mice were deemed to have passed the habituation when they voluntarily explored the entire maze within 30 minutes. Following the habituation, mice were habituated to run on the treadmill. In each treadmill habituation session, the speed of the treadmill was held constant, but the duration of treadmill run was increased from 5s to 15s in 5s increment after every 5 trials (total of 15 trials). The speed was gradually increased from 8.33cm/s to 21.67cm/s with an increment of 3.33cm/s between sessions (5 sessions in total). Following the treadmill training, mice were trained to drink from reward ports which were located at the end of each choice arm. Reward ports were loaded with 0.02mL water and mice were given two minutes to drink from the port. After two minutes, mice were manually transferred to the opposite reward port and given another two minutes to drink. Mice were deemed to have familiarized themselves with the reward ports if they drank 8 out of 10 times and two skipped trials were not from the same side.

Once mice passed all pre-trainings, they were trained to perform a delayed spatial alternation task with a delay of 10s between each alternation. During this 10s delay, mice ran on the motorized treadmill at 21.67cm/s for the entire delay period. Each session started with a 10s

of treadmill run and then a forced trial (forced to go to the left or right with the door to the opposite arm closed). The forced trial was pseudo-randomly selected. After retrieving the water reward of 0.02mL from the reward port, mice had to come back to the treadmill to initiate the second trial. From the second trial, mice were able to freely choose between the left and right arm. However, in order to receive the water reward, they had to choose the arm opposite to the arm they had previously visited. If an incorrect choice was made, mice were placed in a correction trial with the same 10s run on the motorized treadmill until they made a correct choice. Mice were considered to have learned the task if they had 80% correct with more than 30 trials (excluding the forced trial) in 30 minutes for two consecutive sessions.

2.1.4. Optogenetic inhibition of medial septal GABAergic neurons

Once mice reached the criteria, a green laser (520nm wavelength, maximum power output: 60mW, Doric Lenses) was pseudorandomly used to inhibit GABAergic neurons in the MS. In a closed-loop system, the light was turned on in 50% of trials, and triggered on and off by the treadmill start and end TTL, respectively. The estimated light power at the tip of the optic fiber was never allowed to exceed 20mW.

2.1.5. In vivo electrophysiological recordings

Both spikes and local field potential recordings were sampled and digitized at 32kHz using a Digital Lynx recording system (Neuralynx, Inc). Signals were amplified and band-pass filtered between 0.6kHz and 6KHz. Threshold was adjusted prior to each recording, ranging from (30 μV to 65 μV). Sleep recordings were used to guide tetrodes to the CA1 region of the hippocampus while mice were resting in their home cage. Both Neuralynx and Open Ephys systems were used for this purpose.

2.1.6. Analysis of theta power

The power spectrum for local field potentials was obtained using multitaper method included in the Chronux toolbox (*mtspectrumc* with NW = 3 and K = 5; (Mitra & Bokil, 2008). Theta power was calculated by taking the area within 1Hz of the maximum power in the theta range (6-10Hz). Baseline theta power was obtained by taking the average of theta power during laser-off trials, and mean reduction in theta power for each session was obtained by dividing each laser-on trial with baseline theta power and averaging across laser-on trials. For each channel, the theta-delta ratio was obtained by taking the ratio between mean theta power (6-10Hz) and mean delta power (2-4Hz) during laser-off segments. A channel with the highest theta-delta ratio was used in the LFP analysis.

Instantaneous theta power was estimated with the MATLAB built-in function *cwt* using the Morlet wavelet. This was used to calculate the reduction in theta power as a function of time and location. For time, mean reduction in theta power before, during, and after the treadmill run was compared as described above. For location, T-maze was linearized, and x-y coordinates, which are sampled at 30Hz, were linearly interpolated to match the LFP sampling rate (500Hz). After binning theta power, mean reduction in theta power was calculated in the same way as described above. Time points falling into the cone of influence were excluded from these analyses.

2.1.7. Identification of time cells

Spike times on the treadmill were first referenced to the beginning of each treadmill run. Spike times were binned into 200ms bins, and convolved with a Gaussian kernel (S.D. = 400ms). The smoothed spike trains were used throughout the analysis unless specified. Time information I was derived for individual neurons as previously described (Skaggs et al., 1992).

$$I = \sum_{t=1}^{T} t \frac{f_t}{f} log_2 \frac{f_t}{f},$$

To assess the stability of the representations of neurons across trials, a reliability score was obtained by constructing the mean firing rate vectors out of even and odd trials, and by computing the Pearson correlation coefficient between the two vectors. Neurons need to express time information and split-half reliability higher than the 95th percentile of their shuffled distribution. To ensure that cells are active on the treadmill, peak firing rate and mean firing rate had to be greater than 2Hz and 0.5Hz, respectively. Any cells with overall mean firing rate of equal to or greater than 5Hz were excluded from the analysis. Cells had to pass these criteria in either left-going or right-going off/on trials to be identified as a time cell.

2.1.8. Split-half reliability of sequences and single units

For single units, a random set of trials was selected from laser-off and laser-on trials, and Pearson correlation coefficient was calculated using resulting mean firing vectors. For the same laser condition comparison (off vs. off, on vs. on), the second set of trials was randomly selected from left-out trials. This was repeated 5000 times, and the mean of each null distribution was obtained. For sequences, a random set of trials was selected following the same procedure as described above, but was done separately for left off/on and right off/on trials. Pearson correlation coefficient was calculated using concatenated mean firing vectors. For all analyses, a number of trials used to calculate mean firing rate vectors was matched.

2.1.9. Visualization of neural trajectories

For visualization purposes only, principal component analysis was performed as previously described (Cunningham & Yu, 2014) to reduce the dimensionality of smoothed spike trains (bin size = 200ms, S.D. = 1s). First three components were extracted, and PCA scores were plotted in

a 3D state space. Only those sessions with at least six trials in all four conditions (left-going off/on, right-going off/on) were included in this visualization.

2.1.10. Maximum likelihood estimation of delay time

A naive Bayesian classifier (K. Zhang et al., 1998) was implemented to decode time of the treadmill delay period. This classifier was originally intended for place cells and for decoding spatial locations. Accordingly, the prior probability distribution could be constructed out of the spatial occupancy map. However, given that time is constant, this prior probability becomes uniform in our application, and the resulting approach is equivalent to *maximum likelihood estimation*. That is, the log-likelihood is maximized with respect to delay time:

$$\max_t l(t|n) \propto \sum_{i=1}^{N} n_i \log(f_i(t)) - \delta t \sum_{i=1}^{N} f_i(t).$$

Here, for N neurons, the mean number of spikes fired by neuron i at delay time t is given by $f_i(t)$, and the delay time is decoded on the population spike vector n_i. Spike trains were binned using a window size of $\delta t = 200$ms as with before and smoothed using a σ = 1s Gaussian kernel. Firing rates of zero (which normally leads to the undesirable condition of $log\ (0) = -\infty$) were replaced by a constant penalty term of 2^{-52} (eps in MATLAB). Due to the small number of simultaneously recorded time cells within a typical recording session, we pooled together neurons from all recordings that had at least 6 trials in each of four combinations of laser and behavioral choice conditions. An *m-out-of-n bootstrap* method (Bickel & Sakov, 2008) was subsequently used to estimate an empirical distribution of decoding accuracy, where $m = 50$ neurons were sampled from the n total recorded neurons with replacement. This alternative *bootstrap* approach permits the number of neurons to be matched between the ArchT and the YFP groups to control

for bias in sample sizes. The decoding accuracy was measured by *leave-one-out* cross-validation for each bootstrap sample by holding out single trials.

2.1.11. Gini impurity index and decoding of behavioral choice

A custom classifier based on the *Gini impurity index* was used to decode animals' choice (left or right trials) subsequent to the delay period, and hence to serve as a proxy measure of a neuron's trajectory-dependency. This index is related to the measure of *entropy* in information theory and is frequently used for building *decision tree classifiers* (Yang, 2010). Intuitively, if a neuron's firing rate can be used to predict subsequent behavioral choice, then a certain threshold can be set so that trials in which the firing rate falls below the threshold are confined to one side of the maze, while the complement set of trials falls under the other side (**Supplementary Figure 2-6**). In other words, by ordering the trials based on the neuron's firing rate and splitting the trials by some appropriate threshold, a neuron that differentiates between left and right trials will have mostly left-going trials over one side of the threshold, while the other side will be predominantly right-going trials (**Supplementary Figure 2-6**). The Gini index helps in establishing this threshold by quantify the "impurity" of a dataset:

$$g = 1 - P(L)^2 - P(R)^2 = 2\,P(L)\,P(R),$$

where $P(L)$ and $P(R)$ are the fractions of left-going and right-going trials respectively. The resulting measure ranges between 0 and 0.5, with 0 signifying that the data contains only one trial label (e.g., only left-going trials) and 0.5 defining an equally proportioned mixture.

First, a baseline Gini index g_0 is computed from all trials in a given session. Then, the trials are sorted based on the firing rate of a neuron $f_k(t)$ on each trial k at each time bin t, such that

$f_k(t) \leq f_{k+1}(t)$ for all $k \in \{1,2,\ldots,K-1\}$ over a total of K trials. The time series were smooth with a $\sigma = 200$ms Gaussian kernel to compensate for potential jitters in time fields. The trials can then be split into two subsets of trials at any of the $K-1$ locations, in which case we can define the firing rate threshold $\theta_k(t) = \frac{f_{k+1}(t) - f_k(t)}{2} + f_k(t)$ as the midway point between the two firing rates on those trials. After splitting the trials into two subsets (i.e., the upper and lower subsets), we compute the Gini impurity for each of them:

$$g_U(t,k) = 2\,P(L \mid f(t) \leq \theta_k(t))\,P(R \mid f(t) \leq \theta_k(t)) \text{ and}$$

$$g_L(t,k) = 2\,P(L \mid f(t) > \theta_k(t))\,P(R \mid f(t) > \theta_k(t)).$$

Finally, the Gini gain (i.e., the gain in purity) is calculated as the difference in impurity before and after splitting the trials, weighed by the size of the trial subsets:

$$g_{gain}(t,k) = g_0 - \frac{k}{K} g_U(t,k) - \frac{K-k}{K} g_L(t,k).$$

Effectively, a high Gini gain signifies that by placing the trials into two categories based on whether the neuron's firing rate is lesser or greater than a threshold, left- and right-going trials can be accurately dissociated. Therefore, by maximizing Gini gain with respect to t and k, we estimate the time bin during the treadmill delay period and the firing rate threshold that gives the maximal accuracy in classifying behavioral choice. The decoding accuracy was assessed by a *leave-one-out* cross-validation approach.

2.1.12. Identification of trajectory-dependent time cells

Trajectory-dependent time cells were identified following the procedure described previously (Kinsky et al., 2020). In short, the actual difference between mean firing rates of left-

going and right-going trials was compared to the difference obtained by shuffling trial identity. The actual difference had to exceed the shuffled difference for 2850 out of 3000 times (95%). In order to avoid spurious detection of trajectory-dependent cells, cells had to have at least 3 consecutive bins that are significantly different, and at least 3 spikes in 40% of either left-going or right-going trials. Raw spike trains were used to ensure that these criteria are not simply met by smoothing. The identification was done separately for laser-off and on conditions.

2.1.13. Histology

After mice were anesthetized deeply with isoflurane (5%), they were intracardially perfused with 1 x PBS and 4% paraformaldehyde. Brains were retrieved after animal heads were left in 4% paraformaldehyde for at least 48 hours. Subsequently, brains were kept in a 30% sucrose solution until they sank to the bottom. Following these procedures, brains were kept in a -80ºC freezer. Coronal sections were sliced using a cryostat at 20µm or 40µm. Both hippocampal and MS sections were mounted using a fluorescent DAPI labeling medium (Southern Biotechnology), and were imaged using a slide scanner (Olympus, VS120) or Zeiss Axio Observer to confirm tetrode tracks, optic fiber location, and viral vector expression. For YFP controls only, GFP amplification immunohistochemistry was performed. Sections were initially washed 3 x 5 minutes in 1 x PBS, and blocked 3 x 15 minutes in PGT solution (0.45% gelatin and 0.25% triton in 1 x PBS) under gentle agitation. Then, they were incubated in anti-GFP primary antibody (1:1000 dilution in PGT, anti-GFP rabbit (IgG), ThermoFisher, A-11122) overnight at 4°C (up to 24 hours). On the following day, they were washed 3 x 15 minutes in PGT solution and further incubated in Alexa Fluor-488 secondary antibody (1:1000 dilution in PGT, anti-rabbit goat Alexa Fluor-488 (IgG), ThermoFisher, A-21206) for 3 hours. They were washed 3 x 5 minutes in 1 x PBS, and

mounted as described above. Histological data from mice #5653 (ArchT) and #7415 (YFP) could not be recovered due to misplacing their brains during storage, however in both cases the neurophysiology and response to laser were qualitatively similar to their respective groups and were included in the analysis.

2.1.14. Statistical analysis

All statistical evaluations were performed under MATLAB and GNU R. Non-parametric Wilcoxon signed rank tests, Wilcoxon rank sum tests, Kolmogorov-Smirnov tests, and Kruskal-Wallis one-way ANOVAs were used throughout the paper. P-values reported from all *post hoc* tests were Bonferroni-adjusted for multiple comparisons. Robust statistics were performed using the 'WRS' package (Wilcox, 2012). Robust two-way mixed bootstrapped ANOVA was used to compare choice decoding accuracy across training-testing conditions between trajectory-dependent and trajectory-independent cells. Multiple paired bootstrap tests for equal mean was utilized to compare accuracy of time decoding between training-testing conditions. Statistical tests used for each figure were described in the corresponding figure panel. Box and whiskers represent IQR and 1.5 x IQR, respectively. SEM and 95% confidence interval were used throughout, and stated in each figure panel. Correlations were calculated using Pearson's correlation coefficient.

2.2. Results

2.2.1. Theta oscillations are significantly reduced with temporal and spatial specificity

To investigate the contribution of theta oscillations to time cells and memory performance, we applied an optogenetic approach to specifically inhibit GABAergic neurons in the MS. First, the viral vector AAV2/DJ-Ef1α-Flex-ArchT-GFP was injected into the MS of

VGAT::Cre mice to induce Cre-mediated expression of Archaerhodopsin (Han et al., 2011) in GABAergic neurons ($n_{ArchT} = 14$, $n_{YFP} = 7$). The expression was largely confined to the MS and the diagonal band of Broca (**Figure 2-1B and Supplementary Figure 2-1**). Next, microdrives with independently moveable tetrodes were implanted above and lowered into dorsal CA1 of the hippocampus (**Figure 2-1B and Supplementary Figure 2-1**). Mice were then trained in a delayed spatial alternation T-maze task to alternate between the left and the right arm and to run on a motorized treadmill (constant speed of 21.67cm/s) in the delay zone for 10 seconds between each alternation (**Figure 2-1A**). After passing a task performance criterion (80% correct for two consecutive days), the MS was inhibited on a random subset of 50% of trials during the delay period when mice ran on the treadmill. Single units and local field potential (LFP) recordings were simultaneously acquired from the pyramidal cell layer of dorsal CA1.

Hippocampal theta oscillations were substantially reduced when the laser was on in the ArchT group, but not in YFP controls (**Figure 2-1C**), consistent with a previous report during REM sleep (Boyce et al., 2016). Compared to laser-off trials, laser-on trials in the ArchT group had a 73±1.7% (SEM) reduction in theta power while YFP controls were unaffected (**Figure 2-1F**). To further investigate if the disruption was temporally and spatially specific to the delay period, the instantaneous theta power was obtained by continuous wavelet transform. To evaluate the temporal specificity of this effect, theta power was compared between laser-off and on trials before, during, and after the delay period (**Figure 2-1D**). Theta power in the ArchT group was reduced when the laser was turned on, and remained disrupted throughout the delay period before returning to baseline after the laser was turned off. On average, it took 202.26±5.81ms (SEM) to have theta power reduced to 50% of its baseline value. To interrogate if a similar level of specificity could be observed as a function of location, we obtained the occupancy-normalized

theta power for individual bins, and compared between laser-off and on trials, separately for left-going/returning and right-going/returning trials (**Figure 2-1E**). Theta power was disrupted only when the ArchT group was running on the treadmill, but not when they were on the treadmill without running (i.e., waiting for the next trial to start or waiting for the door to open after the delay) or outside of the treadmill area. These results demonstrate that our approach allowed for strong control of the power of theta oscillations with high spatial and temporal precision while animals were performing the task.

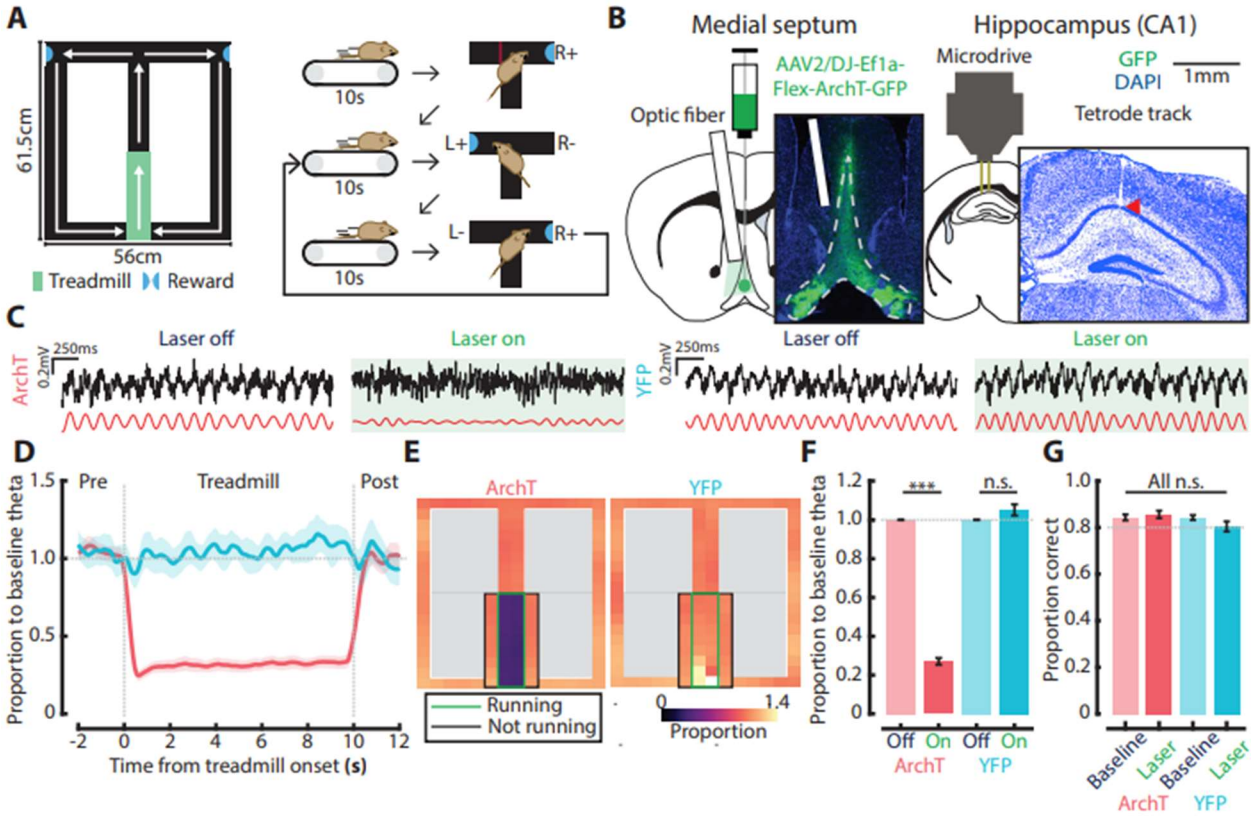

Figure 2-1. Theta oscillations (6-10Hz) are significantly reduced with temporal and spatial specificity during the delay period.

(A) Schematic of the T-maze and overview of the delayed spatial alternation task. Mice were trained to alternate between the left and right arm of the maze while running on the treadmill (green) for 10 seconds between each alternation. Mice were rewarded with 0.02mL of water for a correct choice (+).

(B) Histology of the MS showing virus expression (green), optic fiber location (white bar), and tetrode track tip in dorsal CA1 (red arrow).

(C) Examples of raw (black) and filtered (red) LFP traces during laser-off and on trials in ArchT and YFP animals.

(D) Proportion to baseline theta as a function of time. 2 seconds before and after the treadmill run are shown. Shaded area indicates the 95% confidence interval. Traces were smoothed over a 500ms window with a moving average.

(E) Ratio between laser-on-theta and laser-off-theta as a function of location. Black square indicates the treadmill area while green square shows the proportion to baseline theta during the delay period. Left-going/returning, right-going/returning, and treadmill running periods were smoothed separately (S.D. = 2 bins) for visualization.

(F) Proportion of laser-on-theta was significantly reduced compared to baseline theta in the ArchT group, but not in YFP controls. (Wilcoxon signed-rank test, ArchT: 0.269 (SEM: ± 0.017), $p = 1.11 \times 10^{-9}$ / YFP: 1.04 (SEM: ± 0.023), $p = 0.16$).

(G) Behavioral performance between baseline and sessions with laser was not impaired in the ArchT group and YFP controls. (Wilcoxon signed-rank test, ArchT: baseline = 0.84 (SEM: ± 0.013), laser = 0.86 (SEM: ± 0.016), p = 0.46 / YFP: baseline = 0.84 (SEM: ± 0.011), laser = 0.80 (SEM: ± 0.022), p = 0.30). For all panels, n.s = non-significant, ***P < 0.001.

2.2.2. Intact behavioral performance despite partial remapping of time cells during optogenetic theta reduction

Having established that the reduction in theta oscillations was substantial and confined to the delay period, we investigated if animals' memory performance was disrupted. Surprisingly, we did not observe any impairments in behavioral performance on the T-maze task (**Figure 2-1F**). This was the case even when the performance level was calculated separately for laser-off and on trials (**Supplementary Figure 2-2B**). Moreover, behavioral performance was not correlated with the level of reduction in theta oscillations (**Supplementary Figure 2-2A**).

We subsequently investigated whether temporal tuning of hippocampal CA1 neurons was affected by optogenetic manipulation. All analyses were carried out only using correct trials unless otherwise specified to ensure that provenance and destination are the same for each choice following the treadmill run. First, isolated single units were classified as a time cell when they passed the following criteria: (1) significant time information (bits/spike, (Skaggs et al., 1992)), (2) split-half reliability greater than the 95th percentile of a shuffled distribution, (3) peak firing rate greater than 2Hz, and (4) overall mean firing rate less than 5Hz (to eliminate interneurons). The proportion of time cells identified within each laser condition was similar between the ArchT group and YFP controls (Pearson's χ^2 test of independence, ArchT off: 193 (38.8%), YFP

off: 74 (31.4%), χ^2 = 3.79, p = 0.10, ArchT on: 186 (37.4%), YFP on: 70 (29.7%), χ^2 = 4.17, p = 0.082, corrected for multiple comparisons with Bonferroni).

Consistent with previous reports (Heys & Dombeck, 2018; Kraus et al., 2013, 2015; MacDonald et al., 2011, 2013; MacDonald & Tonegawa, 2021; Pastalkova et al., 2008; N. T. M. Robinson et al., 2017; Salz et al., 2016; Shimbo et al., 2021; Taxidis et al., 2020; Y. Wang et al., 2015), time cells had firing fields at specific moments in time that collectively spanned the entire delay period (**Figures 2-2A and B**). In response to optogenetic manipulation, partial remapping or 're-timing' of time cells was consistently observed. The stability of the rate map between laser-off and on trials was significantly reduced in the ArchT group compared to YFP controls (**Figure 2-2C**). Unlike behavioral performance, the magnitude of time cell remapping was significantly correlated with the magnitude of theta reduction (**Supplementary Figure 2-2C**). Furthermore, the time cell sequence for the ArchT group decorrelated faster over the course of the delay than YFP controls (**Figure 2-2D**). As another proxy measure of remapping, we compared the temporal peak firing location between laser-off and on trials. The conditional probability of the ArchT group had more dispersion from the diagonal compared to YFP controls, suggesting that time representations remapped between laser conditions (**Figure 2-2E**).

Remapping of time cells was accompanied by significant changes in firing rates and time information when these properties were compared within cells between laser conditions (**Figures 2-2F to H**). However, no differences were observed across laser conditions when the shape of population distribution was compared (CDF plots in **Figures 2-2F to H**). These observations suggest that a new, partially remapped sequence emerges during laser-on trials. This indeed was the case when we sorted the sequence again by peak firing locations during laser-on trials

(**Figure 2-2B**). Moreover, the proportion of time cells that were exclusively identified as a time cell in either laser-off or on trials was significantly higher in the ArchT group compared to YFP controls (Pearson's χ^2 test of independence, ArchT: 105/498 (21.1%), YFP: 26/236 (11.0%), $\chi^2 = 11.07$, $p = 8.78 \times 10^{-4}$). However, we did not observe a difference in the proportion of time cells in both laser-off and on trials (Pearson's χ^2 test of independence, ArchT: 137/498 (27.5%), YFP: 59/236 (25.0%), $\chi^2 = 0.52$, $p = 0.47$). Together, these results suggest that time cells remap when theta oscillations are disrupted, and a new sequence emerges to possibly support working memory.

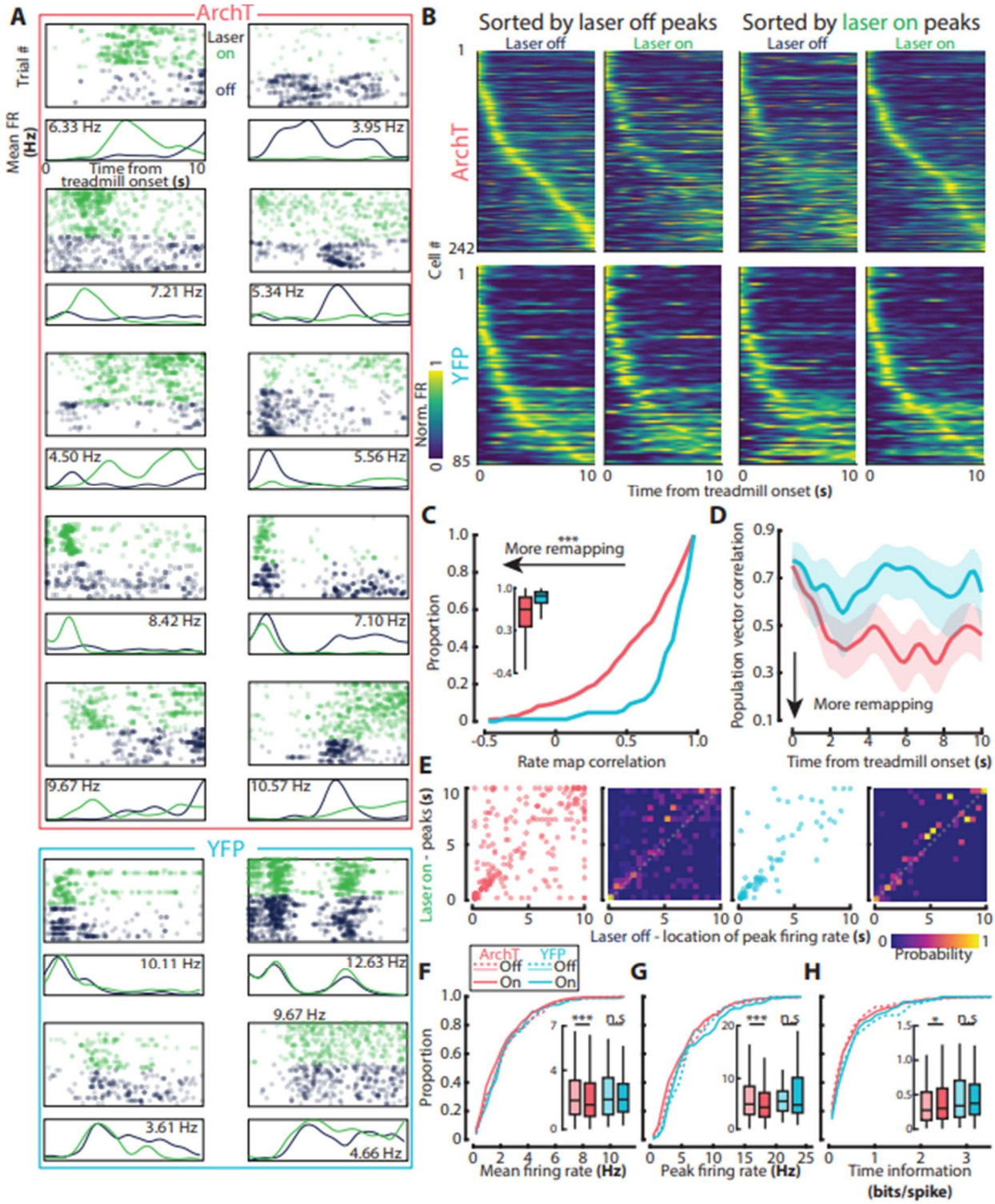
A
ArchT
Trial #
Laser
on
off
Mean FR (Hz)
6.33 Hz
3.95 Hz
0
Time from treadmill onset (s)
10
7.21 Hz
5.34 Hz
4.50 Hz
5.56 Hz
8.42 Hz
7.10 Hz
9.67 Hz
10.57 Hz
YFP
10.11 Hz
12.63 Hz
9.67 Hz
3.61 Hz
4.66 Hz
B
Sorted by laser off peaks
Sorted by laser on peaks
Laser off
Laser on
Laser off
Laser on
ArchT
Cell #
1
242
YFP
1
85
Norm. FR
0
1
0
10
Time from treadmill onset (s)
C
***
More remapping
Proportion
1.0
0.8
0.6
0.4
0.2
0
1.0
0.3
-0.4
-0.5
0
0.5
1.0
Rate map correlation
D
Population vector correlation
0.9
0.7
0.5
0.3
0.1
More remapping
0
2
4
6
8
10
Time from treadmill onset (s)
E
Laser on - peaks (s)
10
5
0
Laser off - location of peak firing rate (s)
Probability
0
1
F
G
H
ArchT
YFP
Off
On
Off
On
Proportion
***
n.s
*
7
4
0
20
10
1.5
1.0
0.5
0
0
2
4
6
8
10
Mean firing rate (Hz)
0
5
10
15
20
25
Peak firing rate (Hz)
0
1
2
3
Time information
(bits/spike)

Figure 2-2. Time cells partially remap when theta oscillations are significantly reduced.

(A) Individual time cell examples showing the effect of optogenetic inhibition of septal GABAergic neurons in ArchT (red box) and YFP (blue box) groups. Rasters for spike times, which are referenced to the beginning of each treadmill run, are shown with mean firing rate curves (laser-off: navy, laser-on: green). The firing rate shown in the box indicates the peak firing rate.

(B) Sequence of time cells sorted by either their laser-off or on peaks.

(C) Temporal rate map correlation coefficient for time cells between laser-off and laser-on conditions was reduced in the ArchT group (Wilcoxon rank-sum test, $p = 4.36 \times 10^{-10}$).

(D) Population vector correlation coefficient of time cells (column-wise correlation in (B)) between laser-off and laser-on conditions over successive 200ms time bins (ArchT: red, YFP: blue). Two-sided confidence intervals were estimated using the procedure described in (Bonett & Wright, 2000).

(E) Peak firing rate location during laser-on condition vs. peak firing rate location during laser-off condition (left) with conditional probability matrix (right). Peak firing rate location was more dispersed in the ArchT group compared to YFP controls, which has their peaks mostly concentrated along the diagonal in both conditions.

(F) Mean firing rate of individual time cells between laser-off (dashed/shaded) and on (solid) conditions. In the ArchT group, there was a significant reduction in mean firing rate with the laser (Wilcoxon pairwise signed-rank test, $p = 7.48 \times 10^{-7}$), but not in YFP controls ($p = 0.54$).

(G) Peak firing rate of individual time cells. Similar to mean firing rate, there was a significant reduction in the ArchT group with the laser (Wilcoxon pairwise signed-rank test, ArchT: $p = 3.39 \times 10^{-4}$, YFP: 0.33).

(H) Time information of individual time cells. Significant increase in the ArchT group was observed (Wilcoxon pairwise signed-rank test, ArchT: $p = 0.02$, YFP: $p = 0.88$). Although there was a significant change in these time cell metrics, the overall shape of population distribution remained the same between laser-off and on conditions (two-sample Kolmogorov-Smirnov test, $p > 0.05$). For all panels, n.s = non-significant, *$P < 0.05$, ***$P < 0.001$.

2.2.3. Temporal encoding is preserved by the emergence of a partially remapped sequence

To confirm that a partially remapped sequence emerges with reduced theta oscillations, we first investigated the split-half reliability between laser-off and on trials. This was done by randomly selecting a matched number of trials from laser-off and laser-on trials and calculating the Pearson correlation between resulting mean firing vectors. In line with our hypothesis, the split-half reliability between laser-off and laser-on trials in the ArchT group was significantly lower than other conditions (**Figure 2-3A**). Moreover, the split-half reliability between off-off and on-on trials did not significantly differ from each other, further suggesting that two representations reliably flip back and forth depending on the power of theta oscillations available for a given trial. Importantly, these changes were not observed in YFP controls (**Figure 2-3A**).

Next, we visualized if a sequence in each trial was reliable within the same laser condition, but different between laser conditions. When visualizing the trial-by-trial sequence for the ArchT group, we observed a checkered pattern, suggestive of a reliable sequence representation within the same laser condition and decorrelated sequence representations

between laser conditions (**Figure 2-3B and Supplementary Figure 2-3B**). This pattern was observed regardless of the minimum number of trials needed to be included in the analysis (**Supplementary Figure 2-3C**). Indeed, Principal Component Analysis (PCA) shows that neural trajectories take markedly different paths depending on the laser condition (**Figure 2-3C**), but this effect was not observed in YFP controls (**Supplementary Figure 2-3**).

To further confirm that a partially remapped sequence emerges between laser conditions, we utilized a maximum likelihood estimator to decode time of treadmill delay based on the population activity. In the ArchT group, the absolute decoding errors were comparable between laser-off and on conditions with a mean of ~0.5s (where the theoretical chance level would be 3.33s) (**Figures 2-3D to F**). However, when the estimator, trained on the neural activities during laser-off trials, was used to decode laser-on trials (or *vice versa*), the absolute error increased substantially. In contrast, the levels of decoding error were maintained across training-testing conditions for YFP controls (**Figure 2-3F and Supplementary Figure 2-4A**). These results were consistent regardless of the number of cells and the minimum number of trials that were included in the training of the decoder (**Supplementary Figures 2-4B and C**). These outcomes further outline the view that an altered, albeit similarly accurate, time sequence emerges with the reduction of theta oscillations.

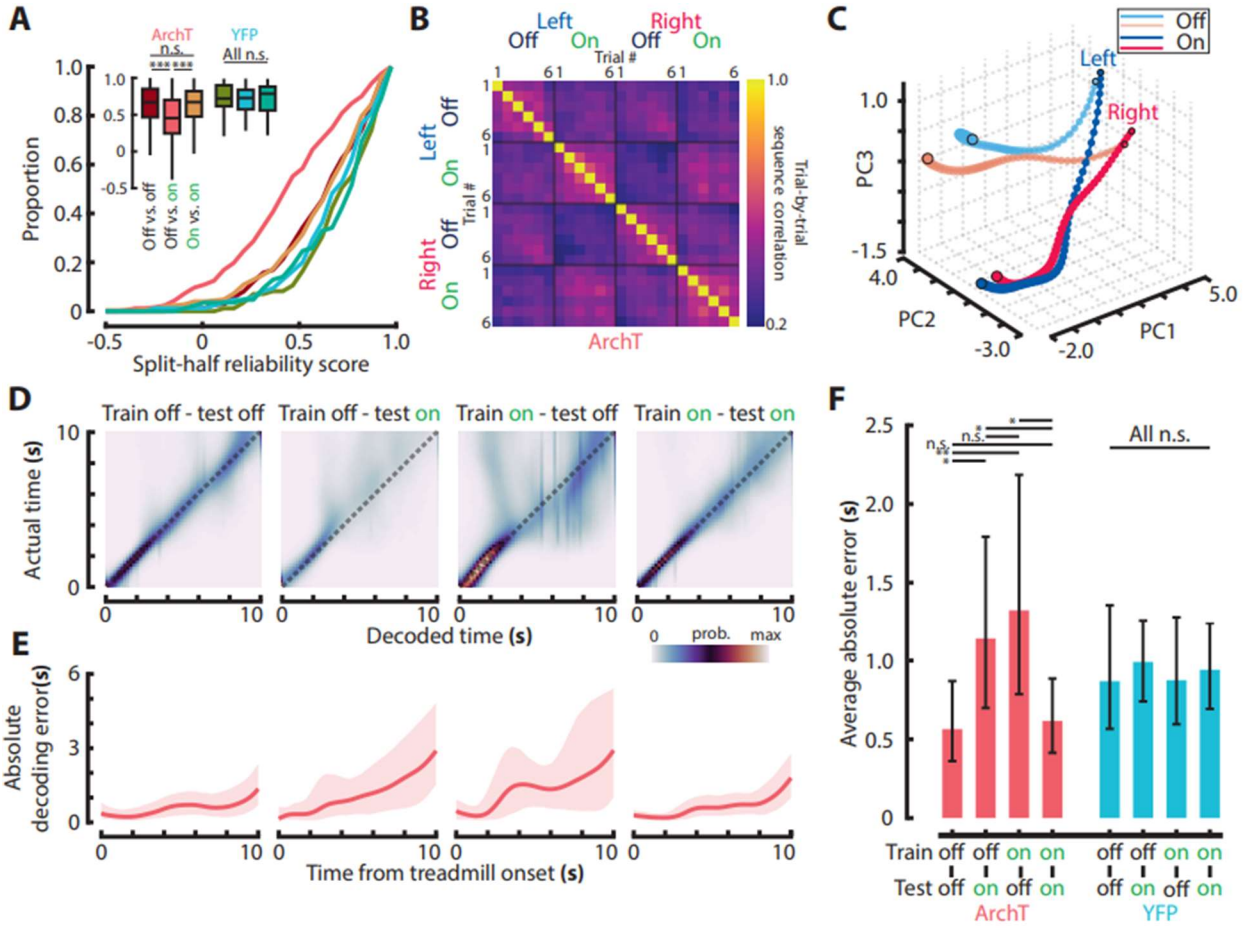

Figure 2-3. Temporal encoding is preserved during septal inactivation by the emergence of a partially distinct time code.

(A) Split-half reliability for spike trains in the same condition (off-off, on-on), or across conditions (off-on). We randomly selected a matched number of trials from each condition and calculated the split-half reliability between resulting mean firing rate vectors. This was repeated 5000 times, and the mean of each null distribution was obtained. (Kruskal-Wallis test followed by post hoc tests, corrected for multiple comparisons with Bonferroni, ArchT: $F(2, 723) = 55.11$, $p = 3.10 \times 10^{-12}$, off-off vs. on-on: $p = 0.99$, off-off vs. off-on: $p = 3.48 \times 10^{-10}$, on-on vs. off-on: $p = 4.39 \times 10^{-10}$,

YFP: $F(2, 252) = 1.38$, $p = 0.50$). Reduced split-half reliability in off-on condition suggests the emergence of remapped time code when theta oscillations are significantly reduced.

(B) Trial-by-trial sequence similarity correlation matrix. Each pixel represents a correlation of sequences between a pair of trials. Note the checkerboard pattern, indicating remapping between laser-off and on conditions. Only those time cells with at least 6 trials in all four conditions were included in this and all subsequent analyses in this figure (ArchT = 178/242, YFP = 69/85).

(C) 3D projection of neural trajectories in all four conditions (red = left, blue = right, graded color = laser-off, solid color = laser-on). The dot size indicates the time from the treadmill onset with larger ones indicating later in time. Black circles mark the beginning and end of the treadmill run. Axes are three first principal components with arbitrary units. This was plotted for visualization purposes only.

(D) Confusion matrices of maximum likelihood decoding of time (see methods above).

(E) Absolute decoding error at each time bin across training conditions. Shaded area is 95% confidence interval.

(F) Average absolute decoding error across training conditions in ArchT (red) and YFP (blue). Mean and 95% confidence interval for each training-testing condition are shown. Multiple paired bootstrap sample tests for equal mean absolute error were used to test the significance across different training conditions within ArchT and YFP groups. P-values were Bonferroni-corrected for multiple comparisons. Refer to Table 2-2 for p-values. For all panels, n.s = non-significant, $*P < 0.05$, $**P < 0.01$, $***P < 0.001$.

2.2.4. Trajectory-dependent time cells were resilient to optogenetic theta reduction

Given that behavioral performance was not disrupted following significant theta reduction and partial remapping between laser conditions, we hypothesized that trajectory-dependent time cells, signaling the past or future trajectories (Ferbinteanu & Shapiro, 2003; Frank et al., 2000; Kinsky et al., 2020; Pastalkova et al., 2008; Wood et al., 2000) of animals, would remain stable despite this perturbation. We reasoned that this subset of time cells may be sufficient to guide behavior when other time cells remap during reduced theta oscillations. Time cells were identified to be significantly modulated by the trajectory when the difference in mean firing rate between left-going and right-going trials was greater than the 95th percentile of a shuffled distribution (Kinsky et al., 2020). This resulted in 46 and 12 trajectory-dependent neurons in the ArchT group and YFP controls, respectively. The proportion of trajectory-dependent neurons did not differ between the ArchT group (19%) and YFP controls (14%) (Pearson's χ^2 test of independence, $\chi^2 = 1.03$, $p = 0.31$) (**Figure 2-4A**).

Trajectory-dependent time cells showed greater rate map stability compared to trajectory-independent time cells (**Figure 2-4B)**. Similar to a previous report (Pastalkova et al., 2008), we observed that trajectory-dependent time cells were highly concentrated towards the beginning of the treadmill run (**Figures 2-4C, D**). Indeed, according to our neural trajectory visualization and time decoding analysis (**Figure 2-3C to E**), decoding error at the beginning was lower compared to later portions of the delay. Thus, we separated time cells by their peak firing location during laser-off trials and compared the rate map correlation between trajectory-dependent time cells and trajectory-independent time cells. This revealed that trajectory-dependent time cells were more stable than trajectory-independent time cells during the first 2 seconds on the treadmill,

while the stability of trajectory-dependent and trajectory-independent cell groups did not differ in the remainder of the treadmill delay period (**Figure 2-4E**).

To further corroborate these findings, we designed a decoder to predict the animals' subsequent choice based on spiking activities during the delay period (see Methods). The decoder was first trained to discriminate between left-going and right-going trials during laser-off and on trials separately, and prediction accuracy was obtained by leave-one-out cross-validation. Under both conditions, cells that expressed high decoding accuracy during laser-off trials maintained their accuracy during laser-on trials (**Figure 2-4F**). To examine if the decoding accuracy was stable across laser conditions, we trained the decoder on laser-off trials and tested the accuracy for decoding laser-on trials, and vice versa. Across train-test conditions, trajectory-dependent time cells had higher decoding accuracy compared to trajectory-independent time cells, while the same level of accuracy was maintained across train-test conditions (**Figure 2-4G**). These results suggest that a small population of cells that are more relevant to behavioral performance maintain stable time representation despite strong theta reduction, which could be sufficient to support working memory.

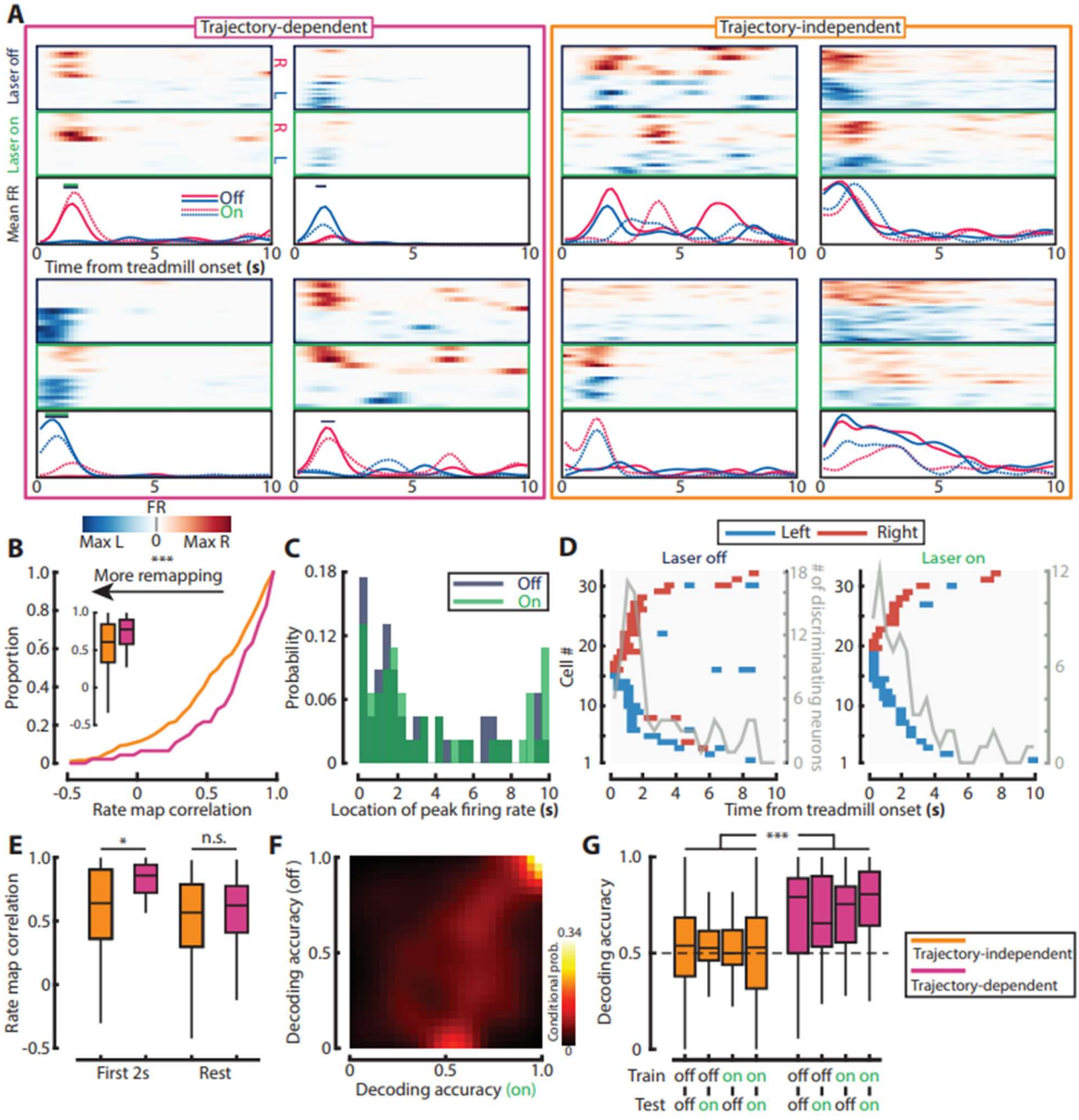

Figure 2-4. Trajectory-dependent time cells maintain more stable representations than trajectory-independent time cells.

(A) Examples of trajectory-dependent (pink box) and trajectory-independent cells (orange box). Trial-by-trial firing rate is shown as a function of time, sorted by their choice following a treadmill

run (left: blue, right: red) and the laser condition (off: blue box, on: green box). Mean firing rate is shown at the bottom for each condition (off: solid, on: dashed, same color scheme as described above). Solid horizontal line on top of the mean firing rate curve indicates significantly discriminating fields (off: blue, on: green)

(B) Temporal rate map correlation coefficient, comparing trajectory-dependent and trajectory-independent cells. (Wilcoxon rank-sum test, ArchT: $p = 0.006$, YFP: $p = 0.79$).

(C) Location of peak firing rate during laser-off (dark blue) and on (green) trials for trajectory-dependent cells.

(D) Location of significantly discriminating fields for each trajectory-dependent cells during laser-off and on. Color scheme is the same as individual examples. The y-axis on the right indicates the number of trajectory-dependent cells that have a significantly discriminating field for a given time period. Note that location of peak firing rate and significantly discriminating fields are largely within the first 2 seconds of the delay period.

(E) Temporal rate map correlation, comparing trajectory-dependent (pink) and trajectory-independent cells (orange) with their peak firing rate within the first 2 seconds or after. (Wilcoxon rank-sum test, first 2 seconds: ArchT: $p = 0.015$, YFP: $p = 0.43$, after 2 seconds: ArchT: $p = 0.52$, YFP: $p = 0.97$).

(F) Conditional probability matrix showing the accuracy of a decoder built to predict the animals' subsequent choice (left or right) based on firing patterns during the delay period. Note the diagonal in the upper right part of the matrix, indicating the consistent accuracy across laser-off and on conditions.

(G) Decoding accuracy of choice (left or right) for trajectory-dependent and trajectory-independent cells (Robust 2-way mixed bootstrapped ANOVA with 20% trimmed means, number of bootstrap: 5000, only main effect of cell identity (trajectory-dependent vs. trajectory-independent) was significant ($p < 1.00 \times 10^{-4}$). Refer to Table 2-3 for ANOVA table, and Supplementary Figure 2-5/ Table 2-3 for data from YFP controls. For all panels, n.s = non-significant, *P < 0.05, ***P < 0.001.

2.3. Supplementary materials

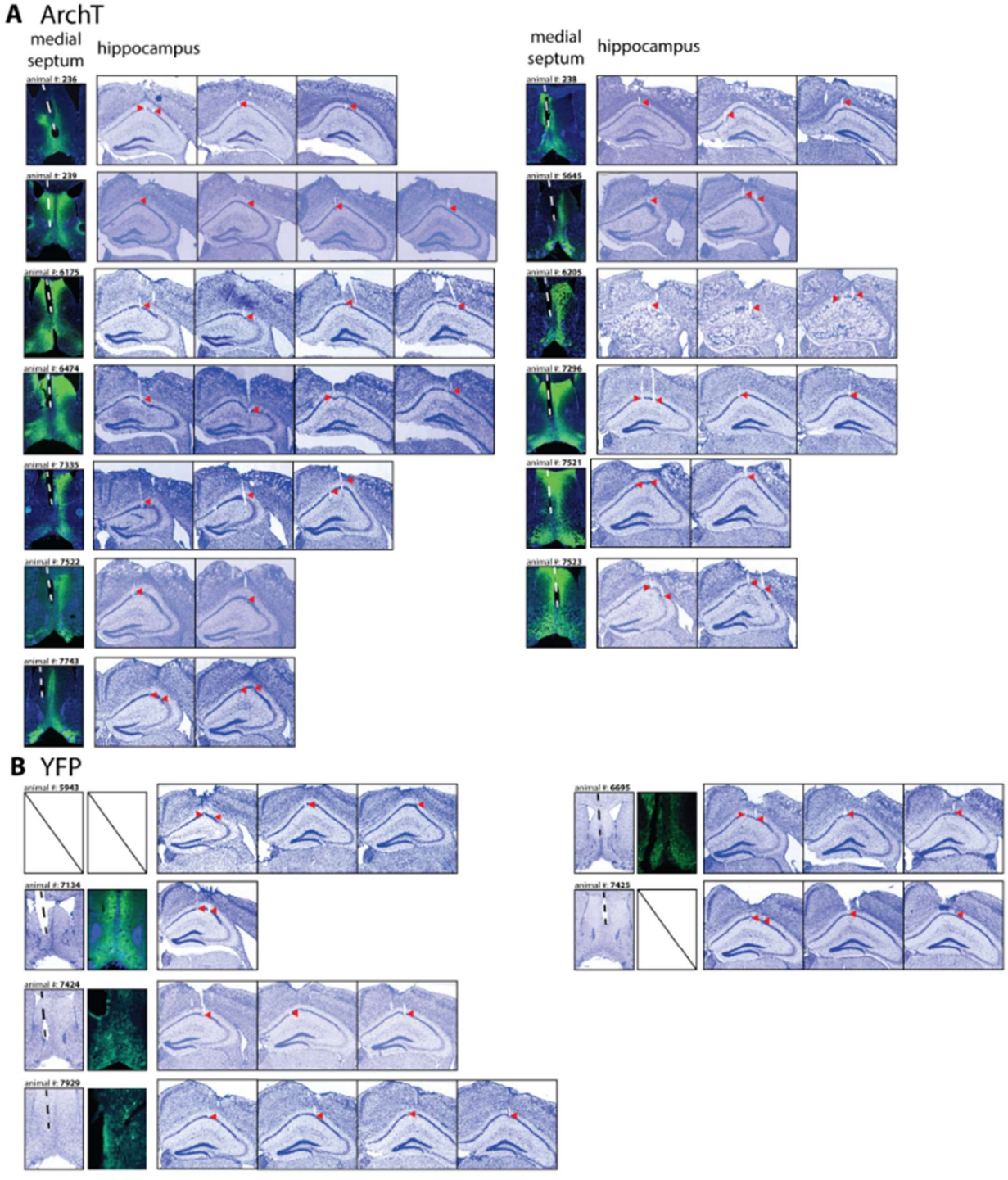

Supplementary Figure 2-1. Histology of CA1 and the MS

(A) Optic fiber track (white dashed line) with GFP expression in the MS for ArchT animals. Tetrode tracks (red arrows) in dorsal CA1 for ArchT animals.

(B) Same as (A), but for YFP controls. Missing panels for YFP animals were due to damage during immunohistochemistry (#5943 / #7425).

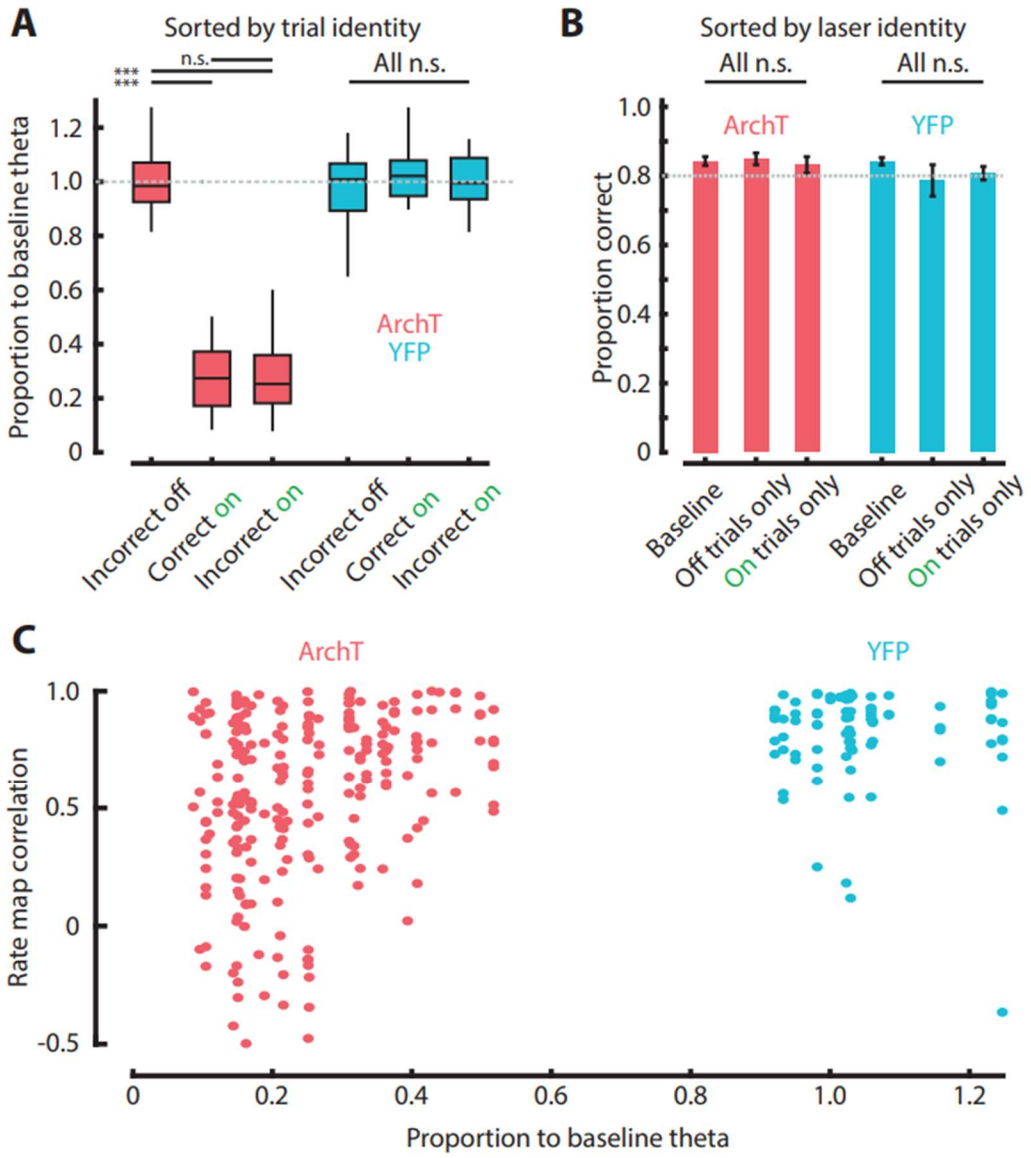

Supplementary Figure 2-2. Reduction in theta power was correlated with stability of time cells, but not with choice

(A) Proportion to baseline theta as a function of correct and incorrect choice. There was no significant change in theta power between correct on and incorrect on trials (Kruskal-Wallis test followed by post hoc test, corrected for multiple comparisons with Bonferroni, ArchT: F(3,152)

= 116.59, $p = 4.18 \times 10^{-25}$, YFP: $F(3, 52) = 0.51$, $p = 0.92$). Refer to Table 2-1 for post hoc test results.

(B) Proportion correct based on laser identity. No behavior disruption was observed (Kruskal-Wallis test, ArchT: $F(2, 39) = 0.61$, $p = 0.74$, YFP: $F(2,18) = 1.87$, $p = 0.39$).

(C) Pearson correlation between rate map correlation and proportion to baseline theta. Significant correlation observed in ArchT ($r = 0.27$, $p = 1.65 \times 10^{-5}$), but not in YFP ($r = -0.05$, $p = 0.68$).

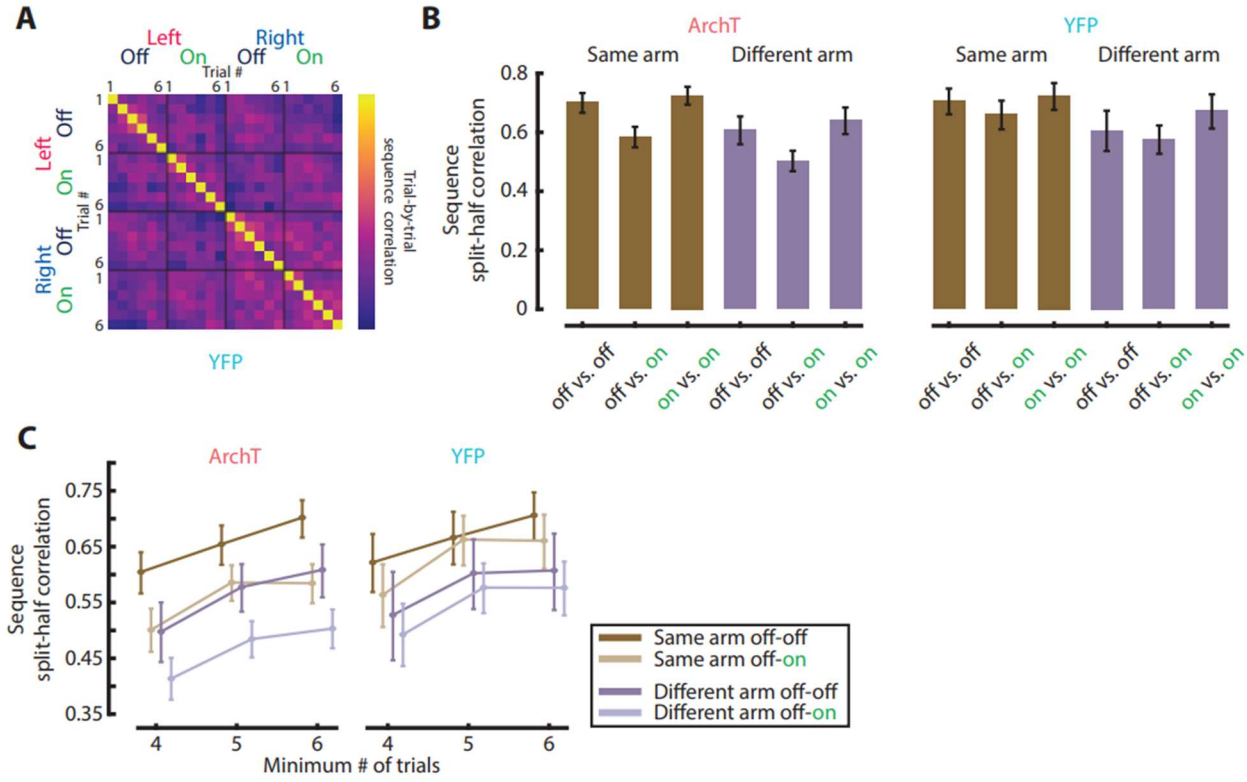

Supplementary Figure 2-3. Trial-by-trial correlation for YFP and split-half correlation of individual sequences

(A) Sequence similarity correlation matrix for YFP controls.

(B) Split-half correlation for sequences. Trials were randomly divided into two parts, and the mean firing rate of these two parts was concatenated to build two sequences. Pearson correlation of these two sequences was obtained. This process was repeated 10,000 times. Bar plots indicate the mean and error bars indicate 95% confidence interval. Sessions with at least 6 trials of leff-going off/on and right-going off/on were used for this analysis.

(C) Change in sequence split-half correlation as a function of minimum number of trials needed to be included in the analysis. Dots indicate the mean and error bars indicate 95% confidence interval. In all cases, cross-training condition (off-on, shaded color) was lower than its counterpart condition

(off-off, solid color). Moreover, sequence split-half correlation for the same arm was higher than the different arm condition, suggesting that a checkered pattern in ArchT animals is observed regardless of threshold used for analysis.

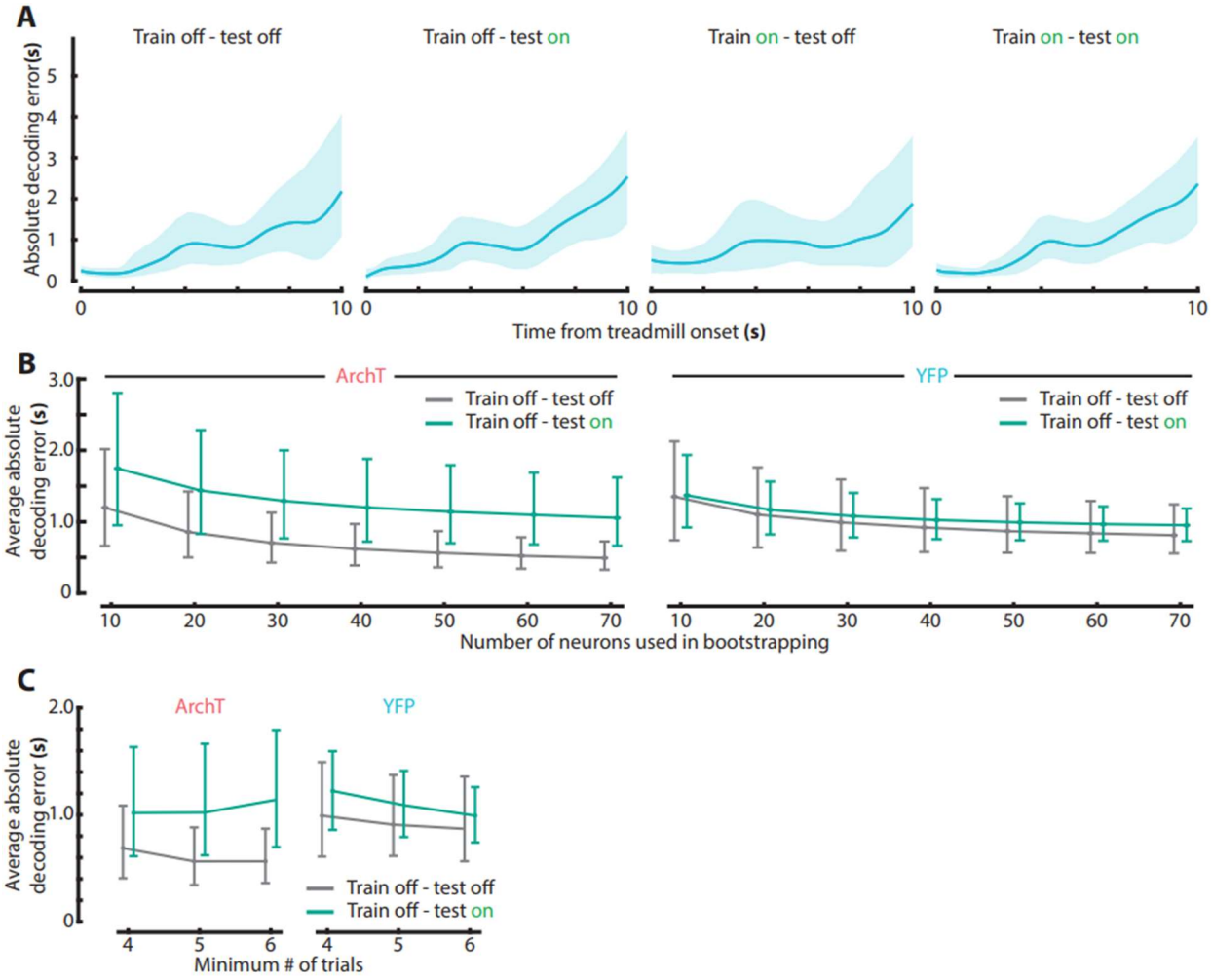

Supplementary Figure 2-4. Maximum likelihood estimator results

(A) Absolute decoding error as a function of time for YFP controls.

(B) Average absolute decoding error as a function of the number of neurons used for bootstrapping. Note that off-off error (grey) is consistently lower than cross-training condition (off-on, green) for the ArchT group, but not for YFP controls. Dots indicate the mean and error bars indicate 95% confidence interval.

(C) Average absolute decoding error as a function of minimum number of trials used. Similar to (B), ArchT animals have lower error in cross-training condition regardless of the minimum number of trials used to select sessions.

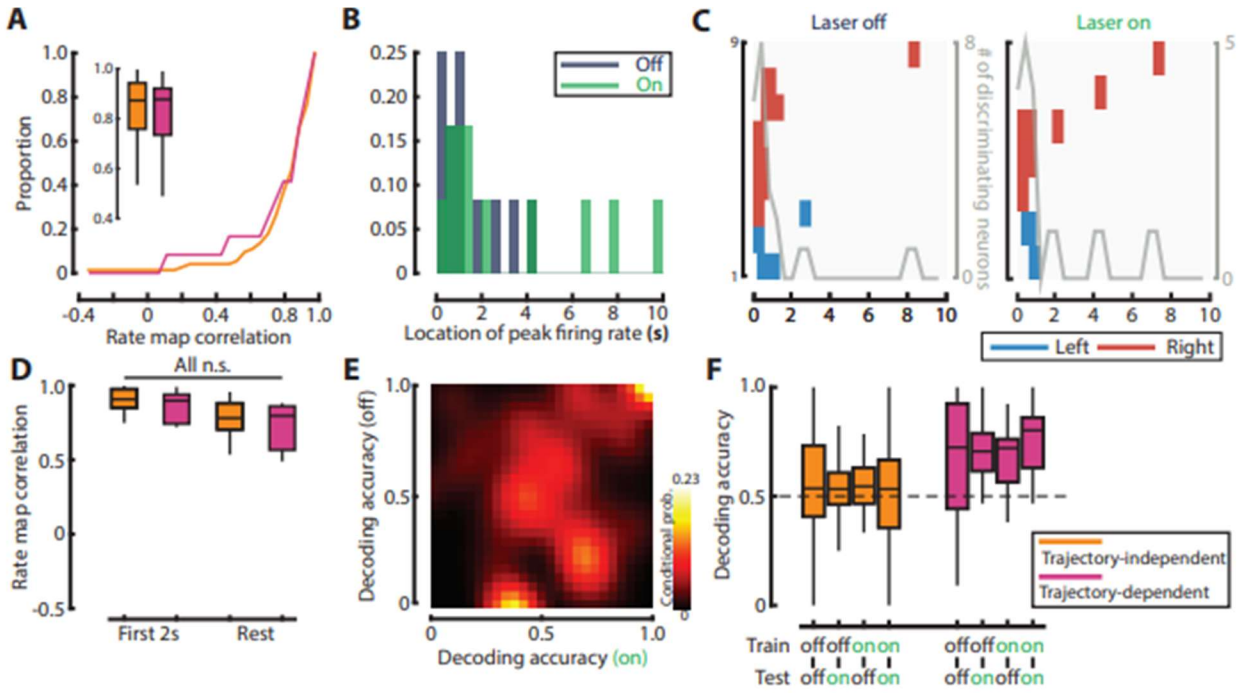

Supplementary Figure.2-5. Trajectory-dependent time cells in YFP

(A) Rate map correlation of YFP trajectory-independent and trajectory-dependent cells (Wilcoxon rank-sum test, YFP: p = 0.79).

(B) Peak firing field location during laser off and on for YFP cells.

(C) Significantly discriminating field locations for YFP. Note that they are concentrated at the beginning similar to ArchT cells.

(D) Rate map correlation separated by the first 2 seconds vs. the rest. No significant difference observed.

(E) Conditional probability matrix for decoding accuracy for YFP controls.

(F) Decoding accuracy for trajectory-independent and trajectory dependent neurons. Refer to Table 2-3 for p values.

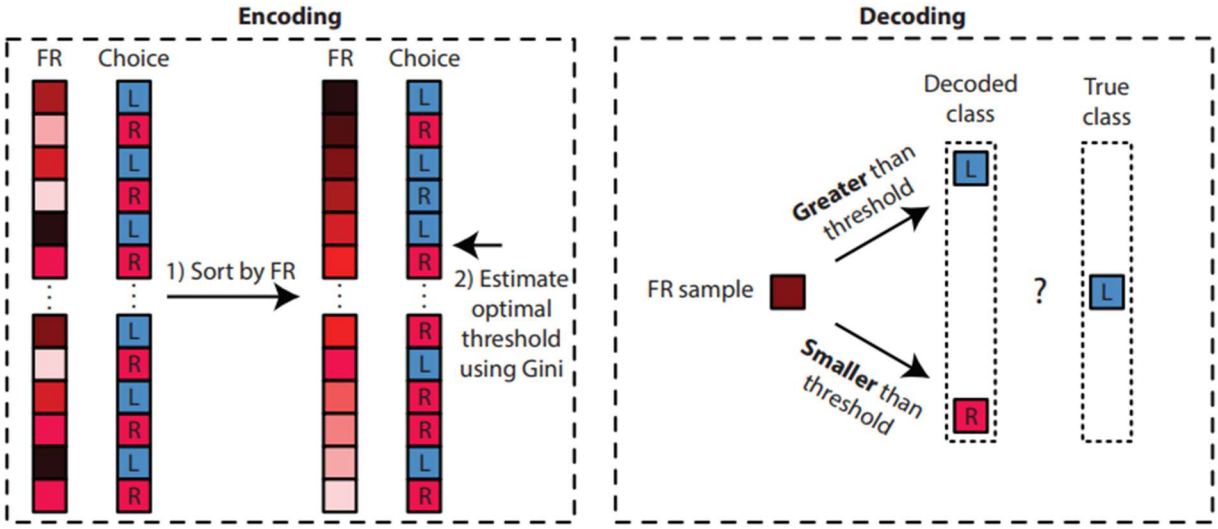

Supplementary Figure 2-6. Overview of decoding method for animals' choice following the treadmill run. Refer to methods for detailed description.

ArchT	Correct off	Correct on	Incorrect off	Incorrect on
Correct off		**2.34×10^{-14}**	1.00	**1.84×10^{-14}**
Correct on			**1.05×10^{-12}**	1.00
Incorrect off				**8.39×10^{-13}**

Table 2-1. Post hoc p-values corrected for multiple comparisons with Bonferroni (Supplementary Figure 2-2B).

ArchT	Train off - test off	Train off - test on	Train on - test off	Train on - test on
Train off - test off		**0.0486**	**0.0042**	1
Train off - test on			1	**0.039**
Train on - test off				**0.014**

YFP	Train off - test off	Train off - test on	Train on - test off	Train on - test on
Train off - test off		1.00	1.00	1.00
Train off - test on			1.00	1.00
Train on - test off				1.00

Table 2-2. Paired-sample bootstrap for equal mean absolute error, Bonferroni corrected for multiple comparisons

ArchT		
Type	**Factor**	**P-value**
Between	Cell identity (Trajectory-dependent vs. independent)	**$<1.00 \times 10^{-4}$**
Within	Decoding condition (off-off, off-on, on-off, on-on)	0.0644
Interaction	Cell identity x decoding condition	0.1560

YFP		
Type	**Factor**	**P-value**
Between	Cell identity (Trajectory-dependent vs. independent)	**0.0062**
Within	Decoding condition (off-off, off-on, on-off, on-on)	0.2008
Interaction	Cell identity x decoding condition	0.1764

Table 2-3. Robust 2-way mixed bootstrapped ANOVA with 20% trimmed means

	Male	Female
8 weeks old (n = 5 per group)	23.8 ± 1.10 (SD)	17.6 ± 0.89 (SD)
16-17 weeks old (n = 6 per group)	28.8 ± 0.98 (SD)	21.8 ± 1.17 (SD)

Table 2-4. Average weight of female and male VGAT::Cre mice.

Chapter 3: Comprehensive discussions and outlook

3.1. Summary of results

Episodic memory is a crucial part of our daily lives. Even though potential neural correlates for 'where' and 'what' components of episodic memory have been identified, research on 'when' component of episodic memory has been lagging behind. Time cells, which are found throughout the hippocampal formation (Kraus et al., 2015; Pastalkova et al., 2008), have been hypothesized to subserve 'when' component of episodic memory by bridging temporal gap between discontinuous events (Eichenbaum, 2014). A recent study that motivated much of the work presented in this thesis suggested that theta oscillations are crucial for time cells and working memory (Y. Wang et al., 2015), but this conclusion is limited because the long-acting pharmacological agent was used, inhibiting theta oscillations throughout behavior.

To disentangle the relationship between theta oscillations, time cell sequences, and working memory, we optogenetically suppressed GABAergic neurons in the MS exclusively during the delay period of a delayed alternation memory task. This approach allowed us to control the power of theta oscillations with temporal and spatial specificity, significantly reducing theta oscillations only when animals were running on the treadmill. This enabled us to investigate a causal role of theta oscillations in working memory and time cells. Surprisingly, we found that strong suppression of theta oscillations did not impair working memory despite leading to remapping and the emergence of a distinct time cell sequence during the delay. The hippocampus was switching between two distinct, albeit similarly accurate time cell sequences depending on the power of theta oscillations available to the system. Moreover, trajectory-dependent time cells maintained more stable representation compared to trajectory-independent

time cells between laser-off and laser-on trials. Our results suggest that, in the absence of theta oscillations, working memory could be supported by intact trajectory-dependent time cells at the beginning of the delay period that signal behaviorally-relevant past and future trajectories. Taken together, these results suggest that theta oscillations are not required during the delay period of a delayed spatial alternation task. While theta oscillations may play a key role in maintaining stable trial-by-trial time cell sequence, a single, task-persistent time cell sequence is not required for working memory.

3.2. Potential mechanisms for time cell sequence generation

Our results speak to the putative mechanisms that support time cell sequences. We demonstrate that the presence of theta oscillations allows for a consistent readout, across trials, of a single sequence. Without theta oscillations, a new sequence emerges, particularly evident after ~2 seconds on the treadmill. The stability of time cells at the beginning of the treadmill may be driven by immediate prior experience and sensory inputs, while expression of the remainder of the sequence - when sensory information is no longer informative - is dependent on an internally driven theta-dependent process, similar to mechanisms proposed in time cell models (Haimerl et al., 2019; Hasselmo & Stern, 2014; Y. Wang et al., 2015). Without this theta-dependent mechanism, retrieval of the original sequence fails and is replaced by a new sequence.

We speculate that this new sequence could emerge due to a shift in temporal information arriving to CA1 from CA3 and the MEC. It was previously reported that both CA3 and the MEC contain time cells (Heys & Dombeck, 2018; Kraus et al., 2015; Salz et al., 2016). Inhibition of MEC input to the hippocampus has been shown to induce remapping of time cells (N. T. M. Robinson et al., 2017), and time cell sequences have been observed to remain intact following

extensive lesions to the MEC (Sabariego et al., 2019). These studies strongly suggest that CA3 provides CA1 with sufficient temporal information to express a time cell sequence.

An important parallel can be drawn with works from the spatial coding literature: neither lesions to CA3 or MEC prevent spatial coding in CA1 (Brun et al., 2002; Brun et al., 2008), demonstrating that either input is sufficient to drive spatial coding in this subregion. Moreover, optogenetic inactivation of CA3 or MEC induces remapping in a subset of CA1 place cells while others either remain unaffected or show increased activity (Davoudi & Foster, 2019; Rueckemann et al., 2016). In septal inactivation studies, which disrupt the tuning of MEC grid cells (Brandon et al., 2011; Koenig et al., 2011), spatial coding in both CA1 and CA3 remains intact (Brandon et al., 2014; Koenig et al., 2011; Y. Wang et al., 2015). Given that grid cells can function as time cells in the delayed T-maze task, it is likely that these cells are similarly disrupted in the temporal, or distance traveled, domain (Kraus et al., 2015) during optogenetic silencing of septal GABAergic populations. Thus, the remapping reported here may result from a disruption in the integration of parallel streams of temporal information arriving from the MEC and CA3, whereby only CA3 temporal inputs remain intact and can drive a new sequence in CA1 without the presence of theta oscillations. Indeed, CA3 is a strong candidate for retrieval of temporal sequences in the absence of changing sensory information due to its recurrent, autoassociative connectivity (Marr, 1971; Mcnaughton & Morris, 1987). Future experiments should confirm if MS inactivation disrupts time cells in the MEC. Moreover, the effects of CA3 inhibition on CA1 time cells should be confirmed to get a complete picture on how disrupting CA3 and MEC pathway influences CA1 time cell code.

One caveat to consider is that a new sequence may have emerged because of changes in cholinergic or glutamatergic tone in the hippocampus. The MS contains GABAergic, cholinergic, and glutamatergic neurons, and these neurons are locally interconnected with each other (Henderson et al., 2001; Manseau et al., 2005). Since our optogenetic inhibition was applied at the level of the MS-DBB, it remains a possibility that we inadvertently inhibited some of cholinergic or glutamatergic neurons that are connected with GABAergic neurons, and this drove remapping of hippocampal time cell sequence instead. However, this is highly unlikely because a previous report that used the same viral construct and mouse line did not observe any changes in SWR occurrences and behavior (Boyce et al., 2016), which are only present when cholinergic levels are low (Y. Zhang et al., 2021). Regardless, future studies are required to identify a role of cholinergic and glutamatergic neurons in time cells in order to further carve out unwanted effects of MS inhibition.

Moreover, to avoid the unwanted effects driven by changes in cholinergic or glutamatergic populations, future studies could inhibit axon collaterals of GABAergic neurons at the level of CA1. This would selectively inhibit GABAergic projections from the MS to the hippocampus while leaving other computations carried out by the MS-DBB completely intact. However, it is unlikely that this will produce similar remapping results because partial remapping we observed is likely to be driven by network level, not local microcircuit level, changes that modulated CA3-MEC inputs converging onto CA1 pyramidal neurons.

3.3. Notable differences from time cell literature

Our results are the first to demonstrate that switching between partially remapped time cell sequences does not impact working memory, which is a markedly different result from prior

reports that used other circuit optogenetic manipulations to degrade time information and memory. In previous work, transient inactivation of the MEC disrupted CA1 time cell sequences substantially and induced memory impairments (N. T. M. Robinson et al., 2017). In this case, time cell information, time cell sequences and behavioral performance were disrupted in both laser-on and laser-off trials, suggesting that direct manipulations of the MEC had a relatively long impact on entorhinal-hippocampal physiology that persisted across trials. Moreover, transient CA2 inactivation did not appear to recruit a new time cell sequence in prior work, and in contrast to that reported here, time cells exhibited increased firing rates and decreased time information (MacDonald & Tonegawa, 2021). Similarly, full MS inactivation with muscimol led to both decreased time field information and memory (Y. Wang et al., 2015). It is noteworthy to add that these behavioral impairments may have also been the consequence of non-selective inhibition of all septal neurons, as recent studies highlight the importance of non-GABAergic septal neurons for working memory performance. Stimulation of cholinergic neurons during the delay (Y. Zhang et al., 2021), and inhibition or random rhythmic perturbation (Etter et al., 2022; Gemzik et al., 2021) of all septal cell types during the delay period led to behavioral impairments. In our study, despite switching to a partially remapped time cell sequence, selective inactivation of septal GABAergic neurons led to decreased firing rates and *increased* time information. In contrast to other reports, the maintenance of high temporal information during septal GABAergic inactivation may help to explain why working memory remained intact.

Furthermore, future studies are needed to identify a mechanism that is responsible for previously reported working memory impairments (Y. Wang et al., 2015). As described previously, the MS is still implicated to be necessary for the delayed spatial alternation task (Etter et al., 2022; Gemzik et al., 2021; Y. Zhang et al., 2021). It has been suggested that

cholinergic neurons may be important because stimulation of cholinergic neurons suppressed SWRs, and in turn, led to behavioral impairments (Y. Zhang et al., 2021). However, this conclusion is limited because behavioral impairments induced by muscimol (Y. Wang et al., 2015) were not coupled with reduction in the number of SWR events as well as changes in the contents of replay (Y. Wang et al., 2016). Rather, muscimol infusion significantly increased the number of SWR events during the delay period, and more SWR events contained time cell sequences (Y. Wang et al., 2016). These findings demonstrate that enhanced SWR activities did not rescue memory, and future studies should continue to investigate a septal cell type subserving working memory in the delayed spatial alternation task.

3.4. Potential mechanisms for intact memory performance

While the baseline and theta-reduced time cell sequences were statistically different, these sequences were not orthogonal. Trajectory-dependent time cells in the first 2 seconds remained stable (**Figure 2-4E**), and the population correlation following the initial 2 seconds was maintained around 0.4 (**Figure 2-2D**). Thus, at any given moment in time, the neural trajectory at the population level could be similar enough for downstream readers to generate correct tuning responses in the delayed spatial alternation task. This view suggests that downstream readers important for behavioral decisions can rapidly interpret information that is degraded, but not completely orthogonal, potentially through a pattern-completion-like mechanism (Stefan Leutgeb et al., 2004; Marr, 1971; Treves & Rolls, 1994). Future experiments should confirm if downstream structures such as prefrontal cortex are able to generate reliable responses when upstream input challenges the circuit with stable and unstable features.

An important perspective concerning the relevance of hippocampal outflow to memory-guided online decision making is generated from the timing of neural representations observed during the delay period. In fact, the population code in the first two seconds of the delay period saw the highest resilience towards theta-disruption, as well as being most explanatory to behavioural choice. This strong bias of trajectory-related representations to the beginning of the delay period has been observed in a previous study as well (Pastalkova et al., 2008). One possibility is that this initial 2 second period is critical to informing downstream regions of the correct behavioural decision. Following this period, persistent neural activity selective to behavior is maintained by other structures such as the prefrontal cortex (Curtis & D'Esposito, 2003; Fuster & Alexander, 1971). Consequently, the type of information relevant to working memory being encoded in hippocampal time cell sequences may themselves be graded temporally. The relevance of neural activities to behavior can be studied by observing their recruitment patterns to SWRs. A recent study demonstrated that CA3 axons were selectively recruited to SWRs depending on their utility to a task at hand (Terada et al., 2022). Specifically, CA3 axons were reliably recruited to SWRs when they encoded task-relevant information such as cues that predicted reward. On the other hand, CA3 axons encoding irrelevant features such as a light cue that did not have any predictive value were suppressed during SWRs (Terada et al., 2022). Future studies should interrogate if time cells are recruited differently during SWRs and if the observed difference is correlated with their preferred firing time point during the delay. The increased recruitment of trajectory-dependent time cells at the beginning of the delay would suggest that these neurons encode more behaviorally relevant information.

An important alternative perspective, given that partially remapped time cell sequences were present both during baseline and theta-reduced trials with high temporal information, is that

animals were capable of using both sequences to perform the task. Similar findings have been reported on the time scale of days and weeks, whereby behavioral performance is maintained despite substantial representational drift (Driscoll et al., 2017; Levy et al., 2021; Taxidis et al., 2020; Ziv et al., 2013). In the current study, representational content was immediately altered optogenetically, yet the hippocampal representation during the delay was sufficient to support behavioral performance. This view suggests that downstream readers important for behavioral decisions can rapidly switch to interpret distinct temporal sequences that subserve the same behavioral outcome. However, whether animals need to learn distinct sequences to guide behavior remains unknown. If learning is required, animals could be erroneous in a very first few trials, but their performance would quickly converge to baseline. On the other hand, if learning is not required, animal's behavior would be intact in these initial trials, indicating that either sequences that are similar or behaviorally relevant neurons that are stable may be sufficient to guide behavior. Future studies should investigate these possibilities to shed light on potential mechanisms used to guide behavior in response to optogenetic manipulations.

A final perspective is that downstream structures were able to decode a remapped sequence because remapping was confined within a microcircuit, which led to similar enough output to be decoded by downstream structures. Specifically, I speculate that (1) time fields that were lost are gained by other pyramidal cells within the same microcircuit, which would generate similar output, and (2) downstream structures are sensitive to the overall output of the microcircuit instead of single-unit responses. A neural microcircuit, defined as a group of interconnected neurons that encode similar locations, needs to be identified in order to support this speculation. CA3 instead of CA1 seems like a good candidate because CA3 has extensive recurrent collaterals, but CA1 lacks such connections. However, numerous studies recently

suggested that CA1 consists of these microcircuits as well, albeit a smaller proportion (Geiller et al., 2022; Huszár et al., 2022; McKenzie et al., 2021; Soltesz & Losonczy, 2018). A recent study showed that stimulation of a single CA1 pyramidal cell, called a seed, caused other nearby pyramidal cells to gain a place field (Geiller et al., 2022). Locations of these optogenetically induced place fields were not random, but rather situated in close proximity to the seed's place field (**Figure 3-1**). Moreover, CA1 neurons that were born together were more likely to fire together within a single cycle of theta and to have place fields in overlapping locations (Huszár et al., 2022). These results strongly suggest that CA1 pyramidal neurons are more interconnected than initially thought, and interconnected neurons have similar functional properties. Thus, remapping or drift confined within this microcircuit could ensure that the overall output is the same despite remapping in a subset of neurons. In other words, regardless of a set of neurons that are firing within the microcircuit, it may be able to maintain similar output by encoding similar locations or time or firing around similar phases of theta oscillations. This may allow downstream structures to reliably decode activities from upstream structures because inputs are arriving around the same time in relation to theta oscillations or spatial location (Geiller et al., 2022; Huszár et al., 2022; Tingley & Buzsáki, 2018). Future studies are needed to test if representational drift is indeed restricted within these CA1 microcircuits.

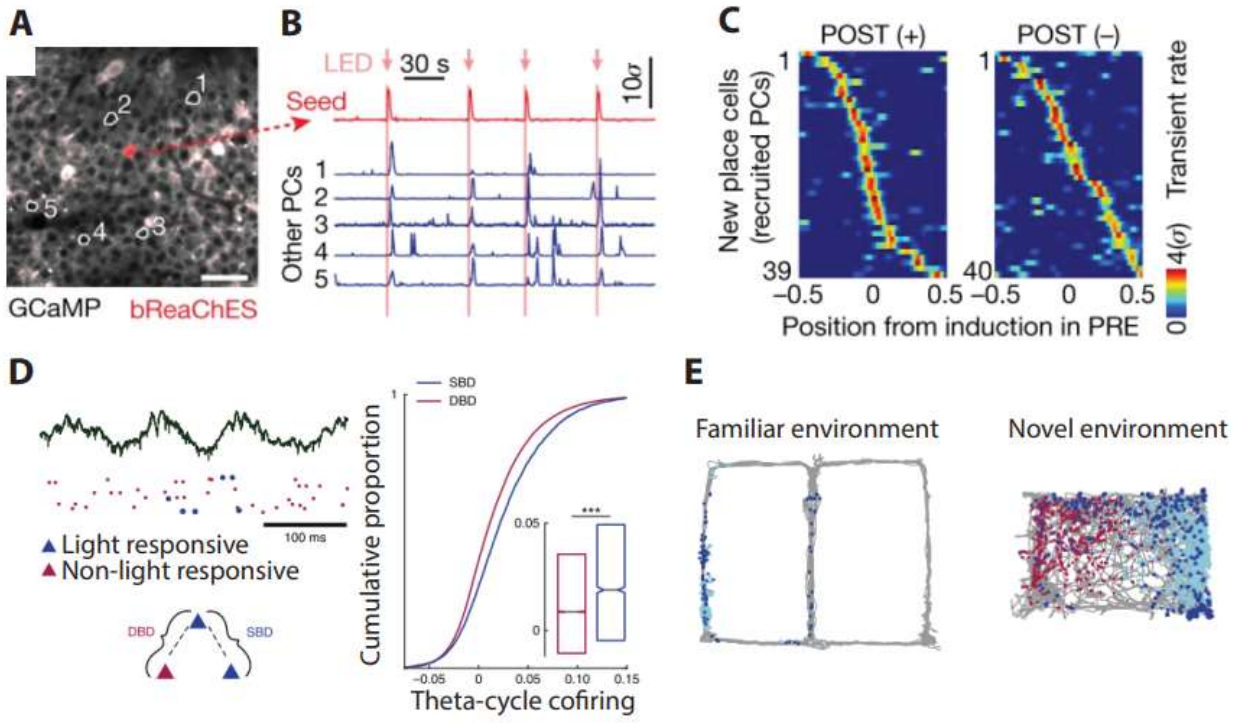

Figure 3-1. Evidence for the presence of connected subnetworks in CA1

(A) Field of view with CA1 pyramidal cells transfected with GCaMP, and a seed neuron (red), which was electroporated with bReaChES, a modified version of channelrhodopsin.

(B) Photostimulation (red arrows) of the seed neuron was able to drive activities of these five pyramidal cells

(C) Place cells that gained their place fields due to photostimulation of a seed neuron (left). Place cells that were not responsive to photostimulation (right). While place cells that were induced by photostimulation had place fields in close vicinity of the seed neuron, place cells that did not respond to photostimulation had more uniformly distributed field locations.

(D) Raw LFP trace with spike rasters showing that spikes from the same birthday neurons (SBD, red). CDF shows that SBD were more likely to fire together within a single cycle of theta compared to different birthday neurons (DBD).

(E) SBD neurons had place fields in overlapping locations in the open field, but DBD had nonoverlapping fields.

Parts **A-C** were adapted from Geiller et al. (2022), and parts **D-E** were adapted Huszar et al. (2022).

3.5. Final conclusion and summary

In this thesis, *in vivo* electrophysiology, optogenetics, and a hippocampal-dependent working memory task were combined in freely moving mice to delineate the role of theta oscillations in working memory and time cells. The optogenetic approach targeting theta-pacing GABAergic neurons in the MS significantly reduced theta oscillations with temporal and spatial specificity (Aim 1). Surprisingly, optogenetic reduction in theta oscillations restricted to the delay period did not cause any behavior deficit in contrast to the prior study (Y. Wang et al., 2015) (Aim2). Single-unit analysis revealed that time cells, which are known to encode the delay period, remapped in response to the optogenetic reduction of theta power (Aim 2). Furthermore, a subset of time cells that encode the animal's past and future trajectories maintained their firing fields in response to optogenetic manipulations, potentially supporting animal's memory performance (Aim 2). These electrophysiological properties of time cells were demonstrated in mice (Aim 3). Together, these results suggest that a reliable time cell sequence is not a prerequisite for stable memory performance. Furthermore, it provides a greater insight into the role of theta oscillations in working memory and hippocampal physiology.

References

Ahmed, M. S., Priestley, J. B., Castro, A., Stefanini, F., Solis Canales, A. S., Balough, E. M., Lavoie, E., Mazzucato, L., Fusi, S., & Losonczy, A. (2020). Hippocampal Network Reorganization Underlies the Formation of a Temporal Association Memory. *Neuron*, *107*(2), 283-291.e6. https://doi.org/10.1016/j.neuron.2020.04.013

Amaral, D. G. (1978). A Golgi study of cell types in the hilar region of the hippocampus in the rat. *The Journal of Comparative Neurology*, *182*(4 Pt 2), 851–914. https://doi.org/10.1002/cne.901820508

Aronov, D., Nevers, R., & Tank, D. W. (2017). Mapping of a non-spatial dimension by the hippocampal-entorhinal circuit. *Nature*, *543*(7647), 719–722. https://doi.org/10.1038/nature21692

Baimbridge, K. G., Peet, M. J., McLennan, H., & Church, J. (1991). Bursting response to current-evoked depolarization in rat CA1 pyramidal neurons is correlated with lucifer yellow dye coupling but not with the presence of calbindin-D28k. *Synapse (New York, N.Y.)*, *7*(4), 269–277. https://doi.org/10.1002/syn.890070404

Bartos, M., Vida, I., & Jonas, P. (2007). Synaptic mechanisms of synchronized gamma oscillations in inhibitory interneuron networks. *Nature Reviews Neuroscience*, *8*(1), 45–56. https://doi.org/10.1038/nrn2044

Belluscio, M. A., Mizuseki, K., Schmidt, R., Kempter, R., & Buzsáki, G. (2012). Cross-frequency phase-phase coupling between theta and gamma oscillations in the hippocampus. *Journal of Neuroscience*, *32*(2), 423–435. https://doi.org/10.1523/JNEUROSCI.4122-11.2012

Berry, S. D., & Thompson, R. F. (1978). Prediction of Learning Rate from the Hippocampal Electroencephalogram. *Science*, *200*(4347), 1298–1300. https://doi.org/10.1126/science.663612

Bickel, P. J., & Sakov, A. (2008). On the choice of m in the m out of n bootstrap and confidence bounds for extrema. *Statistica Sinica*, *18*(3), 967–985.

Bohbot, V. D., Copara, M. S., Gotman, J., & Ekstrom, A. D. (2017). Low-frequency theta oscillations in the human hippocampus during real-world and virtual navigation. *Nature Communications*, *8*, 1–7. https://doi.org/10.1038/ncomms14415

Bonett, D. G., & Wright, T. A. (2000). Sample size requirements for estimating pearson, kendall and spearman correlations. *Psychometrika*, *65*(1), 23–28. https://doi.org/10.1007/BF02294183

Boyce, R., Glasgow, S. D., Williams, S., & Adamantidis, A. (2016). Causal evidence for the role of REM sleep theta rhythm in contextual memory consolidation. *Science*, *352*(6287), 812–816. https://doi.org/10.1126/science.aad5252

Bragin, A., Jandó, G., Nádasdy, Z., Hetke, J., Wise, K., & Buzsáki, G. (1995). Gamma (40-100 Hz) oscillation in the hippocampus of the behaving rat. *Journal of Neuroscience*, *15*(1 I),

47–60. https://doi.org/10.1523/jneurosci.15-01-00047.1995

Brandon, M. P., Bogaard, A. R., Libby, C. P., Connerney, M. A., Gupta, K., & Hasselmo, M. E. (2011). Reduction of Theta Rhythm Dissociates Grid Cell Spatial Periodicity from Directional Tuning. *Science*, *332*(6029), 595–599. https://doi.org/10.1126/science.1201652

Brandon, M. P., Koenig, J., Leutgeb, J. K., & Leutgeb, S. (2014). New and Distinct Hippocampal Place Codes Are Generated in a New Environment during Septal Inactivation. *Neuron*, *82*(4), 789–796. https://doi.org/10.1016/j.neuron.2014.04.013

Brun, Vegard H., Otnæss, M. K., Molden, S., Steffenach, H. A., Witter, M. P., Moser, M. B., & Moser, E. I. (2002). Place cells and place recognition maintained by direct entorhinal-hippocampal circuitry. *Science*, *296*(5576), 2243–2246. https://doi.org/10.1126/science.1071089

Brun, Vegard Heimly, Leutgeb, S., Wu, H. Q., Schwarcz, R., Witter, M. P., Moser, E. I., & Moser, M. B. (2008). Impaired Spatial Representation in CA1 after Lesion of Direct Input from Entorhinal Cortex. *Neuron*, *57*(2), 290–302. https://doi.org/10.1016/j.neuron.2007.11.034

Buzsáki, G. (2002). Theta Oscillations in the Hippocampus. *Neuron*, *33*(3), 325–340. https://doi.org/10.1016/S0896-6273(02)00586-X

Buzsáki, G., & Moser, E. I. (2013). Memory, navigation and theta rhythm in the hippocampal-entorhinal system. *Nature Neuroscience*, *16*(2), 130–138. https://doi.org/10.1038/nn.3304

Canto, C. B., Wouterlood, F. G., & Witter, M. P. (2008). What does the anatomical organization of the entorhinal cortex tell us? *Neural Plasticity*, *2008*. https://doi.org/10.1155/2008/381243

Cardin, J. A., Carlén, M., Meletis, K., Knoblich, U., Zhang, F., Deisseroth, K., Tsai, L. H., & Moore, C. I. (2009). Driving fast-spiking cells induces gamma rhythm and controls sensory responses. *Nature*, *459*(7247), 663–667. https://doi.org/10.1038/nature08002

Cembrowski, M. S., Bachman, J. L., Wang, L., Sugino, K., Shields, B. C., & Spruston, N. (2016). Spatial Gene-Expression Gradients Underlie Prominent Heterogeneity of CA1 Pyramidal Neurons. *Neuron*, *89*(2), 351–368. https://doi.org/10.1016/j.neuron.2015.12.013

Chiba, A. A., Kesner, R. P., & Reynolds, A. M. (1994). Memory for spatial location as a function of temporal lag in rats: Role of hippocampus and medial prefrontal cortex. *Behavioral and Neural Biology*, *61*(2), 123–131. https://doi.org/10.1016/S0163-1047(05)80065-2

Colgin, L. L. (2013). Mechanisms and functions of theta rhythms. In *Annual Review of Neuroscience* (Vol. 36, pp. 295–312). https://doi.org/10.1146/annurev-neuro-062012-170330

Colgin, L. L., Denninger, T., Fyhn, M., Hafting, T., Bonnevie, T., Jensen, O., Moser, M. B., & Moser, E. I. (2009). Frequency of gamma oscillations routes flow of information in the hippocampus. *Nature*, *462*(7271), 353–357. https://doi.org/10.1038/nature08573

Colom, L. V, Castaneda, M. T., Reyna, T., Hernandez, S., & Garrido-Sanabria, E. (2005). Characterization of medial septal glutamatergic neurons and their projection to the hippocampus. *Synapse (New York, N.Y.)*, *58*(3), 151–164. https://doi.org/10.1002/syn.20184

Corkin, S., Amaral, D. G., González, R. G., Johnson, K. A., & Hyman, B. T. (1997). H. M.'s Medial Temporal Lobe Lesion: Findings from Magnetic Resonance Imaging. *The Journal of Neuroscience*, *17*(10), 3964 LP – 3979.

Csicsvari, J., Jamieson, B., Wise, K. D., & Buzsáki, G. (2003). Mechanisms of gamma oscillations in the hippocampus of the behaving rat. *Neuron*, *37*(2), 311–322. https://doi.org/10.1016/S0896-6273(02)01169-8

Cui, Z., Gerfen, C. R., & Young, W. S. (2013). Hypothalamic and other connections with dorsal CA2 area of the mouse hippocampus. *Journal of Comparative Neurology*, *521*(8), 1844–1866. https://doi.org/10.1002/cne.23263

Cunningham, J. P., & Yu, B. M. (2014). Dimensionality reduction for large-scale neural recordings. In *Nature Neuroscience* (Vol. 17, Issue 11, pp. 1500–1509). Nature Publishing Group. https://doi.org/10.1038/nn.3776

Curtis, C. E., & D'Esposito, M. (2003). Persistent activity in the prefrontal cortex during working memory. *Trends in Cognitive Sciences*, *7*(9), 415–423. https://doi.org/10.1016/S1364-6613(03)00197-9

Danielson, N. B. B., Kaifosh, P., Zaremba, J. D. D., Lovett-Barron, M., Tsai, J., Denny, C. A. A., Balough, E. M. M., Goldberg, A. R. R., Drew, L. J. J., Hen, R., Losonczy, A., & Kheirbek, M. A. A. (2016). Distinct Contribution of Adult-Born Hippocampal Granule Cells to Context Encoding. *Neuron*, *90*(1), 101–112. https://doi.org/10.1016/j.neuron.2016.02.019

Danielson, N. B., Zaremba, J. D., Kaifosh, P., Bowler, J., Ladow, M., & Losonczy, A. (2016). Sublayer-Specific Coding Dynamics during Spatial Navigation and Learning in Hippocampal Area CA1. *Neuron*, *91*(3), 652–665. https://doi.org/10.1016/j.neuron.2016.06.020

Dannenberg, H., Kelley, C., Hoyland, A., Monaghan, C. K., & Hasselmo, M. E. (2019). The firing rate speed code of entorhinal speed cells differs across behaviorally relevant time scales and does not depend on medial septum inputs. *Journal of Neuroscience*, *39*(18), 3434–3453. https://doi.org/10.1523/JNEUROSCI.1450-18.2019

Davoudi, H., & Foster, D. J. (2019). Acute silencing of hippocampal CA3 reveals a dominant role in place field responses. *Nature Neuroscience*, *22*(3), 337–342. https://doi.org/10.1038/s41593-018-0321-z

De Lavilléon, G., Lacroix, M. M., Rondi-Reig, L., & Benchenane, K. (2015). Explicit memory creation during sleep demonstrates a causal role of place cells in navigation. *Nature Neuroscience*, *18*(4), 493–495. https://doi.org/10.1038/nn.3970

Deng, W., Aimone, J. B., & Gage, F. H. (2010). New neurons and new memories: How does adult hippocampal neurogenesis affect learning and memory? *Nature Reviews Neuroscience*, *11*(5), 339–350. https://doi.org/10.1038/nrn2822

Deshmukh, S. S., & Knierim, J. J. (2011). Representation of non-spatial and spatial information in the lateral entorhinal cortex. *Frontiers in Behavioral Neuroscience*, *5*(OCTOBER). https://doi.org/10.3389/fnbeh.2011.00069

Driscoll, L. N., Pettit, N. L., Minderer, M., Chettih, S. N., & Harvey, C. D. (2017). Dynamic Reorganization of Neuronal Activity Patterns in Parietal Cortex. *Cell*, *170*(5), 986-999.e16. https://doi.org/10.1016/j.cell.2017.07.021

Dudek, S. M., Alexander, G. M., & Farris, S. (2016). Rediscovering area CA2: Unique properties and functions. *Nature Reviews Neuroscience*, *17*(2), 89–102. https://doi.org/10.1038/nrn.2015.22

Dupret, D., O'Neill, J., Pleydell-Bouverie, B., & Csicsvari, J. (2010). The reorganization and reactivation of hippocampal maps predict spatial memory performance. *Nature Neuroscience*, *13*(8), 995–1002. https://doi.org/10.1038/nn.2599

Eichenbaum, H., Kuperstein, M., Fagan, A., & Nagode, J. (1987). Cue-sampling and goal-approach correlates of hippocampal unit activity in rats performing an odor-discrimination task. *Journal of Neuroscience*, *7*(3), 716–732. https://doi.org/10.1523/jneurosci.07-03-00716.1987

Eichenbaum, Howard. (2014). Time cells in the hippocampus: a new dimension for mapping memories. *Nature Reviews Neuroscience*, *15*(11), 732–744. https://doi.org/10.1038/nrn3827

Engel, A. K., Fries, P., & Singer, W. (2001). Dynamic predictions: Oscillations and synchrony in top–down processing. *Nature Reviews Neuroscience*, *2*(10), 704–716. https://doi.org/10.1038/35094565

Etter, G., van der Veldt, S., Choi, J., & Williams, S. (2022). Optogenetic frequency scrambling of hippocampal theta oscillations dissociates working memory retrieval from hippocampal spatiotemporal codes. *BioRxiv*. https://doi.org/https://doi.org/10.1101/2021.12.24.474139

Ferbinteanu, J., & Shapiro, M. L. (2003). Prospective and Retrospective Memory Coding in the Hippocampus that explicitly vary memory demands while holding con-stant other aspects of behavior. Hippocampal neurons in behaving rodents have long been thought to encode. In *Neuron* (Vol. 40). http://www.

Fernández-Ruiz, A., Oliva, A., de Oliveira, E. F., Rocha-Almeida, F., Tingley, D., & Buzsáki, G. (2019). Long-duration hippocampal sharp wave ripples improve memory. *Science*, *364*(6445), 1082–1086. https://doi.org/10.1126/science.aax0758

Fernández-Ruiz, A., Oliva, A., Soula, M., Rocha-Almeida, F., Nagy, G. A., Martin-Vazquez, G., & Buzsáki, G. (2021). Gamma rhythm communication between entorhinal cortex and dentate gyrus neuronal assemblies. *Science*, *372*(6537). https://doi.org/10.1126/science.abf3119

Fortin, N. J., Agster, K. L., & Eichenbaum, H. B. (2002). Critical role of the hippocampus in memory for sequences of events. *Nature Neuroscience*, *5*(5), 458–462. https://doi.org/10.1038/nn834

Frank, L. M., Brown, E. N., & Wilson, M. (2000). Trajectory encoding in the hippocampus and

entorhinal cortex. *Neuron*, *27*(1), 169–178. https://doi.org/10.1016/S0896-6273(00)00018-0

Freund, T. F., & Antal, M. (1988). GABA-containing neurons in the septum control inhibitory interneurons in the hippocampus. *Nature*, *336*(6195), 170–173. https://doi.org/10.1038/336170a0

Fries, P., Nikolić, D., & Singer, W. (2007). The gamma cycle. *Trends in Neurosciences*, *30*(7), 309–316. https://doi.org/10.1016/j.tins.2007.05.005

Frotscher, M., & Léránth, C. (1985). Cholinergic innervation of the rat hippocampus as revealed by choline acetyltransferase immunocytochemistry: A combined light and electron microscopic study. *Journal of Comparative Neurology*, *239*(2), 237–246. https://doi.org/10.1002/cne.902390210

Fuhrmann, F., Justus, D., Sosulina, L., Kaneko, H., Beutel, T., Friedrichs, D., Schoch, S., Schwarz, M. K., Fuhrmann, M., & Remy, S. (2015). Locomotion, Theta Oscillations, and the Speed-Correlated Firing of Hippocampal Neurons Are Controlled by a Medial Septal Glutamatergic Circuit. *Neuron*, *86*(5), 1253–1264. https://doi.org/10.1016/j.neuron.2015.05.001

Fuster, J. M., & Alexander, G. E. (1971). Neuron Activity Related to Short-Term Memory. *Science*, *173*(3997), 652–654. https://doi.org/10.1126/science.173.3997.652

Geiller, T., Fattahi, M., Choi, J. S., & Royer, S. (2017). Place cells are more strongly tied to landmarks in deep than in superficial CA1. *Nature Communications*, *8*. https://doi.org/10.1038/ncomms14531

Geiller, T., Sadeh, S., Rolotti, S. V., Blockus, H., Vancura, B., Negrean, A., Murray, A. J., Rózsa, B., Polleux, F., Clopath, C., & Losonczy, A. (2022). Local circuit amplification of spatial selectivity in the hippocampus. *Nature*, *601*(7891), 105–109. https://doi.org/10.1038/s41586-021-04169-9

Gemzik, Z. M., Donahue, M. M., & Griffin, A. L. (2021). Optogenetic suppression of the medial septum impairs working memory maintenance. *Learning and Memory*, *28*(10), 361–370. https://doi.org/10.1101/lm.053348.120

Gilbert, P. E., Kesner, R. P., & Lee, I. (2001). Dissociating hippocampal subregions: A double dissociation between dentate gyrus and CA1. *Hippocampus*, *11*(6), 626–636. https://doi.org/10.1002/hipo.1077

Gill, P. R., Mizumori, S. J. Y., & Smith, D. M. (2011). Hippocampal episode fields develop with learning. *Hippocampus*, *21*(11), 1240–1249. https://doi.org/10.1002/hipo.20832

Girardeau, G., Benchenane, K., Wiener, S. I., Buzsáki, G., & Zugaro, M. B. (2009). Selective suppression of hippocampal ripples impairs spatial memory. *Nature Neuroscience*, *12*(10), 1222–1223. https://doi.org/10.1038/nn.2384

Gonzalez-Sulser, A., Parthier, D., Candela, A., McClure, C., Pastoll, H., Garden, D., Surmeli, G., & Nolan, M. F. (2014). GABAergic Projections from the Medial Septum Selectively Inhibit Interneurons in the Medial Entorhinal Cortex. *Journal of Neuroscience*, *34*(50), 16739–16743. https://doi.org/10.1523/JNEUROSCI.1612-14.2014

GoodSmith, D., Chen, X., Wang, C., Kim, S. H., Song, H., Burgalossi, A., Christian, K. M., & Knierim, J. J. (2017). Spatial Representations of Granule Cells and Mossy Cells of the Dentate Gyrus. *Neuron*, *93*(3), 677-690.e5. https://doi.org/10.1016/j.neuron.2016.12.026

Goutagny, R., Jackson, J., & Williams, S. (2009). Self-generated theta oscillations in the hippocampus. *Nature Neuroscience*, *12*(12), 1491–1493. https://doi.org/10.1038/nn.2440

Goyal, A., Miller, J., Qasim, S. E., Watrous, A. J., Zhang, H., Stein, J. M., Inman, C. S., Gross, R. E., Willie, J. T., Lega, B., Lin, J. J., Sharan, A., Wu, C., Sperling, M. R., Sheth, S. A., McKhann, G. M., Smith, E. H., Schevon, C., & Jacobs, J. (2020). Functionally distinct high and low theta oscillations in the human hippocampus. *Nature Communications*, *11*(1), 1–10. https://doi.org/10.1038/s41467-020-15670-6

Graves, A. R., Moore, S. J., Bloss, E. B., Mensh, B. D., Kath, W. L., & Spruston, N. (2012). Hippocampal Pyramidal Neurons Comprise Two Distinct Cell Types that Are Countermodulated by Metabotropic Receptors. *Neuron*, *76*(4), 776–789. https://doi.org/10.1016/j.neuron.2012.09.036

Gray, C. M., König, P., Engel, A. K., & Singer, W. (1989). Oscillatory responses in cat visual cortex exhibit inter-columnar synchronization which reflects global stimulus properties. *Nature*, *338*(6213), 334–337. https://doi.org/10.1038/338334a0

Green, J. D., & Arduini, A. A. (1954). Hippocampal electrical activity in arousal. *Journal of Neurophysiology*, *17*(6), 533–557. https://doi.org/10.1152/jn.1954.17.6.533

Hafting, T., Fyhn, M., Molden, S., Moser, M.-B., & Moser, E. I. (2005). Microstructure of a spatial map in the entorhinal cortex. *Nature*, *436*(7052), 801–806. https://doi.org/10.1038/nature03721

Haimerl, C., Angulo-Garcia, D., Villette, V., Reichinnek, S., Torcini, A., Cossart, R., & Malvache, A. (2019). Internal representation of hippocampal neuronal population spans a time-distance continuum. *Proceedings of the National Academy of Sciences of the United States of America*, *116*(15), 7477–7482. https://doi.org/10.1073/pnas.1718518116

Hainmueller, T., & Bartos, M. (2018). Parallel emergence of stable and dynamic memory engrams in the hippocampus. *Nature*, *558*(7709), 292–296. https://doi.org/10.1038/s41586-018-0191-2

Hales, J. B., Schlesiger, M. I., Leutgeb, J. K., Squire, L. R., Leutgeb, S., & Clark, R. E. (2014). Medial entorhinal cortex lesions only partially disrupt hippocampal place cells and hippocampus- dependent place memory. *Cell Reports*, *9*(3), 893–901. https://doi.org/10.1016/j.celrep.2014.10.009

Han, X., Chow, B. Y., Zhou, H., Klapoetke, N. C., Chuong, A., Rajimehr, R., Yang, A., Baratta, M. V., Winkle, J., Desimone, R., & Boyden, E. S. (2011). A high-light sensitivity optical neural silencer: Development and application to optogenetic control of non-human primate cortex. *Frontiers in Systems Neuroscience*, *5*(APRIL 2011), 1–8. https://doi.org/10.3389/fnsys.2011.00018

Hangya, B., Borhegyi, Z., Szilágyi, N., Freund, T. F., & Varga, V. (2009). GABAergic neurons

of the medial septum lead the hippocampal network during theta activity. *Journal of Neuroscience*, *29*(25), 8094–8102. https://doi.org/10.1523/JNEUROSCI.5665-08.2009

Hargreaves, E. L., Rao, G., Lee, I., & Knierim, J. J. (2005). Major Dissociation Between Medial and Lateral Entorhinal Input to Dorsal Hippocampus. *Science*, *308*(5729), 1792–1794. https://doi.org/10.1126/science.1110449

Hasselmo M. E. (1999). Neuromodulation: acetylcholine and memory consolidation. *Trends in Cognitive Sciences*, *101*(9), 162–183.

Hasselmo, M. E. (2008). Grid cell mechanisms and function: Contributions of entorhinal persistent spiking and phase resetting. *Hippocampus*, *18*(12), 1213–1229. https://doi.org/10.1002/hipo.20512

Hasselmo, M. E., & Stern, C. E. (2014). Theta rhythm and the encoding and retrieval of space and time. *NeuroImage*, *85*, 656–666. https://doi.org/10.1016/j.neuroimage.2013.06.022

Henderson, Z., Morris, N. P., Grimwood, P., Fiddler, G., Yang, H. W., & Appenteng, K. (2001). Morphology of local axon collaterals of electrophysiologically characterised neurons in the rat medial septal/diagonal band complex. *Journal of Comparative Neurology*, *430*(3), 410–432. https://doi.org/10.1002/1096-9861(20010212)430:3<410::AID-CNE1040>3.0.CO;2-I

Heys, J. G., & Dombeck, D. A. (2018). Evidence for a subcircuit in medial entorhinal cortex representing elapsed time during immobility. *Nature Neuroscience*, *21*(11), 1574–1582. https://doi.org/10.1038/s41593-018-0252-8

Hitti, F. L., & Siegelbaum, S. A. (2014). The hippocampal CA2 region is essential for social memory. *Nature*, *508*(1), 88–92. https://doi.org/10.1038/nature13028

Hjorth-Simonsen, A., & Jeune, B. (1972). Origin and termination of the hippocampal perforant path in the rat studied by silver impregnation. *The Journal of Comparative Neurology*, *144*(2), 215–231. https://doi.org/10.1002/cne.901440206

Hjorth-Simonsen, A. (1972). Projection of the lateral part of the entorhinal area to the hippocampus and fascia dentata. *Journal of Comparative Neurology*, *146*(2), 219–231. https://doi.org/10.1002/cne.901460206

Hsu, T. T., Lee, C. T., Tai, M. H., & Lien, C. C. (2016). Differential Recruitment of Dentate Gyrus Interneuron Types by Commissural Versus Perforant Pathways. *Cerebral Cortex*, *26*(6), 2715–2727. https://doi.org/10.1093/cercor/bhv127

Hunt, D. L., Linaro, D., Si, B., Romani, S., & Spruston, N. (2018). A novel pyramidal cell type promotes sharp-wave synchronization in the hippocampus. *Nature Neuroscience*, *21*(7), 985–995. https://doi.org/10.1038/s41593-018-0172-7

Huszár, R., Zhang, Y., Blockus, H., & Buzsáki, G. (2022). Preconfigured dynamics in the hippocampus are guided by embryonic birthdate and rate of neurogenesis. *Nature Neuroscience*. https://doi.org/10.1038/s41593-022-01138-x

Ishizuka, N., Weber, J., & Amaral, D. G. (1990). Organization of intrahippocampal projections originating from CA3 pyramidal cells in the rat. *The Journal of Comparative Neurology*,

295(4), 580–623. https://doi.org/10.1002/cne.902950407

Jadhav, S. P., Kemere, C., German, P. W., & Frank, L. M. (2012). Awake hippocampal sharp-wave ripples support spatial memory. *Science*, *336*(6087), 1454–1458. https://doi.org/10.1126/science.1217230

Jung, M. W., & McNaughton, B. L. (1993). Spatial selectivity of unit activity in the hippocampal granular layer. *Hippocampus*, *3*(2), 165–182. https://doi.org/10.1002/hipo.450030209

Jung, R., & Kornmüller, A. E. (1938). A method of recording localized electrical potentials in subcortical regions of the brain. *Archiv Für Psychiatrie Und Nervenkrankheiten*, *109*, 1–30. https://doi.org/10.1007/BF02157817

Jutras, M. J., Fries, P., & Buffalo, E. A. (2013). Oscillatory activity in the monkey hippocampus during visual exploration and memory formation. *Proceedings of the National Academy of Sciences of the United States of America*, *110*(32), 13144–13149. https://doi.org/10.1073/pnas.1302351110

Karlsson, M. P., & Frank, L. M. (2009). Awake replay of remote experiences in the hippocampus. *Nature Neuroscience*, *12*(7), 913–918. https://doi.org/10.1038/nn.2344

Kesner, R. P., Gilbert, P. E., & Barua, L. A. (2002). The role of the hippocampus in memory for the temporal order of a sequence of odors. *Behavioral Neuroscience*, *116*(2), 286–290. https://doi.org/10.1037//0735-7044.116.2.286

Kinsky, N. R., Mau, W., Sullivan, D. W., Levy, S. J., Ruesch, E. A., & Hasselmo, M. E. (2020). Trajectory-modulated hippocampal neurons persist throughout memory-guided navigation. *Nature Communications*, *11*(1). https://doi.org/10.1038/s41467-020-16226-4

Kitamura, T., Pignatelli, M., Suh, J., Kohara, K., Yoshiki, A., Abe, K., & Tonegawa, S. (2014). Island cells control temporal association memory. *Science (New York, N.Y.)*, *343*(6173), 896–901. https://doi.org/10.1126/science.1244634

Klimesch, W., Doppelmayr, M., Russegger, H., & Pachinger, T. (1996). Theta band power in the human scalp EEG and the encoding of new information. *NeuroReport*, *7*(7), 1235–1240. https://doi.org/10.1097/00001756-199605170-00002

Knierim, J. J., Neunuebel, J. P., & Deshmukh, S. S. (2014). Functional correlates of the lateral and medial entorhinal cortex: Objects, path integration and local - Global reference frames. *Philosophical Transactions of the Royal Society B: Biological Sciences*, *369*(1635). https://doi.org/10.1098/rstb.2013.0369

Koenig, J., Linder, A. N., Leutgeb, J. K., & Leutgeb, S. (2011). The Spatial Periodicity of Grid Cells Is Not Sustained During Reduced Theta Oscillations. *Science*, *332*(6029), 592–595. https://doi.org/10.1126/science.1201685

Kohara, K., Pignatelli, M., Rivest, A. J., Jung, H. Y., Kitamura, T., Suh, J., Frank, D., Kajikawa, K., Mise, N., Obata, Y., Wickersham, I. R., & Tonegawa, S. (2014). Cell type-specific genetic and optogenetic tools reveal hippocampal CA2 circuits. *Nature Neuroscience*, *17*(2), 269–279. https://doi.org/10.1038/nn.3614

Kopsick, J. D., Hartzell, K., Lazaro, H., Nambiar, P., & Michael, E. (2022). *Temporal dynamics of cholinergic activity in the septo-hippocampal system*. *August*, 1–17. https://doi.org/10.3389/fncir.2022.957441

Kramis, R., Vanderwolf, C. H., & Bland, B. H. (1975). Two types of hippocampal rhythmical slow activity in both the rabbit and the rat: Relations to behavior and effects of atropine, diethyl ether, urethane, and pentobarbital. *Experimental Neurology*, *49*(1), 58–85. https://doi.org/10.1016/0014-4886(75)90195-8

Kraus, B. J., Brandon, M. P., Robinson, R. J., Connerney, M. A., Hasselmo, M. E., & Eichenbaum, H. (2015). During Running in Place, Grid Cells Integrate Elapsed Time and Distance Run. *Neuron*, *88*(3), 578–589. https://doi.org/10.1016/j.neuron.2015.09.031

Kraus, B. J., Robinson, R. J., White, J. A., Eichenbaum, H., & Hasselmo, M. E. (2013). Hippocampal "Time Cells": Time versus Path Integration. *Neuron*, *78*(6), 1090–1101. https://doi.org/10.1016/j.neuron.2013.04.015

Krupic, J., Bauza, M., Burton, S., Barry, C., & O'Keefe, J. (2015). Grid cell symmetry is shaped by environmental geometry. *Nature*, *518*(7538), 232–235. https://doi.org/10.1038/nature14153

Landfield, P. W., Mcgaugh, J. L., & Tusa, R. J. (1972). Theta rhythm: A temporal correlate of memory storage processes in the rat. *Science*, *175*(4017), 87–89. https://doi.org/10.1126/science.175.4017.87

Lanuza, E., & Martínez-García, F. (2009). *Evolution of Septal Nuclei BT - Encyclopedia of Neuroscience* (M. D. Binder, N. Hirokawa, & U. Windhorst (eds.); pp. 1270–1278). Springer Berlin Heidelberg. https://doi.org/10.1007/978-3-540-29678-2_3139

Lee, H., GoodSmith, D., & Knierim, J. J. (2020). Parallel processing streams in the hippocampus. *Current Opinion in Neurobiology*, *64*, 127–134. https://doi.org/10.1016/j.conb.2020.03.004

Lee, H., Wang, C., Deshmukh, S. S., & Knierim, J. J. (2015). Neural Population Evidence of Functional Heterogeneity along the CA3 Transverse Axis: Pattern Completion versus Pattern Separation. *Neuron*, *87*(5), 1093–1105. https://doi.org/10.1016/j.neuron.2015.07.012

Lee, I., Yoganarasimha, D., Rao, G., & Knierim, J. J. (2004). Comparison of population coherence of place cells in hippocampal subfields CA1 and CA3. *Nature*, *430*(6998), 456–459. https://doi.org/10.1038/nature02739

Lee, S. H., Marchionni, I., Bezaire, M., Varga, C., Danielson, N., Lovett-Barron, M., Losonczy, A., & Soltesz, I. (2014). Parvalbumin-positive basket cells differentiate among hippocampal pyramidal cells. *Neuron*, *82*(5), 1129–1144. https://doi.org/10.1016/j.neuron.2014.03.034

Leroy, F., Park, J., Asok, A., Brann, D. H., Meira, T., Boyle, L. M., Buss, E. W., Kandel, E. R., & Siegelbaum, S. A. (2018). A circuit from hippocampal CA2 to lateral septum disinhibits social aggression. *Nature*, *564*(7735), 213–218. https://doi.org/10.1038/s41586-018-0772-0

Leutgeb, J. K., Leutgeb, S., Moser, M. B., & Moser, E. I. (2007). Pattern separation in the

dentate gyrus and CA3 of the hippocampus. *Science*, *315*(5814), 961–966. https://doi.org/10.1126/science.1135801

Leutgeb, S., & Mizumori, S. J. Y. (2002). Context-specific spatial representations by lateral septal cells. *Neuroscience*, *112*(3), 655–663. https://doi.org/10.1016/S0306-4522(02)00101-X

Leutgeb, Stefan, Leutgeb, J. K., Barnes, C. A., Moser, E. I., McNaughton, B. L., & Moser, M.-B. (2005). Independent Codes for Spatial and Episodic Memory in Hippocampal Neuronal Ensembles. *Science*, *309*(5734), 619–623. https://doi.org/10.1126/science.1114037

Leutgeb, Stefan, Leutgeb, J. K., Treves, A., Moser, M. B., & Moser, E. I. (2004). Distinct ensemble codes in hippocampal areas CA3 and CA1. *Science*, *305*(5688), 1295–1298. https://doi.org/10.1126/science.1100265

Levy, S. J., Kinsky, N. R., Mau, W., Sullivan, D. W., & Hasselmo, M. E. (2021). Hippocampal spatial memory representations in mice are heterogeneously stable. *Hippocampus*, *31*(3), 244–260. https://doi.org/10.1002/hipo.23272

Li, N., Chen, S., Guo, Z. V., Chen, H., Huo, Y., Inagaki, H. K., Chen, G., Davis, C., Hansel, D., Guo, C., & Svoboda, K. (2019). Spatiotemporal constraints on optogenetic inactivation in cortical circuits. *ELife*, *8*, 1–31. https://doi.org/10.7554/eLife.48622

Li, Y., Xu, J., Liu, Y., Zhu, J., Liu, N., Zeng, W., Huang, N., Rasch, M. J., Jiang, H., Gu, X., Li, X., Luo, M., Li, C., Teng, J., Chen, J., Zeng, S., Lin, L., & Zhang, X. (2017). A distinct entorhinal cortex to hippocampal CA1 direct circuit for olfactory associative learning. *Nature Neuroscience*, *20*(4), 559–570. https://doi.org/10.1038/nn.4517

Liebe, S., Hoerzer, G. M., Logothetis, N. K., & Rainer, G. (2012). Theta coupling between V4 and prefrontal cortex predicts visual short-term memory performance. *Nature Neuroscience*, *15*(3), 456–462. https://doi.org/10.1038/nn.3038

Lorente De Nó, R. (1934). Studies on the structure of the cerebral cortex. II. Continuation of the study of the ammonic system. *Journal Für Psychologie Und Neurologie*, *46*, 113–177.

Lovett-Barron, M., Kaifosh, P., Kheirbek, M. A., Danielson, N., Zaremba, J. D., Reardon, T. R., Turi, G. F., Hen, R., Zemelman, B. V., & Losonczy, A. (2014). Dendritic Inhibition in the Hippocampus Supports Fear Learning. *Science*, *343*(6173), 857–863. https://doi.org/10.1126/science.1247485

Lu, L., Igarashi, K. M., Witter, M. P., Moser, E. I., & Moser, M. B. (2015). Topography of Place Maps along the CA3-to-CA2 Axis of the Hippocampus. *Neuron*, *87*(5), 1078–1092. https://doi.org/10.1016/j.neuron.2015.07.007

Lu Zhou, T., Tamura, R., Kuriwaki, J., & Ono, T. (1999). Comparison of medial and lateral septal neuron activity during performance of spatial tasks in rats. *Hippocampus*, *9*(3), 220–234. https://doi.org/10.1002/(SICI)1098-1063(1999)9:3<220::AID-HIPO3>3.0.CO;2-E

M'Harzi, M., & Jarrard, L. E. (1992). Effects of medial and lateral septal lesions on acquisition of a place and cue radial maze task. *Behavioural Brain Research*, *49*(2), 159–165. https://doi.org/10.1016/S0166-4328(05)80160-3

MacDonald, C. J., Carrow, S., Place, R., & Eichenbaum, H. (2013). Distinct hippocampal time cell sequences represent odor memories in immobilized rats. *Journal of Neuroscience*, *33*(36), 14607–14616. https://doi.org/10.1523/JNEUROSCI.1537-13.2013

MacDonald, C. J., Lepage, K. Q., Eden, U. T., & Eichenbaum, H. (2011). Hippocampal "time cells" bridge the gap in memory for discontiguous events. *Neuron*, *71*(4), 737–749. https://doi.org/10.1016/j.neuron.2011.07.012

MacDonald, C. J., & Tonegawa, S. (2021). Crucial role for CA2 inputs in the sequential organization of CA1 time cells supporting memory. *Proceedings of the National Academy of Sciences*, *118*(3). https://doi.org/10.1073/pnas.2020698118

Macrides, F., Eichenbaum, H. B., & Forbes, W. B. (1982). Temporal relationship between sniffing and the limbic θ rhythm during odor discriminatin reversal learning. *Journal of Neuroscience*, *2*(12), 1705–1717. https://doi.org/10.1523/jneurosci.02-12-01705.1982

Maldonado, M. A., Allred, R. P., Felthauser, E. L., & Jones, T. A. (2008). Motor skill training, but not voluntary exercise, improves skilled reaching after unilateral ischemic lesions of the sensorimotor cortex in rats. *Neurorehabilitation and Neural Repair*, *22*(3), 250–261. https://doi.org/10.1177/1545968307308551

Mann, E. O., Suckling, J. M., Hajos, N., Greenfield, S. A., & Paulsen, O. (2005). Perisomatic feedback inhibition underlies cholinergically induced fast network oscillations in the rat hippocampus in vitro. *Neuron*, *45*(1), 105–117. https://doi.org/10.1016/j.neuron.2004.12.016

Manns, J. R., Howard, M. W., & Eichenbaum, H. (2007). Gradual Changes in Hippocampal Activity Support Remembering the Order of Events. *Neuron*, *56*(3), 530–540. https://doi.org/10.1016/j.neuron.2007.08.017

Manseau, F., Danik, M., & Williams, S. (2005). A functional glutamatergic neurone network in the medial septum and diagonal band area. *Journal of Physiology*, *566*(3), 865–884. https://doi.org/10.1113/jphysiol.2005.089664

Marr, D. (1969). A theory of cerebellar cortex. *The Journal of Physiology*, *202*(2), 437–470. https://doi.org/10.1113/jphysiol.1969.sp008820

Marr, D. (1971). Simple memory: a theory for archicortex. *Philosophical Transactions of the Royal Society of London. B, Biological Sciences*, *262*(841), 23–81. https://doi.org/10.1098/rstb.1971.0078

Mau, W., Sullivan, D. W., Kinsky, N. R., Hasselmo, M. E., Howard, M. W., & Eichenbaum, H. (2018). The Same Hippocampal CA1 Population Simultaneously Codes Temporal Information over Multiple Timescales. *Current Biology*, *28*(10), 1499-1508.e4. https://doi.org/10.1016/j.cub.2018.03.051

McKenzie, S., Huszár, R., English, D. F., Kim, K., Christensen, F., Yoon, E., & Buzsáki, G. (2021). Preexisting hippocampal network dynamics constrain optogenetically induced place fields. *Neuron*, *109*(6), 1040-1054.e7. https://doi.org/10.1016/j.neuron.2021.01.011

McNaughton, B. L., Battaglia, F. P., Jensen, O., Moser, E. I., & Moser, M. B. (2006). Path

integration and the neural basis of the “cognitive map.” *Nature Reviews Neuroscience*, *7*(8), 663–678. https://doi.org/10.1038/nrn1932

Mcnaughton, B. L., & Morris, R. G. M. (1987). *Hippocampal synaptic enhancement and information storage within a distributed memory system*.

McNaughton, B. L., & Nadel, L. (1990). Hebb-Marr networks and the neurobiological representation of action in space. In *Neuroscience and connectionist theory.* (pp. 1–63). Lawrence Erlbaum Associates, Inc.

McNaughton, N., Ruan, M., & Woodnorth, M.-A. (2006). Restoring theta-like rhythmicity in rats restores initial learning in the Morris water maze. *Hippocampus*, *16*(12), 1102–1110. https://doi.org/10.1002/hipo.20235

Middleton, S. J., & McHugh, T. J. (2016). Silencing CA3 disrupts temporal coding in the CA1 ensemble. *Nature Neuroscience*, *19*(7), 945–951. https://doi.org/10.1038/nn.4311

Mikula, S., Trotts, I., Stone, J. M., & Jones, E. G. (2007). Internet-enabled high-resolution brain mapping and virtual microscopy. *NeuroImage*, *35*(1), 9–15. https://doi.org/10.1016/j.neuroimage.2006.11.053

Mitchell, S. J., Rawlins, J. N. P., Steward, O., & Olton, D. S. (1982). Medial septal area lesions disrupt θ rhythm and cholinergic staining in medial entorhinal cortex and produce impaired radial arm maze behavior in rats. *Journal of Neuroscience*, *2*(3), 292–302. https://doi.org/10.1523/jneurosci.02-03-00292.1982

Mitra, P., & Bokil, H. T. A.-T. T.-. (2008). *Observed brain dynamics* (NV-1 onl). Oxford University Press. http://site.ebrary.com/id/10215750

Mizumori, S. J., Perez, G. M., Alvarado, M. C., Barnes, C. A., & McNaughton, B. L. (1990). Reversible inactivation of the medial septum differentially affects two forms of learning in rats. *Brain Research*, *528*(1), 12–20. http://www.ncbi.nlm.nih.gov/pubmed/2245328

Mizuseki, K., Diba, K., Pastalkova, E., & Buzsaki, G. (2011). Hippocampal CA1 pyramidal cells form functionally distinct sublayers. *Nat Neurosci*, *14*(9), 1174–1181. http://dx.doi.org/10.1038/nn.2894

Moser, E. I., Kropff, E., & Moser, M. B. (2008). Place cells, grid cells, and the brain’s spatial representation system. *Annual Review of Neuroscience*, *31*, 69–89. https://doi.org/10.1146/annurev.neuro.31.061307.090723

Muller, R. U., & Kubie, J. L. (1987). The effects of changes in the environment on the spatial firing of hippocampal complex-spike cells. *Journal of Neuroscience*, *7*(7), 1951–1968. https://doi.org/10.1523/jneurosci.07-07-01951.1987

Naber, P. A., Lopes Da Silva, F. H., & Witter, M. P. (2001). Reciprocal connections between the entorhinal cortex and hippocampal fields CA1 and the subiculum are in register with the projections from CA1 to the subiculum. *Hippocampus*, *11*(2), 99–104. https://doi.org/10.1002/hipo.1028

Neunuebel, J. P., & Knierim, J. J. (2012). Spatial firing correlates of physiologically distinct cell

types of the rat dentate gyrus. *Journal of Neuroscience*, *32*(11), 3848–3858. https://doi.org/10.1523/JNEUROSCI.6038-11.2012

Neunuebel, J. P., & Knierim, J. J. (2014). CA3 retrieves coherent representations from degraded input: Direct evidence for CA3 pattern completion and dentate gyrus pattern separation. *Neuron*, *81*(2), 416–427. https://doi.org/10.1016/j.neuron.2013.11.017

O'Keefe, J., & Dostrovsky, J. (1971). The hippocampus as a spatial map. Preliminary evidence from unit activity in the freely-moving rat. *Brain Research*, *34*(1), 171–175. https://doi.org/10.1016/0006-8993(71)90358-1

O'Keefe, John, & Nadel, L. (1978). *The Hippocampus as a Cognitive Map*. Clarendon Press.

Oh, S. W., Harris, J. A., Ng, L., Winslow, B., Cain, N., Mihalas, S., Wang, Q., Lau, C., Kuan, L., Henry, A. M., Mortrud, M. T., Ouellette, B., Nguyen, T. N., Sorensen, S. A., Slaughterbeck, C. R., Wakeman, W., Li, Y., Feng, D., Ho, A., … Zeng, H. (2014). A mesoscale connectome of the mouse brain. *Nature*, *508*(7495), 207–214. https://doi.org/10.1038/nature13186

Oliva, A., Fernández-Ruiz, A., Leroy, F., & Siegelbaum, S. A. (2020). Hippocampal CA2 sharp-wave ripples reactivate and promote social memory. *Nature*, *587*(7833), 264–269. https://doi.org/10.1038/s41586-020-2758-y

Osipova, D., Takashima, A., Oostenveld, R., Fernández, G., Maris, E., & Jensen, O. (2006). Theta and gamma oscillations predict encoding and retrieval of declarative memory. *Journal of Neuroscience*, *26*(28), 7523–7531. https://doi.org/10.1523/JNEUROSCI.1948-06.2006

Otchy, T. M., Wolff, S. B. E., Rhee, J. Y., Pehlevan, C., Kawai, R., Kempf, A., Gobes, S. M. H., & Ölveczky, B. P. (2015). Acute off-target effects of neural circuit manipulations. *Nature*, *528*(7582), 358–363. https://doi.org/10.1038/nature16442

Pastalkova, E., Itskov, V., Amarasingham, A., & Buzsáki, G. (2008). Internally generated cell assembly sequences in the rat hippocampus. *Science*, *321*(5894), 1322–1327. https://doi.org/10.1126/science.1159775

Petersen, P. C., & Buzsáki, G. (2020). Cooling of Medial Septum Reveals Theta Phase Lag Coordination of Hippocampal Cell Assemblies. *Neuron*, *107*(4), 731-744.e3. https://doi.org/10.1016/j.neuron.2020.05.023

Quirk, C. R., Zutshi, I., Srikanth, S., Fu, M. L., Devico Marciano, N., Wright, M. K., Parsey, D. F., Liu, S., Siretskiy, R. E., Huynh, T. L., Leutgeb, J. K., & Leutgeb, S. (2021). Precisely timed theta oscillations are selectively required during the encoding phase of memory. *Nature Neuroscience*, *24*(11), 1614–1627. https://doi.org/10.1038/s41593-021-00919-0

Risold, P. Y., & Swanson, L. W. (1997a). Chemoarchitecture of the rat lateral septal nucleus. *Brain Research Reviews*, *24*(2–3), 91–113. https://doi.org/10.1016/S0165-0173(97)00008-8

Risold, P. Y., & Swanson, L. W. (1997b). Connections of the rat lateral septal complex. *Brain Research Reviews*, *24*(2–3), 115–195. https://doi.org/10.1016/S0165-0173(97)00009-X

Rizzi-Wise, C. A., & Wang, D. V. (2021). Putting together pieces of the lateral septum: Multifaceted functions and its neural pathways. *ENeuro*, *8*(6). https://doi.org/10.1523/ENEURO.0315-21.2021

Robbe, D., & Buzsáki, G. (2009). Alteration of theta timescale dynamics of hippocampal place cells by a cannabinoid is associated with memory impairment. *Journal of Neuroscience*, *29*(40), 12597–12605. https://doi.org/10.1523/JNEUROSCI.2407-09.2009

Robinson, J., Manseau, F., Ducharme, G., Amilhon, B., Vigneault, E., El Mestikawy, S., & Williams, S. (2016). Optogenetic activation of septal glutamatergic neurons drive hippocampal theta rhythms. *Journal of Neuroscience*, *36*(10), 3016–3023. https://doi.org/10.1523/JNEUROSCI.2141-15.2016

Robinson, N. T. M., Priestley, J. B., Rueckemann, J. W., Garcia, A. D., Smeglin, V. A., Marino, F. A., & Eichenbaum, H. (2017). Medial Entorhinal Cortex Selectively Supports Temporal Coding by Hippocampal Neurons. *Neuron*, *94*(3), 677-688.e6. https://doi.org/10.1016/j.neuron.2017.04.003

Roland, J. J., Janke, K. L., Servatius, R. J., & Pang, K. C. H. (2014). GABAergic neurons in the medial septum-diagonal band of Broca (MSDB) are important for acquisition of the classically conditioned eyeblink response. *Brain Structure and Function*, *219*(4), 1231–1237. https://doi.org/10.1007/s00429-013-0560-4

Rolls, E. T. (2016). Pattern separation, completion, and categorisation in the hippocampus and neocortex. *Neurobiology of Learning and Memory*, *129*, 4–28. https://doi.org/10.1016/j.nlm.2015.07.008

Rueckemann, J. W., Dimauro, A. J., Rangel, L. M., Han, X., Boyden, E. S., & Eichenbaum, H. (2016). Transient optogenetic inactivation of the medial entorhinal cortex biases the active population of hippocampal neurons. *Hippocampus*, *26*(2), 246–260. https://doi.org/10.1002/hipo.22519

Rutishauser, U., Ross, I. B., Mamelak, A. N., & Schuman, E. M. (2010). Human memory strength is predicted by theta-frequency phase-locking of single neurons. *Nature*, *464*(7290), 903–907. https://doi.org/10.1038/nature08860

Sabariego, M., Schönwald, A., Boublil, B. L., Zimmerman, D. T., Ahmadi, S., Gonzalez, N., Leibold, C., Clark, R. E., Leutgeb, J. K., & Leutgeb, S. (2019). Time Cells in the Hippocampus Are Neither Dependent on Medial Entorhinal Cortex Inputs nor Necessary for Spatial Working Memory. *Neuron*, *102*(6), 1235-1248.e5. https://doi.org/10.1016/j.neuron.2019.04.005

Sakurai, Y. (2002). Coding of auditory temporal and pitch information by hippocampal individual cells and cell assemblies in the rat. *Neuroscience*, *115*(4), 1153–1163. https://doi.org/10.1016/S0306-4522(02)00509-2

Salz, D. M., Tiganj, Z., Khasnabish, S., Kohley, A., Sheehan, D., Howard, M. W., & Eichenbaum, H. (2016). Time cells in hippocampal area CA3. *Journal of Neuroscience*, *36*(28), 7476–7484. https://doi.org/10.1523/JNEUROSCI.0087-16.2016

Scharfman, H. E. (2016). The enigmatic mossy cell of the dentate gyrus. *Nature Reviews Neuroscience*, *17*(9), 562–575. https://doi.org/10.1038/nrn.2016.87

Schomburg, E. W., Fernández-Ruiz, A., Mizuseki, K., Berényi, A., Anastassiou, C. A., Koch, C., & Buzsáki, G. (2014). Theta Phase Segregation of Input-Specific Gamma Patterns in Entorhinal-Hippocampal Networks. *Neuron*, *84*(2), 470–485. https://doi.org/10.1016/j.neuron.2014.08.051

Scoville, W. B., & Milner, B. (1957). Loss of recent memory after bilateral hippocampal lesions. *Journal of Neurology, Neurosurgery, and Psychiatry*, *20*(1), 11–21.

Sekino, Y., Obata, K., Tanifuji, M., Mizuno, M., & Murayama, J. (1997). Delayed signal propagation via CA2 in rat hippocampal slices revealed by optical recording. In *Journal of Neurophysiology* (Vol. 78, Issue 3). https://doi.org/10.1152/jn.1997.78.3.1662

Senzai, Y., & Buzsáki, G. (2017). Physiological Properties and Behavioral Correlates of Hippocampal Granule Cells and Mossy Cells. *Neuron*, *93*(3), 691-704.e5. https://doi.org/10.1016/j.neuron.2016.12.011

Sheehan, T. P., Chambers, R. A., & Russell, D. S. (2004). Regulation of affect by the lateral septum: Implications for neuropsychiatry. *Brain Research Reviews*, *46*(1), 71–117. https://doi.org/10.1016/j.brainresrev.2004.04.009

Shimbo, A., Izawa, E.-I., & Fujisawa, S. (2021). Scalable representation of time in the hippocampus. In *Sci. Adv* (Vol. 7). http://advances.sciencemag.org/

Shinohara, Y., Hosoya, A., Yahagi, K., Ferecskó, A. S., Yaguchi, K., Sík, A., Itakura, M., Takahashi, M., & Hirase, H. (2012). Hippocampal CA3 and CA2 have distinct bilateral innervation patterns to CA1 in rodents. *European Journal of Neuroscience*, *35*(5), 702–710. https://doi.org/10.1111/j.1460-9568.2012.07993.x

Simon, A. P., Poindessous-Jazat, F., Dutar, P., Epelbaum, J., & Bassant, M. H. (2006). Firing properties of anatomically identified neurons in the medial septum of anesthetized and unanesthetized restrained rats. *Journal of Neuroscience*, *26*(35), 9038–9046. https://doi.org/10.1523/JNEUROSCI.1401-06.2006

Skaggs, W. E., Mcnaughton, B. L., Gothard, K. M., & Markus, E. J. (1992). *An Information-Theoretic Approach to Deciphering the Hippocampal Code*.

Sohal, V. S., Zhang, F., Yizhar, O., & Deisseroth, K. (2009). Parvalbumin neurons and gamma rhythms enhance cortical circuit performance. *Nature*, *459*(7247), 698–702. https://doi.org/10.1038/nature07991

Solstad, T., Boccara, C. N., Kropff, E., Moser, M.-B., & Moser, E. I. (2008). Representation of Geometric Borders in the Entorhinal Cortex. *Science*, *322*(5909), 1865–1868. https://doi.org/10.1126/science.1166466

Soltesz, I., & Losonczy, A. (2018). CA1 pyramidal cell diversity enabling parallel information processing in the hippocampus. *Nature Neuroscience*, *21*(4), 484–493. https://doi.org/10.1038/s41593-018-0118-0

Sotty, F., Danik, M., Manseau, F., Laplante, F., Quirion, R., & Williams, S. (2003). Distinct electrophysiological properties of glutamatergic, cholinergic and GABAergic rat septohippocampal neurons: Novel implications for hippocampal rhythmicity. *Journal of Physiology*, *551*(3), 927–943. https://doi.org/10.1113/jphysiol.2003.046847

Stanfield, B. B., Caviness, V. S., & Cowan, W. M. (1979). The organization of certain afferents to the hippocampus and dentate gyrus in normal and reeler mice. *Journal of Comparative Neurology*, *185*(3), 461–483. https://doi.org/10.1002/cne.901850304

Stark, E., Roux, L., Eichler, R., Senzai, Y., Royer, S., & Buzsáki, G. (2014). Pyramidal cell-interneuron interactions underlie hippocampal ripple oscillations. *Neuron*, *83*(2), 467–480. https://doi.org/10.1016/j.neuron.2014.06.023

Stensola, T., Stensola, H., Moser, M. B., & Moser, E. I. (2015). Shearing-induced asymmetry in entorhinal grid cells. *Nature*, *518*(7538), 207–212. https://doi.org/10.1038/nature14151

Stevenson, E. L., & Caldwell, H. K. (2014). Lesions to the CA2 region of the hippocampus impair social memory in mice. *European Journal of Neuroscience*, *40*(9), 3294–3301. https://doi.org/10.1111/ejn.12689

Sun, Q., Sotayo, A., Cazzulino, A. S., Snyder, A. M., Denny, C. A., & Siegelbaum, S. A. (2017). Proximodistal Heterogeneity of Hippocampal CA3 Pyramidal Neuron Intrinsic Properties, Connectivity, and Reactivation during Memory Recall. *Neuron*, *95*(3), 656-672.e3. https://doi.org/10.1016/j.neuron.2017.07.012

Sun, Y., Nguyen, A. Q., Nguyen, J. P., Le, L., Saur, D., Choi, J., Callaway, E. M., & Xu, X. (2014). Cell-type-specific circuit connectivity of hippocampal CA1 revealed through cre-dependent rabies tracing. *Cell Reports*, *7*(1), 269–280. https://doi.org/10.1016/j.celrep.2014.02.030

Swanson, L. W., & Cowan, W. M. (1979). The connections of the septal region in the rat. *Journal of Comparative Neurology*, *186*(4), 621–655. https://doi.org/10.1002/cne.901860408

Takamura, Y., Tamura, R., Zhou, T. L., Kobayashi, T., Tran, A. H., Eifuku, S., & Ono, T. (2006). Spatial firing properties of lateral septal neurons. *Hippocampus*, *16*(8), 635–644. https://doi.org/10.1002/hipo.20196

Tamamaki, N., & Nojyo, Y. (1995). Preservation of topography in the connections between the subiculum, field CA1, and the entorhinal cortex in rats. *Journal of Comparative Neurology*, *353*(3), 379–390. https://doi.org/10.1002/cne.903530306

Taube, J. S., Muller, R. U., & Ranck, J. B. (1990). Head-direction cells recorded from the postsubiculum in freely moving rats. II. Effects of environmental manipulations. *The Journal of Neuroscience : The Official Journal of the Society for Neuroscience*, *10*(2), 436–447. http://www.ncbi.nlm.nih.gov/pubmed/2303852

Taxidis, J., Pnevmatikakis, E. A., Dorian, C. C., Mylavarapu, A. L., Arora, J. S., Samadian, K. D., Hoffberg, E. A., & Golshani, P. (2020). Differential Emergence and Stability of Sensory and Temporal Representations in Context-Specific Hippocampal Sequences. *Neuron*.

https://doi.org/10.1016/j.neuron.2020.08.028

Terada, S., Geiller, T., Liao, Z., O'Hare, J., Vancura, B., & Losonczy, A. (2022). Adaptive stimulus selection for consolidation in the hippocampus. *Nature*, *601*(7892), 240–244. https://doi.org/10.1038/s41586-021-04118-6

Tingley, D., & Buzsáki, G. (2018). Transformation of a Spatial Map across the Hippocampal-Lateral Septal Circuit. *Neuron*, *98*(6), 1229-1242.e5. https://doi.org/10.1016/j.neuron.2018.04.028

Tóth, K., Freund, T. F., & Miles, R. (1997). Disinhibition of rat hippocampal pyramidal cells by GABAergic afferents from the septum. *Journal of Physiology*, *500*(2), 463–474. https://doi.org/10.1113/jphysiol.1997.sp022033

Treves, A., & Rolls, E. T. (1994). Computational analysis of the role of the hippocampus in memory. *Hippocampus*, *4*(3), 374–391. https://doi.org/10.1002/hipo.450040319

Tulving, E. (1972). Episodic and Semantic Memory. In E. Tulving & W. Donaldson (Eds.), *Organization of Memory* (pp. 381–403). Academic Press.

Tzakis, N., & Holahan, M. R. (2019). Social Memory and the Role of the Hippocampal CA2 Region. *Frontiers in Behavioral Neuroscience*, *13*(October), 1–15. https://doi.org/10.3389/fnbeh.2019.00233

Unal, G., Joshi, A., Viney, T. J., Kis, V., & Somogyi, P. (2015). Synaptic Targets of Medial Septal Projections in the Hippocampus and Extrahippocampal Cortices of the Mouse. *The Journal of Neuroscience : The Official Journal of the Society for Neuroscience*, *35*(48), 15812–15826. https://doi.org/10.1523/JNEUROSCI.2639-15.2015

Valero, M., Cid, E., Averkin, R. G., Aguilar, J., Sanchez-Aguilera, A., Viney, T. J., Gomez-Dominguez, D., Bellistri, E., & De La Prida, L. M. (2015). Determinants of different deep and superficial CA1 pyramidal cell dynamics during sharp-wave ripples. *Nature Neuroscience*, *18*(9), 1281–1290. https://doi.org/10.1038/nn.4074

van der Veldt, S., Etter, G., Mosser, C. A., Manseau, F., & Williams, S. (2021). Conjunctive spatial and self-motion codes are topographically organized in the GABAergic cells of the lateral septum. In *PLoS Biology* (Vol. 19, Issue 8). https://doi.org/10.1371/journal.pbio.3001383

Van Strien, N. M., Cappaert, N. L. M., & Witter, M. P. (2009). The anatomy of memory: An interactive overview of the parahippocampal- hippocampal network. *Nature Reviews Neuroscience*, *10*(4), 272–282. https://doi.org/10.1038/nrn2614

Vandecasteele, M., Varga, V., Berényi, A., Papp, E., Barthó, P., Venance, L., Freund, T. F., & Buzsáki, G. (2014). Optogenetic activation of septal cholinergic neurons suppresses sharp wave ripples and enhances theta oscillations in the hippocampus. *Proceedings of the National Academy of Sciences of the United States of America*, *111*(37), 13535–13540. https://doi.org/10.1073/pnas.1411233111

Vanderwolf, C. . (1969). Hippocampal electrical activity and voluntary movement in the rat. *Electroencephalography and Clinical Neurophysiology*, *26*(4), 407–418.

https://doi.org/10.1016/0013-4694(69)90092-3

Varga, V., Hangya, B., Kránitz, K., Ludányi, A., Zemankovics, R., Katona, I., Shigemoto, R., Freund, T. F., & Borhegyi, Z. (2008). The presence of pacemaker HCN channels identifies theta rhythmic GABAergic neurons in the medial septum. *Journal of Physiology*, *586*(16), 3893–3915. https://doi.org/10.1113/jphysiol.2008.155242

Wang, C., Chen, X., Lee, H., Deshmukh, S. S., Yoganarasimha, D., Savelli, F., & Knierim, J. J. (2018). Egocentric coding of external items in the lateral entorhinal cortex. *Science*, *362*(6417), 945–949. https://doi.org/10.1126/science.aau4940

Wang, Y., Romani, S., Lustig, B., Leonardo, A., & Pastalkova, E. (2015). Theta sequences are essential for internally generated hippocampal firing fields. *Nature Neuroscience*, *18*(2), 282–288. https://doi.org/10.1038/nn.3904

Wang, Y., Roth, Z., & Pastakova, E. (2016). Synchronized excitability in a network enables generation of internal neuronal sequences. *ELife*, *5*(September2016), 1–15. https://doi.org/10.7554/eLife.20697

Wersinger, S. R., Ginns, E. I., O'Carroll, A. M., Lolait, S. J., & Young, W. S. (2002). Vasopressin V1b receptor knockout reduces aggressive behavior in male mice. *Molecular Psychiatry*, *7*(9), 975–984. https://doi.org/10.1038/sj.mp.4001195

Wersinger, Scott R, Temple, J. L., Caldwell, H. K., & Young, W. S. 3rd. (2008). Inactivation of the oxytocin and the vasopressin (Avp) 1b receptor genes, but not the Avp 1a receptor gene, differentially impairs the Bruce effect in laboratory mice (Mus musculus). *Endocrinology*, *149*(1), 116–121. https://doi.org/10.1210/en.2007-1056

Widmer, H., Ferrigan, L., Davies, C. H., & Cobb, S. R. (2006). Evoked slow muscarinic acetylcholinergic synaptic potentials in rat hippocampal interneurons. *Hippocampus*, *16*(7), 617–628. https://doi.org/10.1002/hipo.20191

Wilcox, R. (2012). *Introduction to Robust Estimation and Hypothesis Testing* (3rd ed. NV). Elsevier. https://doi.org/10.1016/C2010-0-67044-1

Wilson, M. A., & McNaughton, B. L. (1994). Reactivation of Hippocampal Ensemble Memories During Sleep. *Science*, *265*(5172), 676–679. https://doi.org/10.1126/science.8036517

Winson, J. (1978). Loss of Hippocampal Theta Rhythm Results in Spatial Memory Deficit in the Rat. *Science*, *201*(4351), 160–163. https://doi.org/10.1126/science.663646

Wirtshafter, H. S., & Wilson, M. A. (2020). Title: Differences in reward biased spatial representations in the lateral septum and hippocampus. *ELife*, *9*, 1–20. https://doi.org/10.7554/eLife.55252

Witter, M. P. (1993). Organization of the entorhinal—hippocampal system: A review of current anatomical data. *Hippocampus*, *3*(1 S), 33–44. https://doi.org/10.1002/hipo.1993.4500030707

Witter, M. P. (2007a). Intrinsic and extrinsic wiring of CA3: Indications for connectional heterogeneity. *Learning and Memory*, *14*(11), 705–713. https://doi.org/10.1101/lm.725207

Witter, M. P. (2007b). The perforant path: projections from the entorhinal cortex to the dentate gyrus. *Progress in Brain Research*, *163*, 43–61. https://doi.org/10.1016/S0079-6123(07)63003-9

Witter, M. P., Doan, T. P., Jacobsen, B., Nilssen, E. S., & Ohara, S. (2017). Architecture of the entorhinal cortex a review of entorhinal anatomy in rodents with some comparative notes. *Frontiers in Systems Neuroscience*, *11*(June), 1–12. https://doi.org/10.3389/fnsys.2017.00046

Wong, L. C., Wang, L., D'Amour, J. A., Yumita, T., Chen, G., Yamaguchi, T., Chang, B. C., Bernstein, H., You, X., Feng, J. E., Froemke, R. C., & Lin, D. (2016). Effective Modulation of Male Aggression through Lateral Septum to Medial Hypothalamus Projection. *Current Biology*, *26*(5), 593–604. https://doi.org/10.1016/j.cub.2015.12.065

Wood, E. R., Dudchenko, P. A., Jonathan Robitsek, R., & Eichenbaum, H. (2000). Hippocampal Neurons Encode Information about Different Types of Memory Episodes Occurring in the Same Location. In *Neuron* (Vol. 27). http://www.neuron.org/cgi/content/full/27/3/623/DC1

Yang, Z. R. (2010). Machine Learning Approaches to Bioinformatics. In *Science, Engineering, and Biology Informatics: Vol. Volume 4*. WORLD SCIENTIFIC. https://doi.org/doi:10.1142/7454

Yassa, M. A., & Stark, C. E. L. (2011). Pattern separation in the hippocampus. *Trends in Neurosciences*, *34*(10), 515–525. https://doi.org/10.1016/j.tins.2011.06.006

Young, W. S., Li, J., Wersinger, S. R., & Palkovits, M. (2006). The vasopressin 1b receptor is prominent in the hippocampal area CA2 where it is unaffected by restraint stress or adrenalectomy. *Neuroscience*, *143*(4), 1031–1039. https://doi.org/10.1016/j.neuroscience.2006.08.040

Zhang, K., Ginzburg, I., McNaughton, B. L., & Sejnowski, T. J. (1998). Interpreting neuronal population activity by reconstruction: Unified framework with application to hippocampal place cells. *Journal of Neurophysiology*, *79*(2), 1017–1044. https://doi.org/10.1152/jn.1998.79.2.1017

Zhang, L., & Hernández, V. S. (2013). Synaptic innervation to rat hippocampus by vasopressin-immuno-positive fibres from the hypothalamic supraoptic and paraventricular nuclei. *Neuroscience*, *228*, 139–162. https://doi.org/10.1016/j.neuroscience.2012.10.010

Zhang, Y., Cao, L., Varga, V., Jing, M., Karadas, M., Li, Y., & Buzsáki, G. (2021). Cholinergic suppression of hippocampal sharp-wave ripples impairs working memory. *Proceedings of the National Academy of Sciences*, *118*(15). https://doi.org/10.1073/pnas.2016432118

Zhao, C., Eisinger, B., & Gammie, S. C. (2013). Characterization of GABAergic Neurons in the Mouse Lateral Septum: A Double Fluorescence In Situ Hybridization and Immunohistochemical Study Using Tyramide Signal Amplification. *PLoS ONE*, *8*(8), 1–24. https://doi.org/10.1371/journal.pone.0073750

Ziv, Y., Burns, L. D., Cocker, E. D., Hamel, E. O., Ghosh, K. K., Kitch, L. J., Gamal, A. El, & Schnitzer, M. J. (2013). Long-term dynamics of CA1 hippocampal place codes. *Nature*

Neuroscience, *16*(3), 264–266. https://doi.org/10.1038/nn.3329

Zutshi, I., Brandon, M. P., Fu, M. L., Donegan, M. L., Leutgeb, J. K., & Leutgeb, S. (2018). Hippocampal Neural Circuits Respond to Optogenetic Pacing of Theta Frequencies by Generating Accelerated Oscillation Frequencies. *Current Biology*, *28*(8), 1179-1188.e3. https://doi.org/10.1016/j.cub.2018.02.061